Ground Vibrations: Effects of masses placed on or in the ground.

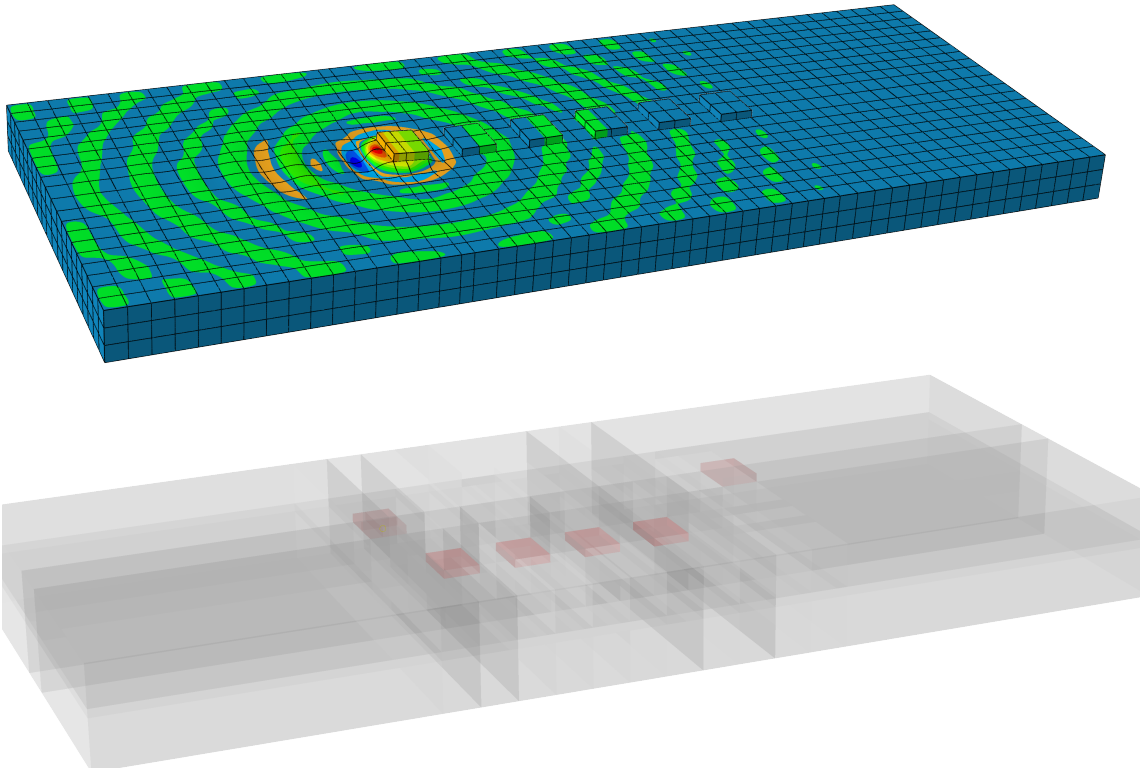

M.Sc Thesis Project

Authors: Mihai Mureşan, Ioan-Oreste Paven,
Liviu Ionuţ Mureşan
Structural and Civil Engineering
Aalborg University

09 June 2016

The Faculty of Engineering and Science
Department of Civil Engineering
Fibigerstræde 10
9220 Aalborg Øst
Phone: 99 40 84 84
http://www.byggeri.aau.dk

Title: Ground Vibrations: Effects of masses placed on or in the ground
Theme: Influence of added masses on the vibrations magnitude
Project period: University Year 2015-2016
Participants:

Mihai Muresan

Ioan-Oreste Paven

Liviu Ionuţ Mureşan

Supervisor: Lars Vabbersgaard Andersen

Copies in circulation: 5
Number of pages: 131
Appendix: 1
Delivered: 09-06-2016

Synopsis:

The project focuses on the vibrations propagation through solids and studies solutions to reduce the magnitude of these vibrations. The problem is investigated from two different approaches, a small scale laboratory experiment and by use of numerical models. Two main test setups are considered. One setup simulates a single soil layer with masses positioned on the surface between an exciter and a receiver. The second model resembles a thicker layer of soil and the masses embedded in the soil volume. The experimental work was performed at Aalborg University laboratory on Sohngaardsholmsvej 52, where with the use of accelerometers and a specialized software, Pulse a FRF analysis was conducted. The same test setup was then modeled using the commercial software Abaqus CAE making possible a comparison between the two different approaches. It was discovered that the the model numerical model behaves better if the experiment is less complex and consequently less uncertainties introduced. Regarding vibration attenuation, mitigation trends were observed at some models but in the same time increased response was present at some frequency ranges.

Preface

This is the 2nd year Master's program project serving as thesis which is written by a group of students from the institution of Structural and Civil Engineering on Aalborg University. The project considers the vibrations propagation through solids and mitigation applications for the vibrations. The project was carried out in the period from 1st of September 2015 to 8th of June 2016. The report is based on the knowledge gained from the courses attended throughout the Master's program and on a theory research on the available publications in relation with the analyzed problem. The report considers different approaches of analysing the problem, this being an experimental study and a numerical study. To understand the content of this project report, the reader must have a certain amount of technical knowledge and understanding of structural dynamics, geotechnical engineering and material modelling.

Readers guide

The report is divided into 7 chapters: Introduction, Ground vibrations analysis, Design of an appropriate study setup, Analysis strategies, Models compatibility using FRF analysis, Vibration mitigation analysis and Conclusion. Furthermore, an appendix is attached on a data CD. Sources used are indicated by the Harvard -method. Books are referenced by author, publish year, ISBN-number, version and publisher. Figures and tables are numbered related to the individual chapter. Figures and tables without sources, are created by the project group. All sources, figures and tables are listed in the back of the report in alphabetic order.

Abstract

This report concerns a real and actual problem of buildings affected by vibrations generated by various urban activities. The project focuses on the vibrations propagation through ground and investigates solutions to reduce the magnitude of these vibrations. In order to mitigate vibrations a relative new idea is studied by using masses placed in between the vibration source and the receiver which can be either placed on the ground surface or embedded in the ground.

The problem is studied from two different approaches, a small scale laboratory experiment and by numerical models. The research work starts with the task of scaling the vibrations characteristics to convenient laboratory dimensions while using accessible materials. Furthermore the behavior of the materials and of the test setup is investigated step by step using specialized equipment (accelerometers , impact hammer and a data processing software PULSE) in the format of a frequency response function (FRF) analysis. The investigation lead to a number of two final experimental test setups, each of them having the possibility to be adapted to a series of added masses configurations. The first model simulates a single soil layer with masses positioned on the surface between an exciter and a receiver. The second model resembles a thicker layer of soil with the masses imbedded in the ground volume. Subsequently, using the commercial software Abaqus CAE a series of numerical models are modeled with the same boundary conditions and the same materials used in the experimental analysis. The results from the experimental and numerical analysis are then compared and the ability of the numerical models of simulating this phenomenon is tested.

It was discovered that the numerical model matches better relative simple models where less uncertainties are likely to be introduced. The effect of added masses could be observed in all test setups configurations for both experimental and numerical analyses. The response recorded attenuation of the accelerations at some frequency ranges but in the same time increased response could be observed at other frequencies. The most significant positive influence was observed when multiple masses were placed in between the exciter and receiver simulating a periodic configuration of the masses.

Abstrakt

Denne rapport omhandler et reelt og aktuelt problem for bygninger påvirket af vibrationer genereret af forskellige årsager. Projektet fokuserer på formering af vibrationer gennem jorden og undersøger løsninger for at mindske størrelsen af disse vibrationer. En relativ ny teori er analyseret for at forhindre vibrationerne ved at placere en masse mellem vibrationens kilde og modtageren, som enten kan være placeret på jorden eller indlejret i jorden.

Problemet er analyseret gennem to metoder; laboratorie tests foretaget på en skaleret model og numerisk analyse. Forskningsarbejdet er startet med at skalere vibrationernes karakteristika ved brug af tilgængelige materialer til anvendelige laboratorie dimensioner. Derudover er materialernes og set uppets adfærd trin-for-trin undersøgt ved at bruge specialiseret udstyr (accelerometer, impulshammer og Pulse software til at bearbejde data) i format af frekvensresponsfunktioner (FRF) analyse. Undersøgelsen leder op til to endelige forsøgsopstillinger, og hver af dem med mulighed for at blive tilpasset med en række masse konfigurationer. Den første model simulerer et enkelt jordlag hvor massen er placeret på overfladen mellem exciter og en modtager. Den anden model forestiller et tykkere jordlag med massen indlejret i selve jorden. Efterfølgende er en række numeriske modeller simuleret med software programmet Abaqus CAE med de samme randbetingelser og materiale data, som blev brugt i forsøgene. Resultaterne fra laboratorie forsøgene og de numeriske modeller er derefter sammenlignet, hvorefter de numeriske modeller er valideret.

Det er observeret, at den numeriske model matcher de relative simple modeller bedre, hvor sandsynligheden for usikkerheder er mindre. Effekten af at tilføje masse kunne observeres ved alle test set ups både eksperimentelt og numerisk. Den respons registreres dæmpning af de accelerationer på nogle frekvensområder, men på samme tid øget respons kunne observeres ved andre frekvenser. Den væsentligste positive indflydelse observeres ved at tilføje flere masser mellem exciter og modtager der simulerer en periodisk konfiguration af masserne.

Contents

1 Introduction **3**
1.1 Background . . . 3
1.2 Objective . . . 3

2 Ground vibrations analysis **5**
2.1 Nature and type of vibrations . . . 5
2.2 Analytical description . . . 8
2.3 Dispersion and dissipation . . . 12
2.4 Mitigation solutions . . . 13

3 Design of an appropriate study setup **17**
3.1 Problem formulation . . . 17
3.2 Suitable domain dimensions and material . . . 18
3.3 Means and tools . . . 20
3.4 Strategies of studying the phenomenon . . . 20

4 Analysis strategies **23**
4.1 Equipment and software specifications . . . 23
4.2 Finite-element model . . . 33
4.3 Verification of Abaqus for wave propagation . . . 36

5 Models compatibility using FRF analysis **41**
5.1 Simply supported model of a beam . . . 41
5.2 Numerical analysis of the simple beam . . . 44
5.3 Dry foam . . . 51
5.4 Wet foam . . . 60

6 Vibration mitigation analysis **69**
6.1 Introduction . . . 69
6.2 Data processing . . . 69
6.3 One layer mattress . . . 70
6.4 Two-layers mattress: Experiment . . . 78
6.5 Two-layers mattress: Numerical model . . . 83
6.6 Vibration screen influence . . . 88

7 Conclusion **93**

8 Bibliography **97**

I Appendix **101**

A Additional wave theory description

A.1 Derivation of the body wave velocities 103

B Wave propagation-mathematical verification

B.1 Verification of Abaqus for wave propagation 107

C FRFs provided by analyzing the simple beam

C.1 Experimental results 109

C.2 Numerical results 111

C.3 Comparing the results 114

D Electronic appendix

Chapter 1

Introduction

1.1 Background

With an increasing world population the urban areas become more and more crowded. To accommodate the growth of population the cities are developing new buildings and the necessary infrastructure: motorways, railways, tramways. This expansion trend reduces the amount of unbuilt areas within cities shortening the distances between buildings and possible vibration sources such as construction sites or nearby transportation links. The vibrations generated by the above mentioned sources affects the inhabitants as well as the structure of the surrounding buildings. Moreover buildings with highly sensitive equipment, such as hospitals, laboratories or radar towers require a very stable environment and therefore a low level of vibrations. In order to allow the expansion of the cities, vibration levels have to be taken in consideration and controlled. Hence solutions for mitigation of vibration have to be studied and implemented. The effectiveness of these solutions can be evaluated using small scaled experiments or numerical models. The numerical models, however, presents more interest since they are cheaper and more less time consuming.

1.2 Objective

The goal of this project is to evaluate the effect of added masses on the surface or embedded in the ground, placed in between a source and a receiver. The efficiency of these solutions is determined by the means of a laboratory experiment accompanied by numerical model with the same setup. The results provided by the two approaches are interpreted, the efficiency of added masses as mitigation solution is examined as well as the capacity of the numerical model to predict the development and the mitigation of the vibration in the ground.

Chapter 2

Ground vibrations analysis

This chapter presents the basic theory of vibrations which is required for a good understanding of the phenomenons of vibration propagation and mitigation. The mitigation problem starts by identifying specific vibration sources. Furthermore simplifying assumptions are considered and a mathematical description is presented. With the velocity definitions determined the interest is turned to vibration interaction and vibration dissipation. Finally, some mitigating solutions are analyzed and discussed.

2.1 Nature and type of vibrations

The soil is subjected to various vibrations generated by different sources. First studies were done on the earthquake generated vibrations which lead to the implementation of the wave propagation theory. This phenomenon was extensively studied and numerous articles were written on the subject, [B.Dasgupta, E. Beskos, 1990], [P. Coulier, G. Degrande, 2015]. Another type of vibrations which can create problems for the structures and their foundations are the man-made vibrations.

The vibration mitigation of structures from ground transmitted waves is a very sensitive, actual and important engineering problem. There can be various causes that generate these vibration waves such as human activities, traffic, machines operating nearby the structures or blasting. This brings the question of how to mitigate these vibrations in order to protect the structures foundation, reduce the vibrations of buildings that are housing sensitive machines and equipment and increase the human comfort. Studies show that man made ground vibrations are usually in the range of 4-80 Hz which corresponds to 'whole body' vibration perception, [P. Coulier, 2011] and furthermore [Woods, 1967] have shown that 67 % of the wave energy is characterized by the Rayleigh waves while just 26 % and 7 % are characterized by the S-wave respectively P-wave. The idea is to study an effective barrier that can diffract the surface vibration waves and reduce their amplitude. Regarding how these barriers behave there are two types, active and passive barriers depending on where they are positioned, see Figure 2.1.

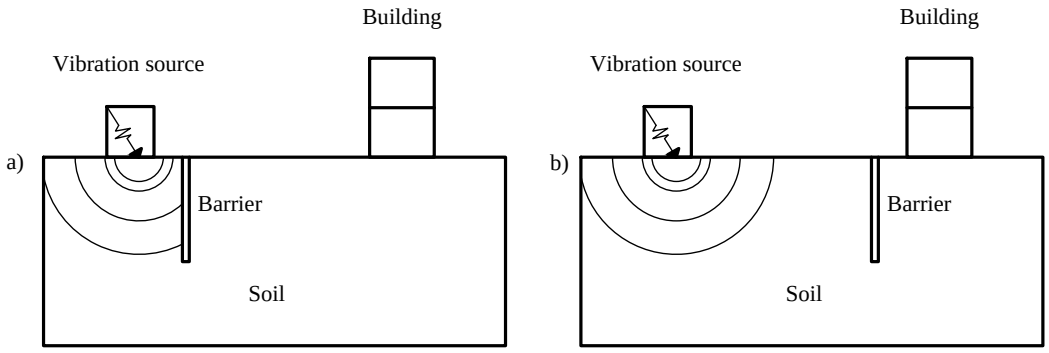

Figure 2.1: Mitigation types depending on the barrier position: a) active mitigation, b) passive mitigation.

Field experiments of the ground response showed that there are two principal type of vibrations, P-waves and S-waves. More vibrations types can be defined such as Rayleigh waves or Love waves which are a result of P-wave and S-wave interaction on the ground surface or special ground conditions. The classification was done considering the velocities and also the propagation direction relative to the particle motion, see Figure 2.3. It also has to be mentioned that some vibrations are propagating in the whole body while others propagate only in the surface (Rayleigh waves), in an interface (Stonely waves) or in a layer (Love waves).

The P-wave is the fastest wave and therefore called the primary wave. It propagates through the soil volume and the particle motion is associated to pure dilation or compression, see Figure 2.3(a).

The S-wave is the second wave to arrive to a receptor and therefore called secondary wave. It travels through space and the particle motion is associated with shear, see Figure 2.3(b). The phase velocity is typically about $c_S = 0.5c_P$ in soil but the ratio varies with the soil Poisson's ratio. The S-wave can be decomposed in two components: a horizontal component SH-wave and a vertical one SV-wave as illustrated in Figure 2.2.

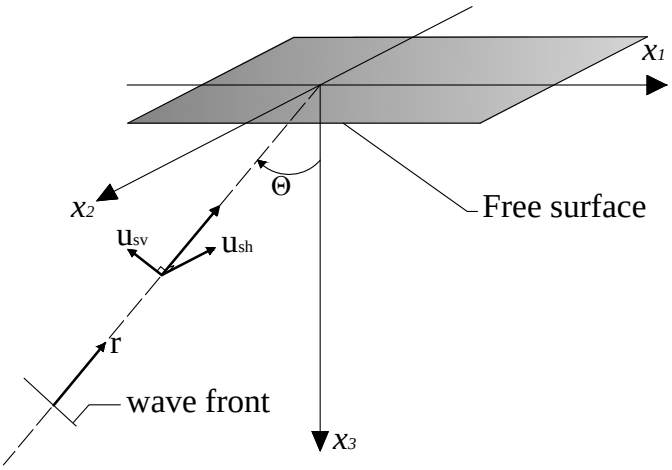

Figure 2.2: Components of the displacement field in a plane elastic wave.

The Rayleigh waves were first discovered by Lord Rayleigh in 1885. In contrast with the P-waves and S-waves, Rayleigh waves propagate in the surface of the soil. It is the slowest wave with a velocity close to the S-wave, $c_R \approx 0.9c_S$. The Rayleigh waves contain both dilatational and shear components, see Figure 2.3(c).

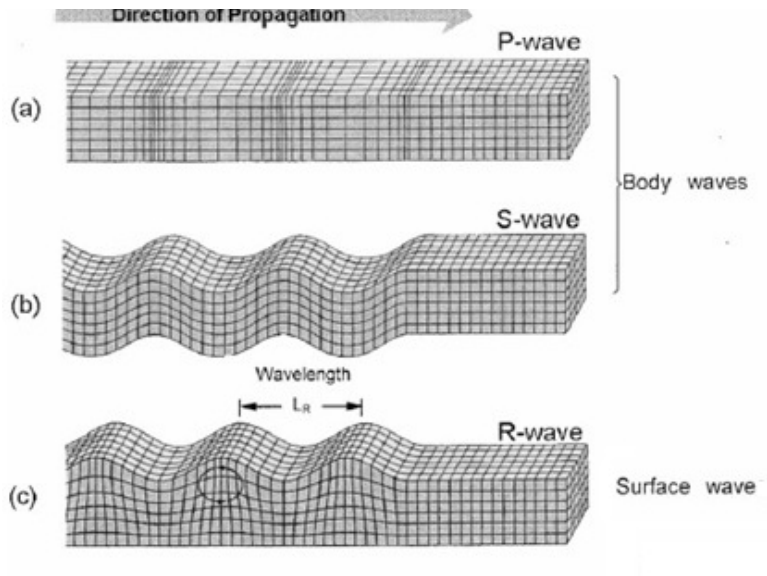

Figure 2.3: Soil deformation subjected to wave type vibrations [L.A-2006].

2.2 Analytical description

2.2.1 Material model

Soil is one of the most complex materials encountered in civil engineering. The complexity is introduced by its mechanical properties. Usually soil is a non-homogeneous material with numerous changes in its structure which also leads to an anisotropic behavior. Furthermore, when loaded it may present plastic deformations and its properties depends on the load history and the water content assimilated in its structure. Numerous studies were made in order to describe this type of behavior but no exact solutions were discovered. Most of the relations are empirical and in order to model accordingly, extensive site investigations are required which usually is not cost effective while a numerical model containing all the parameters becomes complex and time consuming.

In order to reduce the complexity of the problem and to increase the efficiency of the model a closer look to the zone of interest is required. In the case of man-made vibrations plastic deformations may occur or not depending on how the soil is loaded. For instance plasticity is observed for pile driving works while for other vibration sources where the load is distributed over larger areas the deformations remain elastic. However, typically the surveyed areas for the transmission and attenuation of the vibrations are at a significant distance for the source and therefore a linear model is usually used which can be elastic or viscoelastic. The model can be further simplified by considering the soil homogeneous. This is possible because the wavelengths of the vibrations are considerably larger compared with the grain sizes. The soil stratification should be as well taken in consideration, but it may be fair to model the soil in each layer as homogeneous.

In the elasto-dynamics the difference between an isotropic and an anisotropic material is that the in the isotropic case the wave velocity is the same all directions. Usually the soil deposits are layered and therefore anisotropic. However, because only some wave types are affected for a simple analysis the soil can be considered isotropic.

2.2.2 Equations of motion

As discussed above, in the following analysis the soil is regarded as a linear, homogeneous and isotropic material. By isolating a cubic infinitesimal element and by making the summation of all linear contributions of the internal and external forces in each coordinate direction and use of Newton's second law, the Cauchy's equation of motion can be written.

$$\frac{\partial \sigma_{ij}}{\partial x_j} + \rho b_i = \rho \frac{\partial^2 u_i}{\partial t^2}. \tag{2.1}$$

Here σ_{ij} is the Cauchy stress tensor, ρ is the mass density, $b_i = b_i(x,t)$ stands for a component of the body force per unit mass and $u_i = u_i(x,t)$ is a component of the displacement field.

Assuming that the material is linear and isotropic the Cauchy equation of motion reduces to the Navier's equations.

$$(\lambda + \mu)\frac{\partial^2 u_j}{\partial x_i \partial x_j} + \mu \frac{\partial^2 u_i}{\partial x_i \partial x_j} + \rho b_i = \rho \frac{\partial^2 u_i}{\partial t^2}. \tag{2.2}$$

Where λ and μ are the Lame's constants defined as

$$\lambda = \frac{\nu E}{(1+\nu)(1-2\nu)}, \qquad \mu = \frac{E}{2(1+\nu)}. \tag{2.3}$$

2.2.3 Body waves

The P-wave and S-wave are also called body or volume waves because they propagate through the entire volume of the soil. Making use of the Navier's equations the velocities of these waves are expressed as in the following.

P-waves

The phase speed of the P-wave c_P is defined as

$$c_P = \sqrt{\frac{\lambda + 2\mu}{\rho}}. \tag{2.4}$$

S-waves

In contrast with the P-waves, S-waves are rotational and are expressed as

$$c_S = \sqrt{\frac{\mu}{\rho}}. \tag{2.5}$$

A more detailed derivation of the body wave velocities is presented in Appendix A.

2.2.4 Surface waves

Rayleigh waves

As mentioned before Rayleigh waves propagate at the surface through a relative shallow layer of soil. The existence of these waves is a consequence of the interaction of P-waves and SV-waves that are trapped at the surface. The particle motion resembles with a water wave with some differences. In Figure 2.4 the general shape of the wave along with the particle motions are sketched.

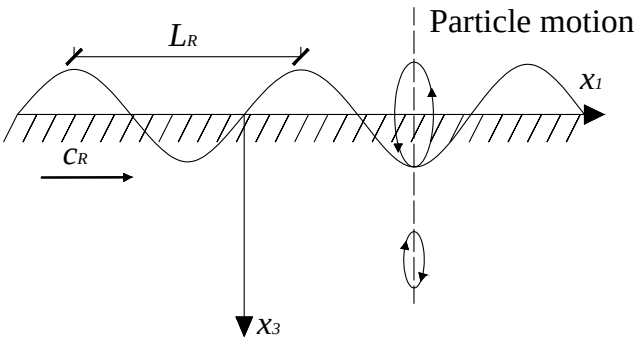

Figure 2.4: Rayleigh wave.

The particles describe ellipses stretched in the vertical, X_3 direction. This is caused because the horizontal displacement amplitude is smaller at any depth than the vertical component. Another particularity is the sense of rotation. At shallow depths for a propagation direction as seen in Figure 2.4 the particles move retrograde and from an approximate depth of about $0.2L_R$ the rotation changes to clockwise.

The amplitude of the Rayleigh waves decay with depth as seen in Figure 2.5.

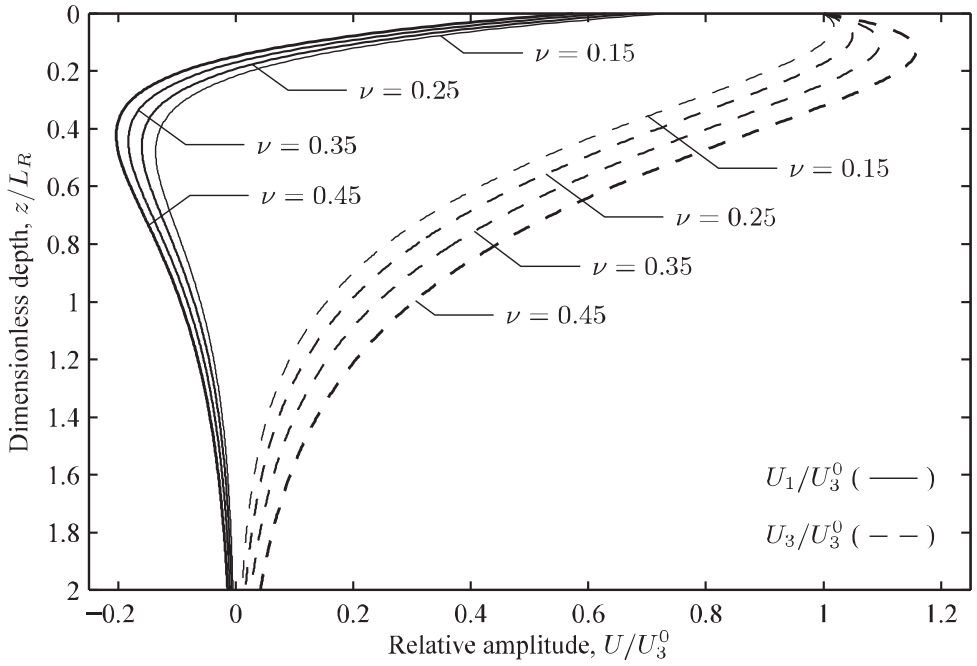

Figure 2.5: Rayleigh wave. Amplitude variation with depth.

It can be observed that the decay patterns depend of the Poisson's ratio and that the wave almost dissipates at a depth of two wavelengths, L_R.

Rayleigh wave velocity

The Rayleigh wave equation can be written as a third order polynomial equation in c_R^2/c_S^2

$$\left(\frac{c_R}{c_S}\right)^6 - 8\left(\frac{c_R}{c_S}\right)^4 + (24 - 16\alpha^{-2})\left(\frac{c_R}{c_S}\right)^2 - 16(1 - \alpha^{-2}) = 0. \tag{2.6}$$

Where α represents the velocity ratio of the principal and secondary wave. The Rayleigh velocity is extracted from this equation and implies that the other two velocities are known. Three roots are obtained but only one is valid. The root must be real and respect the condition $c_R/c_S < 1$ since the Rayleigh wave is slower than the S-wave.

Figure 2.6 presents the variation of the presented wave velocities with respect to the Poisson's ratio.

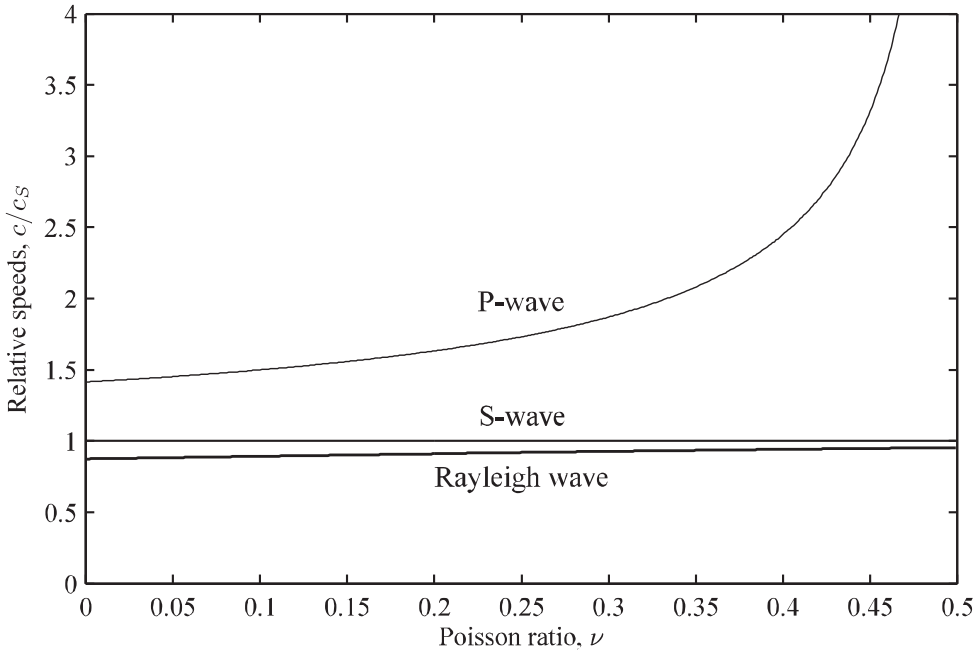

Figure 2.6: Relative wave velocities.

It can be observed that the relative primary wave speed increases significantly with the increase in Poisson's ratio. In the case of the Rayleigh wave velocity, an increase from $c_R = 0.862c_S$ to $c_R = 0.955c_S$ is observed in the interval $\nu = [0 : 0.5]$.

2.3 Dispersion and dissipation

In the previous sections of this chapter the three main waves were described in terms of propagation equations, particle motion and velocities. For a better description of these waves the phenomenons of dispersion and dissipation has to be discussed. Even though in some contexts these terms may have the same meaning in the field of waves analysis they are different.

2.3.1 Dispersion

The dispersion of a wave means that the wave propagation velocity depends on the wave number and implicitly on the frequency. For instance, if a short broad banded pulse is generated, a receiver place at a considerable distance will not receive the signal as a short pulse but as a signal spread over time. Waves with this quality are called dispersive and the others non-dispersive.

In the previous sections it was proven that the primary and secondary wave velocities depend solely on the Lame constants and the soil density. Because these are material

characteristics it can be concluded that both P-wave and S-wave are non-dispersive. Furthermore, the Rayleigh wave velocity is derived from the other two previously mentioned which means that the Rayleigh wave is non-dispersive. This property is only valid for homogenous elastic materials. In reality, depending on the soil structure, dispersion can be observed for all wave types.

2.3.2 Dissipation

Energy loss during wave propagation leads to the notion of dissipation. There are two types of dissipation or energy losses: geometrical dissipation which accounts for the energy spread over the volume and material dissipation which takes in consideration the loss in energy caused by the conversion of the mechanical energy into heat. Their magnitude differs with the type of wave and the soil characteristics. The geometrical dissipation, for instance, is more striking at the volume waves (P-waves and S-waves). The volume waves propagate through a much larger space compared with the surface waves and therefore the geometrical dissipation has an important impact on them.

2.4 Mitigation solutions

2.4.1 Wave mitigation using trenches

The first studies on the mitigation of vibrations problem were conducted by [Barkan, 1962] and [Woods, 1965] and these involved field experiments to observe how efficient are empty trenches to reduce the amplitude of vibrations. Since then a lot of articles and papers appeared regarding these problem but still a perfect solution has yet to be found. This is because there are various variables that characterize this problem, such as soil parameters, barrier geometry and filling material parameters. The next paragraph presents some early considerations about the studied barriers from the experience that previous studies provided. In quest of finding efficient vibration mitigation ways the first proposed barriers were the trenches, see Figure 2.7 at the beginning empty ones obtaining a perfect wave reflection. But then it was observed that the efficiency of the trenches increases with the depth so another problem arises; because the ground waves hitting the trenches could cause failure in the trenches walls a filling material had to be found. Studies were conducted on water [Woods, 1968], concrete, bentonite [Dooling, 1970, Haupt, 1981] and more recently (EPS) geofoam [Alzawi and El Naggar, 2011]. It was shown that wave propagation is better in stiff soils and materials with low impedance which reduce better the amplitude of the waves. So materials with low Young's modulus behave well in reducing vibrations in stiff soil and studies show that trenches filled with geofoam have a better attenuation efficiency than water filled trenches being similar to the open ones. In soils characterized by low stiffness geofoam is not an viable solution. Further on it

was shown that trenches are not the best solution when it comes to long Rayleigh wave lengths, because construction of these trenches is impractical. Sheet pile or vertical pile is the only practical solution for the mitigation of these long Rayleigh wave lengths but these sheet pile walls are very expensive to build and they can also be an important vibration generator when they are executed.

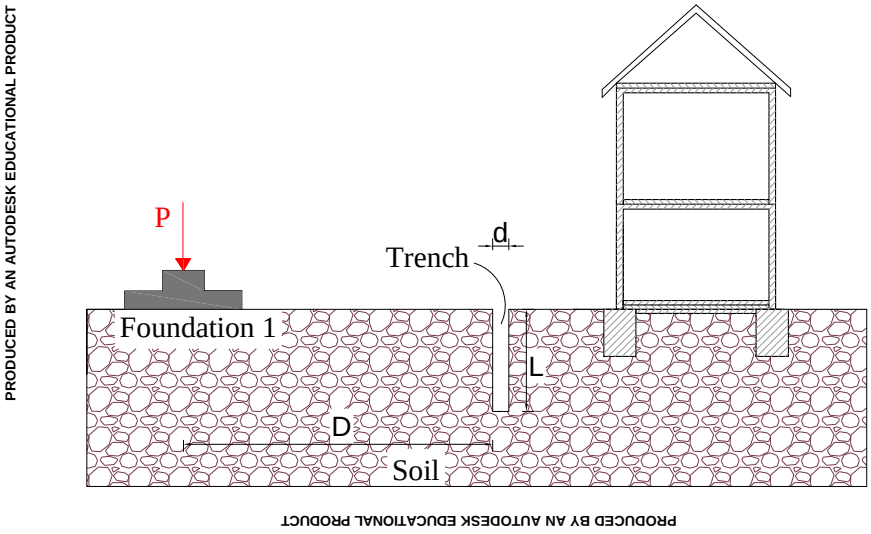

Figure 2.7: Example of trench.

These types of wave barriers can be active or passive, relatively to their position from the excitation source as depicted in Figure 2.8. Studies show that passive trenches tend to be a better choice for wave mitigation.

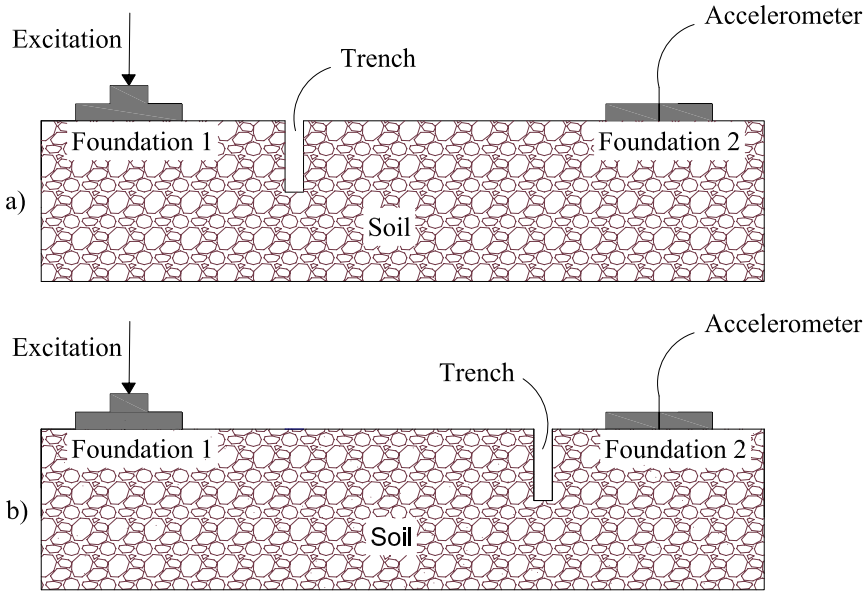

Figure 2.8: Active trench a), passive trench b).

In the last years various articles studied the mitigation of vibrations using added mass on the ground surface see Figure 2.9. Given that the Rayleigh waves propagate at the surface of the soil it was found that correlating the positioning of the mass added with the wave length can attenuate the vibration and reduce their amplitude.

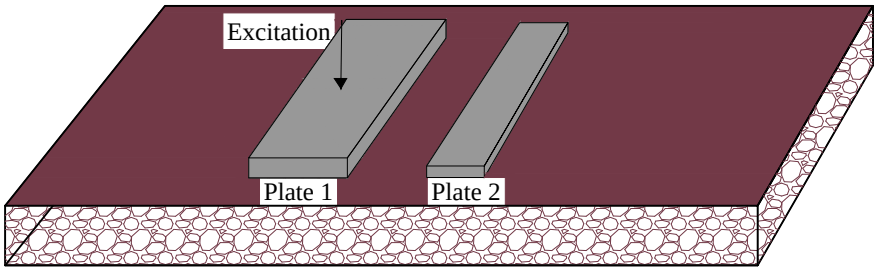

Figure 2.9: Example of added mass.

Table 2.1 presents a short history of the mittigation solutions proposed along time.

Table 2.1: Mittigation solution history.

Mittigattion solution	First studies
Empty Trenches	Barkan (1962) and Woods (1967, 1968)
Water filled trenchest	Woods (1968)
Bentonite filled trenches	Dooling (1970)
Stiff materials filled trenches	Haupt (1981)
Geofoam filled trenches	Alzawi and El Naggar (2011)
Gas cushion concept	K.R. Massarsch and Ersson (1985)
Vertical and Sheet pile walls	Woods, Barnett and Saggeser (1974); Liao and Sangrey (1978)
Added mass	Relatively new, Grau and Laulagnet (2015)

Chapter 3

Design of an appropriate study setup

The aim of this chapter is to present the development process of an experiment setup capable to model similar wave characteristics with those generated by human activities in urban environments. The model design starts with an investigation about the possible infield vibrations followed by a second part consisting of a quest for finding the appropriate materials and dimensions for the setup. The analysis strategies and the expected results are presented in the end of the chapter.

3.1 Problem formulation

In order to design an experiment setup, first it is necessary to investigate the real, infield response of the soil subjected to various excitations. As mentioned before in Chapter 2 human made vibrations are generally spread over a frequency range of 4 Hz to 100 Hz. Combining this information with some common materials encountered in construction works and assuming a viscoelastic behavior some of the vibrations characteristics are estimated as, see Table 3.1.

Table 3.1: Wave characteristics.

Material	c_P [m/s]	c_S [m/s]	c_R [m/s]	L_S(1-100)[Hz] [m]
Wet clay	1.26e+3	248.8	237.06	62.2-2.5
Dry sand	683.13	418.33	381.1	104-4.18
Concrete	2.94e+3	2.66e+3	237.06	737-29
Water	1.42e+3	-	-	-

It can be observed that in the case of soils the generated waves have lengths situated in a range from 100m (4Hz) down to 3 m (100 Hz) while the shear wave velocities are generally under 500 m/s. Judging these results an appropriate laboratory model would be at a scale between 1:50 and 1:100. In order to study wave propagation through media a number of setups have to be designed. To obtain small-scale models representative for the full-scale conditions the wavelengths should be scaled correctly. In the same time the models have to be adaptable to both laboratory environment and numerical modeling. Hence the designs must adhere to the following rules.

- The geometries of the models are simple and clear so the experimental setups and the numerical models are easier to build and model;
- The static schemes should be simple with well-defined boundary conditions; a sketch with the geometry of the model and the boundary conditions is required before building the models;
- The dimensions of the structures in or on the ground measured relatively to the wavelengths must be equivalent in full scale and model scale;
- The distance between source and receiver points as well as between structures added within or on the ground must be equivalent in the two scales;
- The mass and stiffness properties of the materials representing soil and structural elements must have the same relative proportions in model scale and reality;
- It should be possible to analyze the frequency range 0–100 Hz which is of primary concern in relation to vibrations produced by road and railway traffic as well as construction work.

Considering all criteria presented above two setups are going to be designed. A primary model which is supposed to simulate vibrations through soil like material and a secondary model used for equipment and numerical modeling calibration. The primary model consists of a 3D rectangular hexahedron at an approximate scale of 1:50. This scale allows the generation and propagation of the target wave lengths and it fits the laboratory rooms. The secondary model consists of a small simple supported beam.

3.2 Suitable domain dimensions and material

This section concerns the construction of the experimental setup witch is created according to the above mentioned rules, see Section 3.1. Creating the laboratory model is requiring two important steps, which consists of defining the model dimensions and the material used in the analysis.

The model used for this study is constructed in the following manner, a foam mattress is introduced in a watertight wooden box with the inner dimensions of 2450 mm x 1015 mm x 130 mm and the mattress dimensions are presented in Table 3.2. An argumentation for the use of the presented setup is given, later in this section.

Table 3.2: Mattress dimensions.

Dimensions	L [m]	l [m]	h [m]
	2.45	1.015	0.12

An illustration of the mattress and its boundary conditions is presented in Figure 3.1

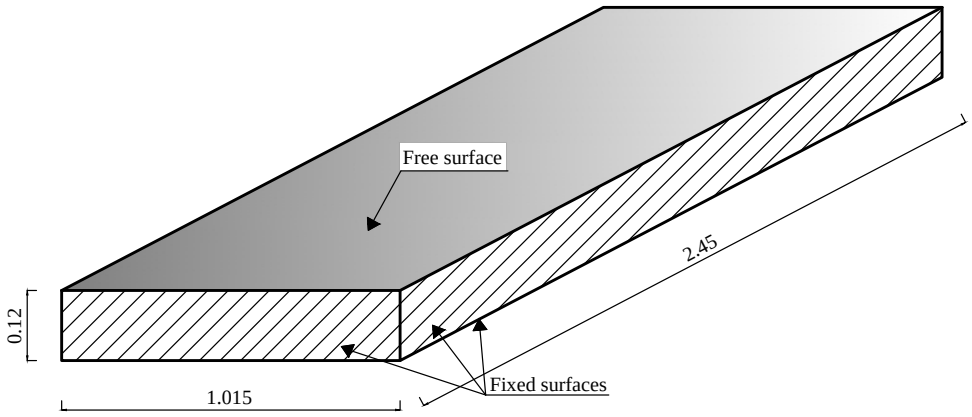

Figure 3.1: Static scheme for the main model.

According to the first rule the geometry of the model has to be simple and clear which lead to a rectangular shape of the model. This shape is easy to reproduce in the laboratory and for the numerical model is more suitable to use a rectangular shape since the required time in building the model is less.

In Figure 3.1 is observed that the hexaedrom is fixed on five faces and free at the surface. Satisfying rule number two, it was decided to use the encastration because it is easy to reproduce both in experimental and numerical models and in the same time reduces the complexity of the system. While the numerical software has predefined settings for this kind of boundary conditions, in the experimental part problems can occur if the locked surfaces presents contact imperfections.

The resulted dimensions of the model are chosen due to rule number three and four, the larger the model the more realistic dynamic response is achieved. The mattress had the thickness of 120 mm and as expected in the section above, the model has a scale of approximate 1:50 which corresponds to an approximately 6 m deep soil layer in full scale. Space limitations given by the use of laboratory and the available dimensions of the mattress are providing the final dimensions of the model setup, see Table 3.2. It was decided to construct a watertight wooden box since the material was available in the laboratory and it easily reproduces the boundary conditions.

Since the use of real soil is considered to be inadequate in the laboratory due to uncertainties that could be introduced in the system, the use of another material that could substitute it was taken into consideration. The material chosen for the experimental work is the foam

which similar to soil, presents a significant amount of damping. Foam is a porous material which can be soaked in water, increasing the density but basically will not affect the shear stiffness of the material. This represents some additional tuning keys for the properties of the material, changing some parameters without changing other parameters. Soaking the mattress will mimic the behavior of a dense ground, satisfying rule number five.

The setup produces an approximately 1:50 model regarding the length and about a 1:100 regarding the mass, so the wavelengths produced at a given frequency will match the full-scale problem at the same frequency, time being scaled 1:1. If real soil and concrete were used much higher frequencies would have to be analyzed, i.e. up to 10 kHz.

3.3 Means and tools

In quest of finding an optimal mitigation solution for vibrations the problem is analyzed by means of numerical and experimental procedures.

For the experimental analysis an excitation hammer and an exciter are used to excite the studied medium. Accelerometers are installed and used to record the data. The LabShop software is then used to perform a time and frequency domain analysis. A detailed explanation for the hardware and software used is given in Section 4.1

In the numerical analysis two approaches are used; a user defined coding program, MATLAB and a commercial finite element software program Abaqus CAE. MATLAB is used to perform a 1D analysis of wave propagation in a bar. The results are compared with the output Abaqus CAE software provided for the same type of analysis. This is done for a very simple model in order to verify if Abaqus works with the same sets of equations and if the output that it provides fits our needs. A good match is found between the results, see Apendix B so all the future numerical analysis is carried out with the numerical software Abaqus CAE.

Models are created in the software that perfectly match the experimental setup, in terms of dimensions, material properties, loads, boundary conditions and observation points. Steady state dynamics analysis were performed in order to obtain the frequency response functions (FRFs) of the model. These FRFs are later compared with the ones obtained in the experimental analysis and an observation will be made regarding how accurate the numerical program can reproduce the real experiment.

3.4 Strategies of studying the phenomenon

In the quest of finding good mitigation solutions some strategies to study the phenomenon have to be reasoned beforehand.

Firstly the phenomenon is tackled starting with the real experiment. The data recorded when the medium is excited with the hammer is used to create a FRF, to identify the natural frequencies of the system.

A frequency sweep analysis, where accelerations are recorded for a chosen range of frequencies, for each frequency for some proposed setups.

As a benchmark a frequency sweep is made for the simple model without any mitigation solution. The setup can be seen in Figure 3.2

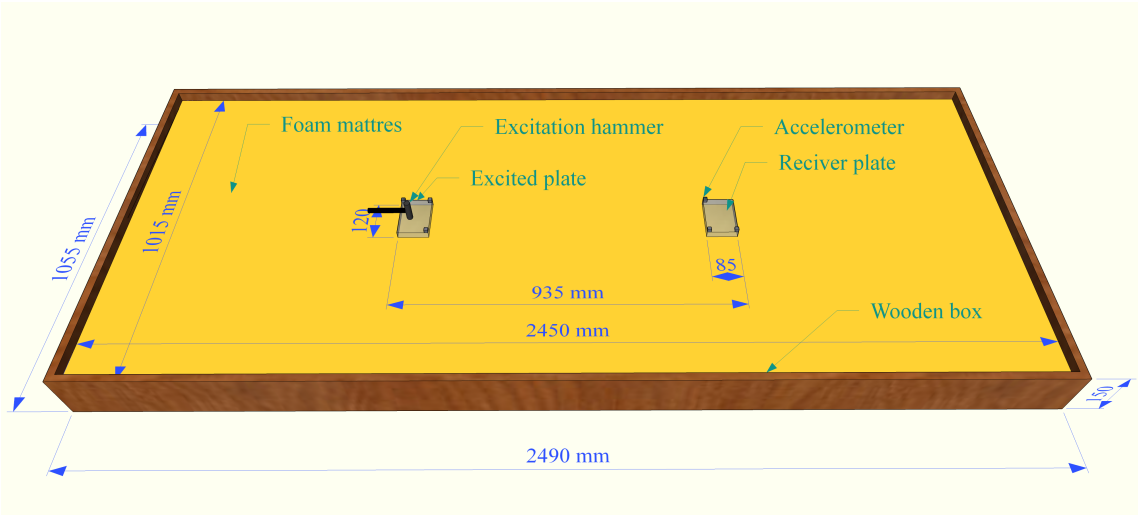

Figure 3.2: Benchmark setup

Next frequency sweeps are made for models with proposed mitigation solutions in quest to find the optimal one. A modular model is set up with proposed mitigation solutions and it can be seen in Figure 5.27.

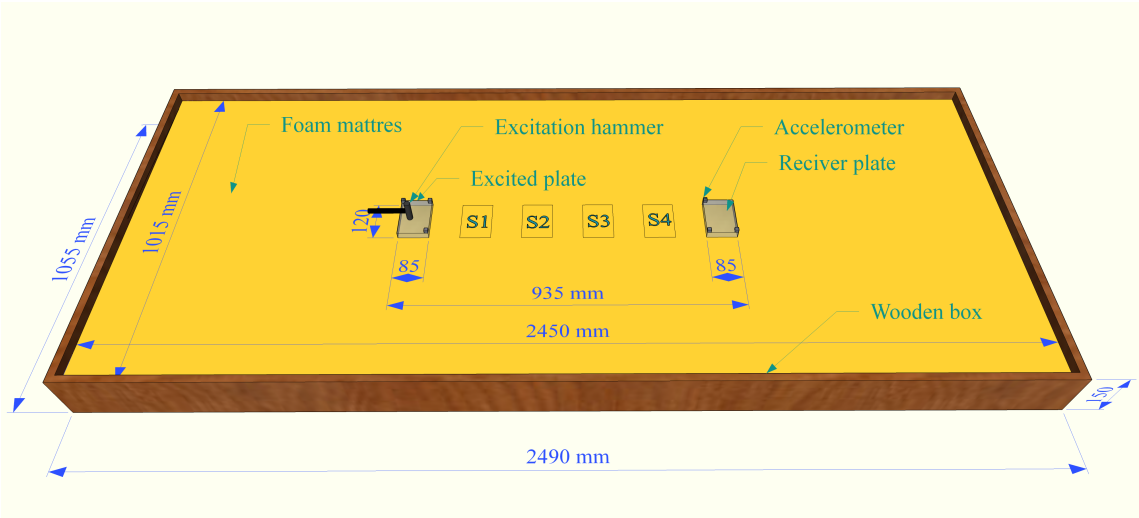

Figure 3.3: Modular set up with proposed mittigation solutions

The numerical analysis will consider the same setups, performing a sweep on the same range, with a frequency increment of 1. Later on the output from the numerical analysis will be compared with the one from the experimental part. Conclusions regarding the analysis correlations and their accuracy will be drawn out.

Chapter 4

Analysis strategies

This chapter presents a detailed description of the equipment and software used for the experimental and numerical part. First section presents the experimental equipment and the necessary software to process the data from the equipment. Second section introduces the finite element software Abaqus and the procedures used for this project.

4.1 Equipment and software specifications

4.1.1 Equipment specifications

The tests are performed using the measuring equipment and computer software produced by Brüel & Kjær (B&K).

In order to excite the system and to obtain the frequency response functions an impact hammer is used, see Figure 4.1. The hammer type is 8202 and it is supplied with four changeable tips of aluminium, plastic and two of rubber, see Figure 4.2. The choice of impact tips is determined by what impulse shape is desired, regarding the amplitude and duration, and also the bandwidth of the excitation. An extra head extender of 40 g is available for increased head mass. The impact hammer is designed to excite and measure impact forces on structures with masses in the range of 2 kg to 3000 kg, range which is very dependent on the structures mechanical properties and the mechanical background noise induced by the ambient conditions.

Figure 4.1: Impact hammer type 8202.

Figure 4.2: Impact hammer tips.

The built-in force transducer, type 8200, measured the force while the accelerometers, type 4507 Bx, see Figure 4.3, measured the structural response, every single accelerometer being calibrated using accelerometer calibrator, type 4294.

Figure 4.3: Accelerometer type 4507 Bx.

Beside the impact hammer, a vibrator produced by Brüel & Kjær, type 4809, see Figure 4.4, is available in order to be able to excite different frequencies in a range of 1 Hz to 1 000 000 Hz, being controlled by a TCELLNER Function Generator, type 7405, see Figure 4.5.

Figure 4.4: Impact hammer type 8202.

Figure 4.5: TCELLNER Function Generator.

The signal is transmitted from the impact hammer to an amplifier, NEXUS Conditioning Amplifier Type 2692-C, see Figure 4.6. It contains four charge channels and it is designed for applications with high charge inputs.

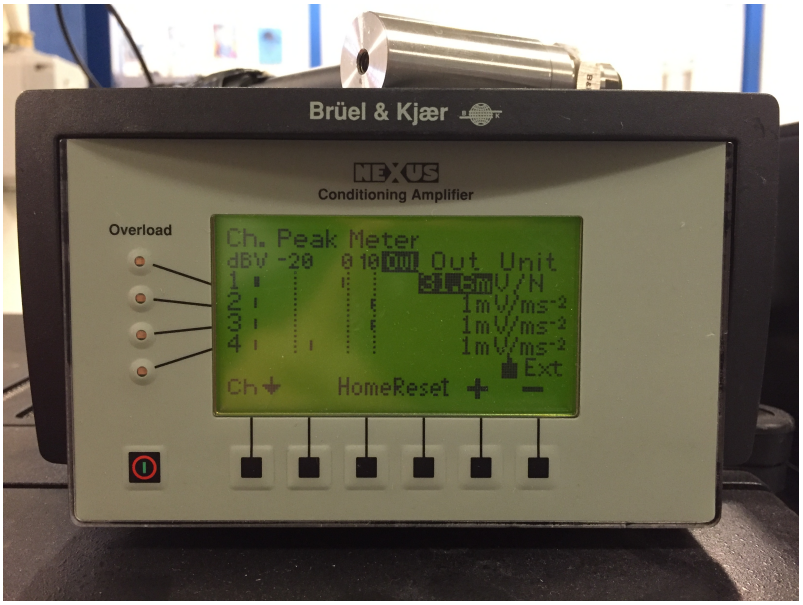

Figure 4.6: Amplifier Type 2692-C.

All the signals provided by the accelerometers are transmitted to the front-end, type 3560 D. The accelerometers are connected to the front-end through one of the five input modules, type 3038 B, and each one is equipped with 12-channels, allowing to connect a maximum of 60 accelerometers to a system in total, see Figure 4.7. The front-end also contains a controller module and a DC power supply unit.

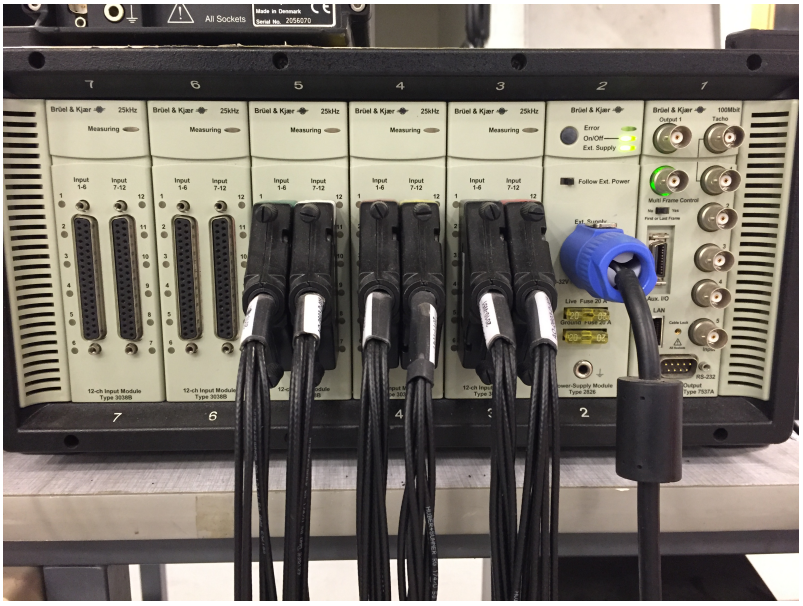

Figure 4.7: Front-end, type 3560 D.

The data processed by the front-end is then transmitted to the PC through the Pulse LabShop software for further analysis. The software can be used for both impact hammer and vibrator, using certain templates.

For the vibrator no template is needed, setting up only the type of analysis, FFT in this case, and the frequency range needed. A time series and the frequency response function is provided. It is noted that the time series does not represent the direct measurement, but the result of Inverse Fast Fourier Transformation function (IFFT) of the frequency spectrum.

4.1.2 Software specifications

Exciting the structure with an impact hammer the frequency response function is obtained using the MTC Hammer template in Pulse LabShop. This template requires several steps in order to have a working model. The steps are presented in the following part.

Step 1

First the accelerometers are placed on the structure, connected to the front end and the software is opened. The connection to the front end is checked and all the accelerometers available are listed and recognized automatically. The hammer is introduced, depending on its type and serial number. All the connected transducers have a green light in Hardware Setup window, see Figure 4.8, indicating that the hardware is working properly and it is ready to perform the analysis.

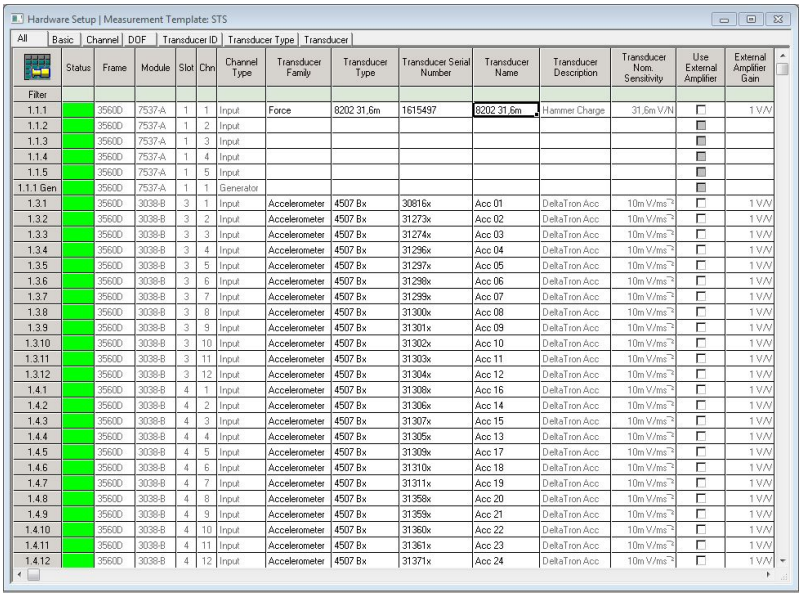

Hardware Setup | Measurement Template: STS

All | Basic | Channel | DOF | Transducer ID | Transducer Type | Transducer

Status	Frame	Module	Slot	Chn	Channel Type	Transducer Family	Transducer Type	Transducer Serial Number	Transducer Name	Transducer Description	Transducer Nom. Sensitivity	Use External Amplifier	External Amplifier Gain
Filter													
1.1.1	3560D	7537-A	1	1	Input	Force	8202 31,6m	1615497	8202 31,6m	Hammer Charge	31,6m V/N	☐	1 V/V
1.1.2	3560D	7537-A	1	2	Input							■	
1.1.3	3560D	7537-A	1	3	Input							■	
1.1.4	3560D	7537-A	1	4	Input							■	
1.1.5	3560D	7537-A	1	5	Input							■	
1.1.1 Gen	3560D	7537-A	1	1	Generator							■	
1.3.1	3560D	3038-B	3	1	Input	Accelerometer	4507 Bx	30816x	Acc 01	DeltaTron Acc	10m V/ms⁻²	☐	1 V/V
1.3.2	3560D	3038-B	3	2	Input	Accelerometer	4507 Bx	31273x	Acc 02	DeltaTron Acc	10m V/ms⁻²	☐	1 V/V
1.3.3	3560D	3038-B	3	3	Input	Accelerometer	4507 Bx	31274x	Acc 03	DeltaTron Acc	10m V/ms⁻²	☐	1 V/V
1.3.4	3560D	3038-B	3	4	Input	Accelerometer	4507 Bx	31296x	Acc 04	DeltaTron Acc	10m V/ms⁻²	☐	1 V/V
1.3.5	3560D	3038-B	3	5	Input	Accelerometer	4507 Bx	31297x	Acc 05	DeltaTron Acc	10m V/ms⁻²	☐	1 V/V
1.3.6	3560D	3038-B	3	6	Input	Accelerometer	4507 Bx	31298x	Acc 06	DeltaTron Acc	10m V/ms⁻²	☐	1 V/V
1.3.7	3560D	3038-B	3	7	Input	Accelerometer	4507 Bx	31299x	Acc 07	DeltaTron Acc	10m V/ms⁻²	☐	1 V/V
1.3.8	3560D	3038-B	3	8	Input	Accelerometer	4507 Bx	31300x	Acc 08	DeltaTron Acc	10m V/ms⁻²	☐	1 V/V
1.3.9	3560D	3038-B	3	9	Input	Accelerometer	4507 Bx	31301x	Acc 09	DeltaTron Acc	10m V/ms⁻²	☐	1 V/V
1.3.10	3560D	3038-B	3	10	Input	Accelerometer	4507 Bx	31302x	Acc 10	DeltaTron Acc	10m V/ms⁻²	☐	1 V/V
1.3.11	3560D	3038-B	3	11	Input	Accelerometer	4507 Bx	31303x	Acc 11	DeltaTron Acc	10m V/ms⁻²	☐	1 V/V
1.3.12	3560D	3038-B	3	12	Input	Accelerometer	4507 Bx	31304x	Acc 12	DeltaTron Acc	10m V/ms⁻²	☐	1 V/V
1.4.1	3560D	3038-B	4	1	Input	Accelerometer	4507 Bx	31308x	Acc 16	DeltaTron Acc	10m V/ms⁻²	☐	1 V/V
1.4.2	3560D	3038-B	4	2	Input	Accelerometer	4507 Bx	31306x	Acc 14	DeltaTron Acc	10m V/ms⁻²	☐	1 V/V
1.4.3	3560D	3038-B	4	3	Input	Accelerometer	4507 Bx	31307x	Acc 15	DeltaTron Acc	10m V/ms⁻²	☐	1 V/V
1.4.4	3560D	3038-B	4	4	Input	Accelerometer	4507 Bx	31305x	Acc 13	DeltaTron Acc	10m V/ms⁻²	☐	1 V/V
1.4.5	3560D	3038-B	4	5	Input	Accelerometer	4507 Bx	31309x	Acc 17	DeltaTron Acc	10m V/ms⁻²	☐	1 V/V
1.4.6	3560D	3038-B	4	6	Input	Accelerometer	4507 Bx	31310x	Acc 18	DeltaTron Acc	10m V/ms⁻²	☐	1 V/V
1.4.7	3560D	3038-B	4	7	Input	Accelerometer	4507 Bx	31311x	Acc 19	DeltaTron Acc	10m V/ms⁻²	☐	1 V/V
1.4.8	3560D	3038-B	4	8	Input	Accelerometer	4507 Bx	31358x	Acc 20	DeltaTron Acc	10m V/ms⁻²	☐	1 V/V
1.4.9	3560D	3038-B	4	9	Input	Accelerometer	4507 Bx	31359x	Acc 21	DeltaTron Acc	10m V/ms⁻²	☐	1 V/V
1.4.10	3560D	3038-B	4	10	Input	Accelerometer	4507 Bx	31360x	Acc 22	DeltaTron Acc	10m V/ms⁻²	☐	1 V/V
1.4.11	3560D	3038-B	4	11	Input	Accelerometer	4507 Bx	31361x	Acc 23	DeltaTron Acc	10m V/ms⁻²	☐	1 V/V
1.4.12	3560D	3038-B	4	12	Input	Accelerometer	4507 Bx	31371x	Acc 24	DeltaTron Acc	10m V/ms⁻²	☐	1 V/V

Figure 4.8: Hardware setup window.

Step 2

The geometry of the structure has to be created in the Geometry Basis window, see Figure 4.9, by creating the structure with specified dimensions. The lines can be drawn on the structure and connected them at the nodes in order to create the desired mesh and measuring points. The created nodes are also used as degrees of freedom, later on.

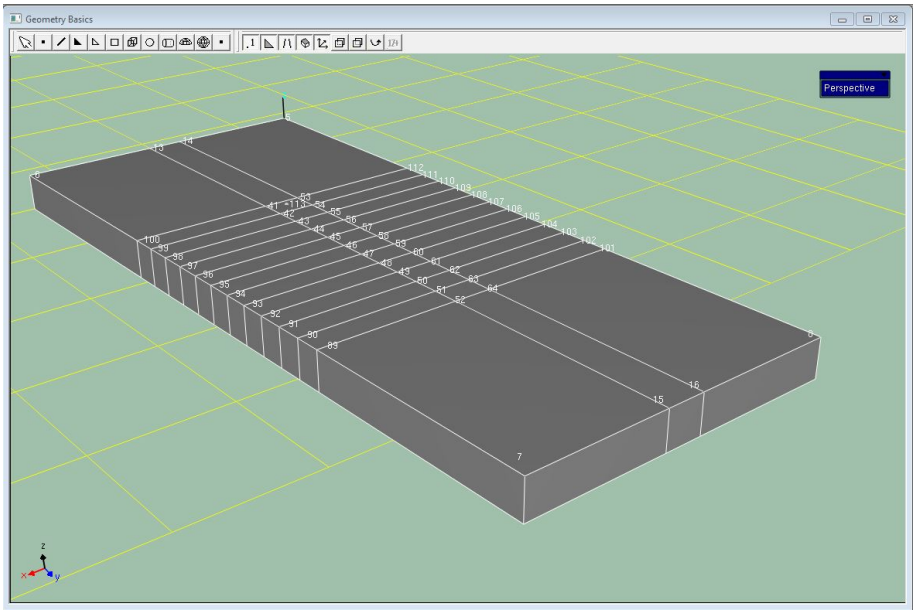

Figure 4.9: Geometry Basis window.

Step 3

The geometry being created, the transducers can be assigned to the nodes, in the exact position as in reality for accurate results. This is done in the Geometry Measurement Points window, see Figure 4.10. It is important to know that the accelerometers has to be assigned exactly at the nodes, in the other case the software will not assign the accelerometer to the model geometry, acting as a single point. The red arrows denote the accelerometers and the black hammer denotes the excitation point.

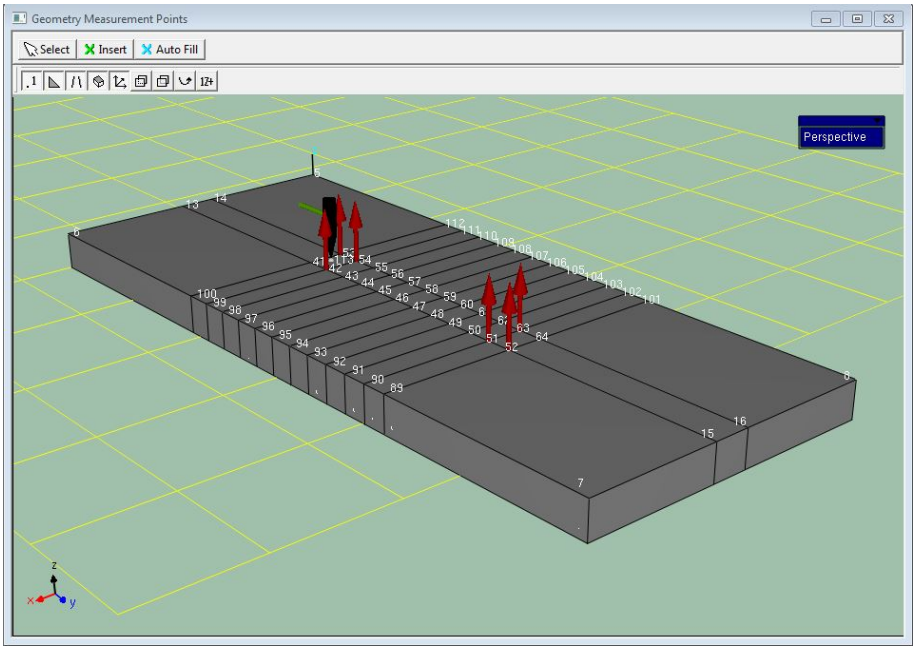

Figure 4.10: Geometry Measurement Points window.

Step 4

In the Analysis Setup window, see Figure 4.11, the analysis configuration is set. It is very important that the selected span to be choose wisely because all the frequencies in the span need to be excited during the tests in order to avoid failure due to too big spans. It is clear that the higher frequencies can be also excited, adding a harder tip for the hammer, but the double hit detector will be activated, leading to the failure of the tests. For this project a frequency span of 200 Hz is selected. In order to avoid the time delays due to long time of measurements a number of just 400 lines is selected, since a higher number does not have a big influence on the results, just increasing the recording time.

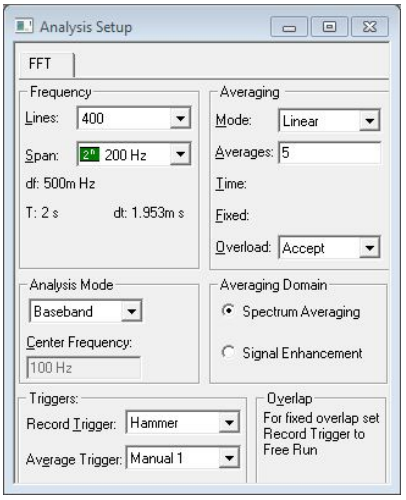

Figure 4.11: Analysis Setup window.

Step 5

Since the frequency span is just 200 Hz, the tip of the hammer does not need to be too stiff, the rubber tip being suitable for this project. In the Hammer Trigger window, see Figure 4.12, pressing the start button the recording begins and the system is excited multiple times. On the graph in Figure 4.12 the impact of the hammer could be clearly seen and the hysteresis lines are set to an appropriate amount in order to account also for weak hits.

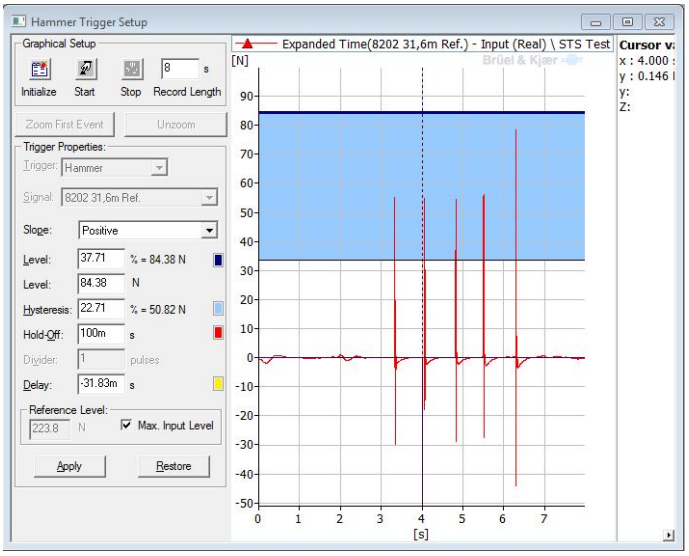

Figure 4.12: Hammer Trigger window.

Step 6

Having the hammer trigger set up the hammer weighting has to be configured, performing a single proper hit. The hit should excite all frequencies in the frequency span set in Step 4, but also it has to be not too weak or a double hit. In the Hammer Weighting Setup window, see Figure 4.13, the proper values are selected for leading, shift, length and trailing parameters. This is used for trimming the signal from both sides, leaving just one peak caused by an impulse load and also to remove the noise.

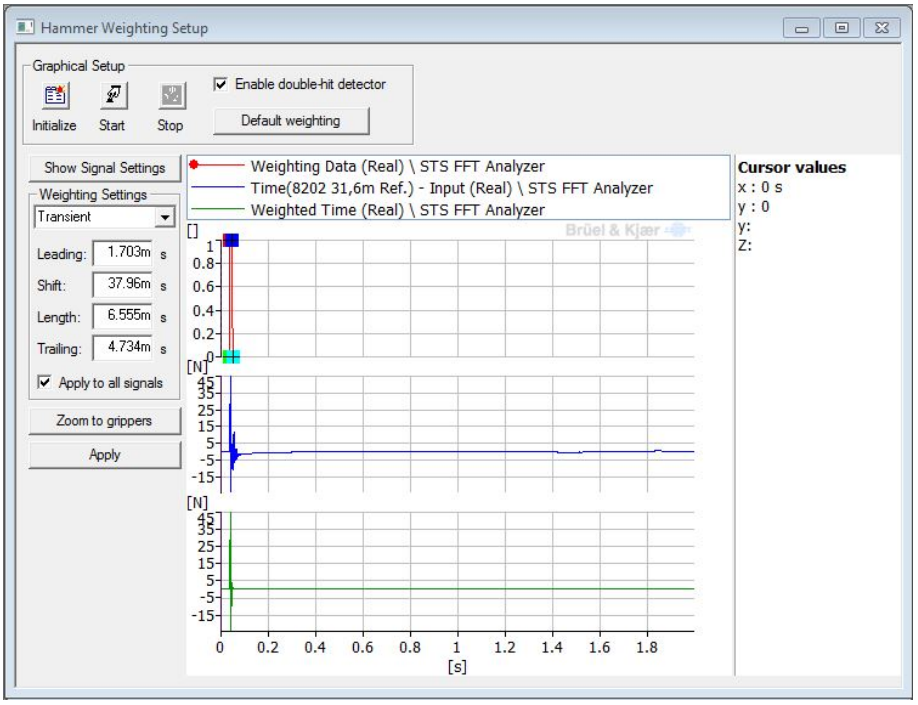

Figure 4.13: Hammer Weighting Setup window.

Step 7

The response weighting is done in the same manner as the hammer weighting described in Step 6. The structure is excited again by a single proper hit and the values for leading, shift and tau parameters are chosen in the Response Weighting Setup window, as it can be seen in Figure 4.14. Here, the values are selected depending on how much damping has to be introduced into the system, the noise has to be damped out of the system.

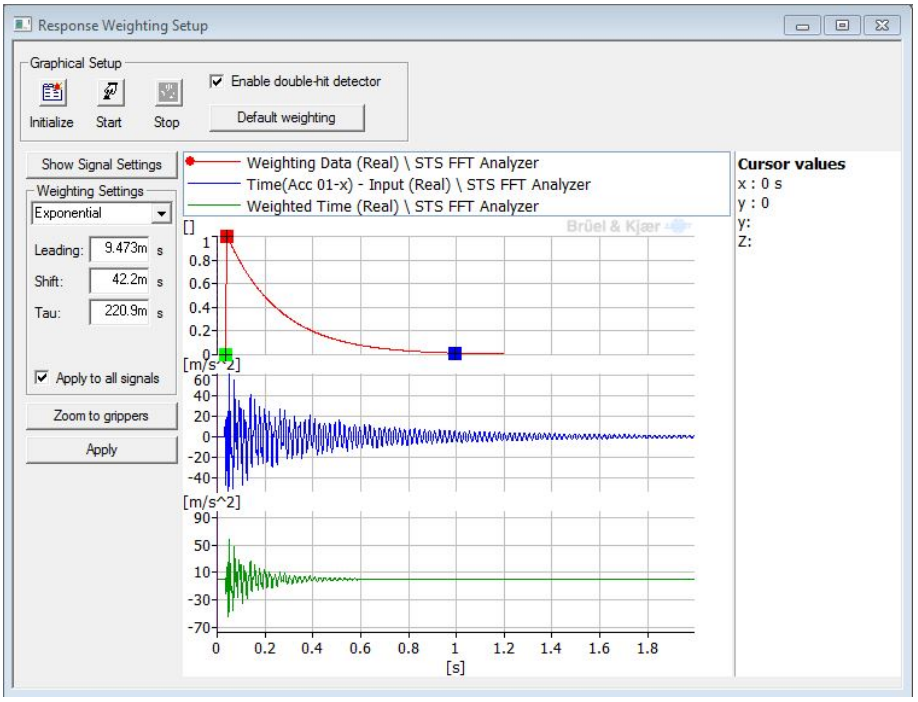

Figure 4.14: Response Weighting Setup window.

Step 8

The above steps being done, the measurements can be performed, in the Measurements tab, see Figure 4.15 by pressing the start button. The system has to be excited by proper hits, as many as they were set in Step 4. For this project a number of five recordings, consisting in five averaged hits, were selected and one excitation point was defined for each measurement.

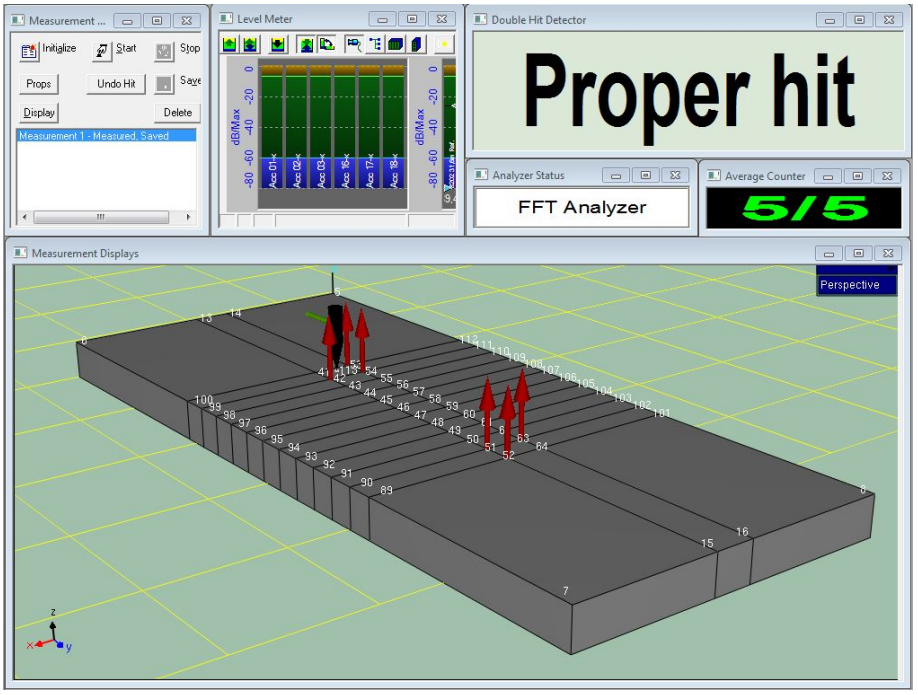

Figure 4.15: Measurements tab, Level Meter, Analyzer Status, Average Counter, Double Hit Detector and Measurement Displays.

Step 9

In the last step the response of the system is obtained by performing an FFT analysis and the FRFs are plotted for each accelerometer according to the reference point, see Figure 4.16. An animation is available for particular frequencies which can be used for inspecting the behavior of the structure. As it was said before, in Step 3, the nodes without accelerometers or the accelerometers assigned to single points will remain fixed, so the animation would not fully represent the actual motion of the model. Just the nodes with accelerometers and the ones excited by the hammer will move.

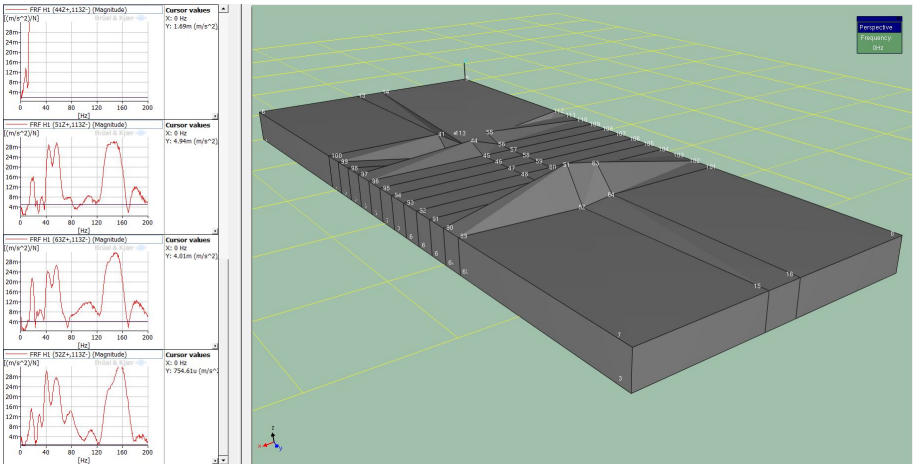

Figure 4.16: FRF validation window with frequency response functions (right) and deformed animated geometry (left).

4.2 Finite-element model

4.2.1 Physical description

The geometry of the model is introduced as in Chapter 3 with the material properties determined in Section 5.3 and 5.4. The studied medium, in this case the foam mattress is considered fully soaked and fixed on 5 sides which is modeled accordingly in Abaqus by locking all displacements and rotations for these surfaces. The loads are defined depending on the analysis procedure as presented in the following sections.

4.2.2 Element types

Abaqus offers a diverse element library which is organized by 5 main criteria: family, degrees of freedom, number of nodes, integration and formulation. All these aspects must be taken in consideration when choosing the appropriate element for an analysis. To begin with, the elements type is selected. Since the material is considered fully soaked with a fully undrained behavior the continuum elements are considered suitable for the analysis. Moreover the continuum elements are appropriate for all the parts involved in the analysis (wave transmission media, masses positioned on surface) so the models have only one element type.

The next step is choosing the integration order and the number of nodes which are directly related with the results accuracy. For the continuum elements there is the option of reduced integration denoted with a capital R and full integration. Taking in consideration that the accuracy is a priority for this project the full integration is chosen even though this option

will increase the computational time. Similar with the integration, the number of nodes used for the elements is another characteristic that dictates the accuracy of the models. There are two types of elements defined by this aspect, first order elements with nodes only at the corner of the element and second order elements with extra mid side nodes, see Figure 4.17.

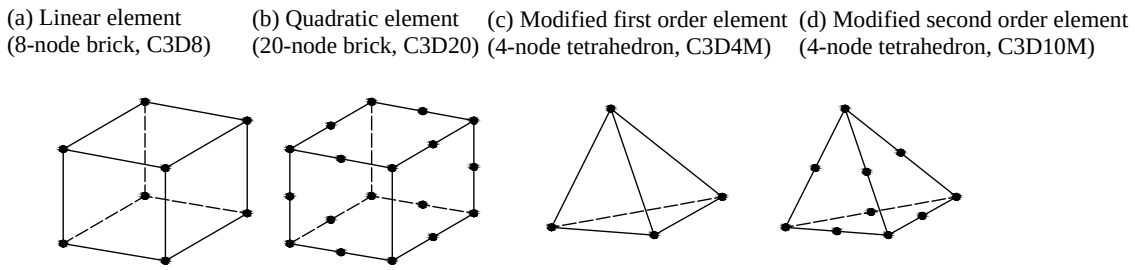

Figure 4.17: First order versus second order elements

The first order elements use the linear interpolation while the second order elements allows a quadratic interpolation which is better at modeling curved surfaces and bending dominated problems. Again with the accuracy in mind and since the expected response is wave shaped deformed material, good accuracy can only be obtained by choosing the second order elements for analysis. Another measure taken in order to have accurate results was to adopt a hybrid element formulation. The option is valid only in Abaqus/Standard element library and in addition to the nodal displacements, this type of element treats the mean stress as a degree of freedom and it therefore produces reliable results for Poisson ratios near 0.5, which is necessary in the present analyses.

The formulation regards the mathematical description of the element and typically the Lagrangian description in which the elements deforms with the material is used when analyzing solids. Having models that deals with solids or other materials that can be regarded as solids the formulation was kept Lagrangian as default.

4.2.3 Dynamic analysis procedures

There are several procedures available that can be used to perform a dynamic analysis when using Abaqus. Depending on their mathematical description they are are divided in direct integration methods and modal methods. The direct methods are mostly used when the the response is characterized of non linearity while the modal procedure are typically used for linear analyses. Even though the direct methods are more computational expensive they were considered more suitable for the present project in behalf of good accuracy.

4.2.4 Natural frequencies. Mode shapes

One of the most frequently used procedures in the project is the natural frequency extraction procedure, *'Frequency'*. This is a linear perturbation scheme that solves the eigen value problem and extracts the eigen-frequencies and the eigen-modes of a given model. The eigenvalue problem of a undamped system is defined as

$$(\mathbf{K} - \lambda \mathbf{M})\mathbf{\Phi} = \mathbf{0}. \tag{4.1}$$

Where $\lambda = \omega^2$ is the eigenvalue, $\omega = 2\pi f$ is the circular frequency and f is the natural frequency, $\mathbf{M}$ is the mass matrix, $\mathbf{K}$ is the stiffness matrix and $\mathbf{\Phi}$ is the eigenmode. For each eigenvalue λ_j a solution $\mathbf{\Phi}^{(j)}$ exists. Here $\mathbf{\Phi}^{(j)}$ contains the information of the jth mode shape.

There are 3 eigenvalue extraction methods to choose from: Lanczos, Automatic multi-level substructuring (AMS) and subspace iteration. The eigenvalue problem was studied intensively during the years resulting in a collection of different methods. [Wilkinson, 1965] and [Ramaswami, 1979] as referred by Abaqus Theory Guide provides an excellent compendium on the problem and the methods available. Another aspect that has to be considered is the software architecture which is used for the subsequent modal superposition procedures. It can be chosen either the traditional architecture or SIM. The eigenfrequency results are independent of the architecture type, the only difference is that SIM architecture is significantly more efficient for subsequent mode-based steady-state or transient dynamic procedures. Since in this project the direct methods are preferred over less accurate modal procedures the Lanczos method with the traditional architecture is used. Using Lanczos the eigenmodes are extracted either by requesting the number of modes or by introducing a frequency range of interest.

The results are used for a preliminary comparison with the response from the experiment as well as to determine the mode shapes and implicitly the nodes of vibration modes. With their position determined, a grid with possible locations for accelerometers is created in a way so they are positioned outside of these areas.

4.2.5 Steady state dynamics direct

The steady state dynamics analysis provides the response of a system in terms of amplitude and phase when subjected to a harmonic load at a certain frequency. The procedure is performed by loading the system at different frequencies as a frequency sweep and recording the response. Unlike the modal based methods, within the *'direct'* procedure the global equations of motion are solved in frequency domain and the results are calculated directly

in terms of physical degrees of freedom of the model. This increases the accuracy with the downside of more computational resources required. The procedure is also good in modeling any form of damping: structural damping, vicous damping, discrete damping such as mass, dashpot, spring or conecting elements. The formulation of the method is based on the following equation of motion

$$Re\Big(\Big(\big(-\omega^2\mathbf{M}+\mathrm{i}\omega\mathbf{C}+\mathbf{K}\big)\tilde{\mathbf{X}}-\tilde{\mathbf{F}}\Big)\exp\mathrm{i}\omega t\Big)=\mathbf{0}. \tag{4.2}$$

Where ω is circular frequency, $\mathbf{M}$ is the mass matrix, $\mathbf{C}$ is the damping matrix, $\mathbf{K}$ is the stiffness matrix, $\tilde{\mathbf{X}}$,$\tilde{\mathbf{F}}$ are complex amplitude vectors of the displacement and of the load respectively and t is the time.

This is only fulfilled when

$$\tilde{\mathbf{X}}=(-\omega^2\mathbf{M}+i\omega\mathbf{C}+\mathbf{K})^{-1}\tilde{\mathbf{F}}. \tag{4.3}$$

In Abaqus the procedure is introduced as *'Linear perturbation'-'Steady state dynamics direct'*. The frequency sweep is performed over the frequencies of interest which are introduced as an interval. Furthermore the number of calculation points have to be defined. By default, the points are equally spaced on a logarithmic scale but there is also the option of the linear scale as well as the possibility to bias the points towards meaningful areas.

4.3 Verification of Abaqus for wave propagation

Since the fundamental problem of this project represents the wave propagation through soil, the mathematical description of the waves in the numerical analysis has to be validated. Basically in this section is verified if Abaqus is able to reproduce the correct wave propagation. This is done by reducing the problem to one dimensional (1D) wave traveling only in one direction.

The validation is done by a simple 1D exercise done in MATLAB and Abaqus, the model being as simple as possible. Basically the model is reduced to a bar element which is excited at one end and the response is recorded at the other end. The only difference between the models, created in the two numerical software, is that for Abaqus the model is still a 3D solid model, with one dimension larger than the other two. Basically is a 3D model but it is a 1D wave propagation problem. In the FE MATLAB code a 1D model is created using a bar element. Both models have no boundary conditions, meaning that all surfaces are

free to move, and they are excited at one end. In Figure 4.18 and 4.19 the two models are presented.

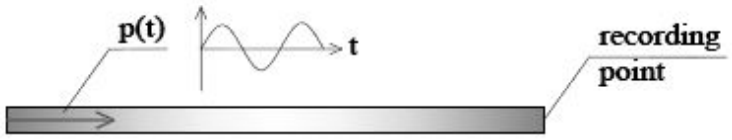

Figure 4.18: 1D model in MATLAB

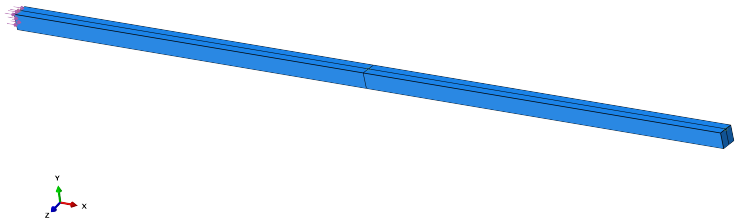

Figure 4.19: 1D model in Abaqus

In Figure 4.18 it is observed the bar element with the excitation and recording point, while in Figure 4.19 the 3D solid model with the same points it can be seen. The two models being exited at one end should provide the same wavelengths. The problem is analyzed by studying the phase velocity of longitudinal waves given by Equation 4.4.

$$c = \sqrt{\frac{E}{\rho}}. \tag{4.4}$$

The mesh or the dimension of elements is chosen in order not have numerical problems and to be able to fully simulate the wave propagation. Courant number has to be less than 1 or equal to 1. A good practice is to have a Courant number around 0.5 since linear elements are used. Courant number is defined as:

$$C = \frac{c\Delta t}{L_e} \rightarrow 0.5 \tag{4.5}$$

It can be seen that the Courant number depends on the phase velocity (c), time step (Δt) and element length (L_e). In other words with a $C = 0.5$ the wave travels a length equal to one half of the element size within a single time step.

The angular frequency and the wave number are given by Equation 4.6 and 4.7.

$$\omega = 2\pi f \tag{4.6}$$

$$k = \frac{\omega}{c} = \frac{2\pi f}{L} \tag{4.7}$$

So the wavelength is calculated by Equation 4.8.

$$L = \frac{2\pi f}{k} \tag{4.8}$$

The length of the models is chosen to be 5 m and by introducing all the material properties with unit values, the phase velocity and elements length must have an unit value as well. It is known that for good results and good approximation a number of 10 elements per wave length should be used. For an element of 5 m length, 50 elements are needed in total for the 1D model created in MATLAB. The analysis is done for a total time of 5 sec with a time step Δt of 0.05 sec, the time step being calculated from the Equation 4.9 and is given as:

$$C = \frac{c\Delta t}{L_e} \rightarrow \Delta t = 0.05 \tag{4.9}$$

A harmonic load is applied at one end of the model. The results are presented in Figure 4.20.

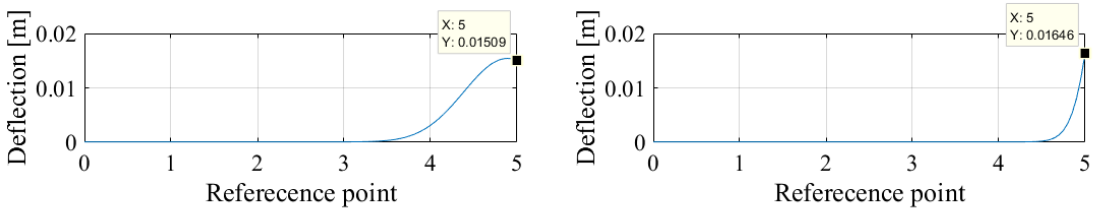

Figure 4.20: MATLAB (left) and Abaqus (right) results for 1D model at t=5 sec.

As it was expected, the Abaqus numerical modeled in Abaqus satisfies the mathematical description of the wave propagation. The difference between the results is of 0.001 37 m. Moreover after 5 s the MATLAB model does not provide the maximum value of displacement, this value being reached at 4.8 s. These differences in results are caused by the fact that the Abaqus is actually a 3D solid model and not a bar element as the MATLAB code. However the models created further with the help of Abaqus software should provide accurate results, depending on the model complexity and model dimensions. More details regarding the build up of the models are presented in Appendix B.

Chapter 5

Models compatibility using FRF analysis

This chapter covers the Frequency Response analysis for more models, starting with a model with less complicity, used for calibration, and then continuing with the analysis of the foam mattress.

Because of the uncertainties presented by the foam's properties, boundary conditions and for the equipment calibration a simpler problem has to be studied.

5.1 Simply supported model of a beam

The purpose of this test is to calibrate the available equipment and also to have a better overview about the results provided by the software. It consists in creating an experimental and numerical model, with the same setup and same problem formulation. The results will be further compared in between and it is expected for the results provided both from experimental and numerical models to match. Using a less complex model, the correlations between the results are more clear and reliable, since the uncertainties are reduced. Moreover the resources and the time used for these models is less than a complex one.

The experimental model consists of analyzing a Plexiglas beam with known properties and dimensions.

These are presented in Table 5.1.

Table 5.1: Plexiglas beam properties and dimensions.

Characteristics	h [cm]	w [cm]	l [cm]	V [cm^3]	m [g]	ρ [g/cm^3]	E [MPa]	ν [-]
-	0.95	2.51	86.55	206.37	243.28	1.17	2371	0.3

The static scheme of the studied beam is presented in Figure 5.1.

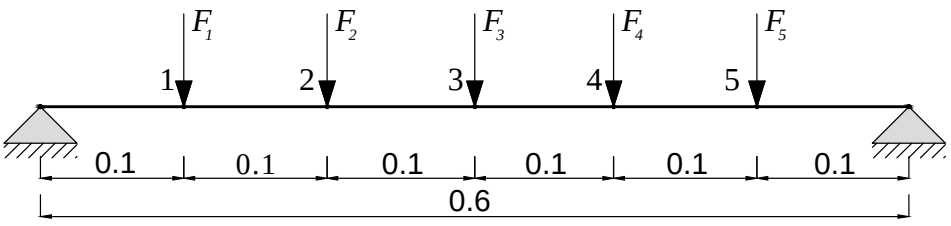

Figure 5.1: Static scheme for the simple beam.

The beam is loaded separately in each position from 1 to 5, $F1$ corresponding to measurement number 1, and during each measurement the response is recorded in all five positions. The response is gathered in the frequency response matrix, which has to be the same with the matrix provided by the numerical model.

The beam is designed as simply supported and this is reproduced by placing it on two cylinders, which are glued to a metal plate, see Figure 5.2. This setup allows rotation in one direction and restrains the displacement in vertical and horizontal directions.

The purpose of this test is to determine the frequency response of the beam. The test is conducted by exciting the beam in five different positions with the hammer and recording the response in each five positions, see Figure 5.2.

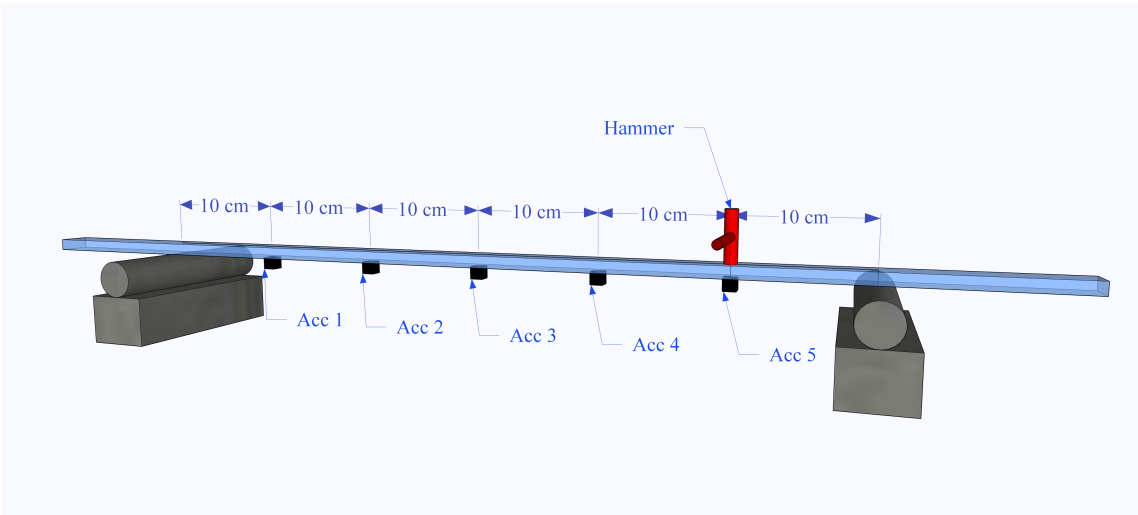

Figure 5.2: Model setup.

Having this set up the responses from each position can be structured in a frequency response matrix, see Equation 5.1

$$\mathbf{H} = \begin{bmatrix} H_{11} & H_{12} & H_{13} & H_{14} & H_{15} \\ H_{21} & H_{22} & H_{23} & H_{24} & H_{25} \\ H_{31} & H_{32} & H_{33} & H_{34} & H_{35} \\ H_{41} & H_{42} & H_{43} & H_{44} & H_{45} \\ H_{51} & H_{52} & H_{53} & H_{54} & H_{55} \end{bmatrix} \tag{5.1}$$

The matrix is assembled with the frequency response functions provided by the software. The functions are denoted as H_{ij} where i represents the recording point for the excitation in node j. By plotting a line of the matrix an overview of the response as it is illustrated in Figure 5.3 making possible a better interpretation as. The rest of the response is attached to the Appendix C.

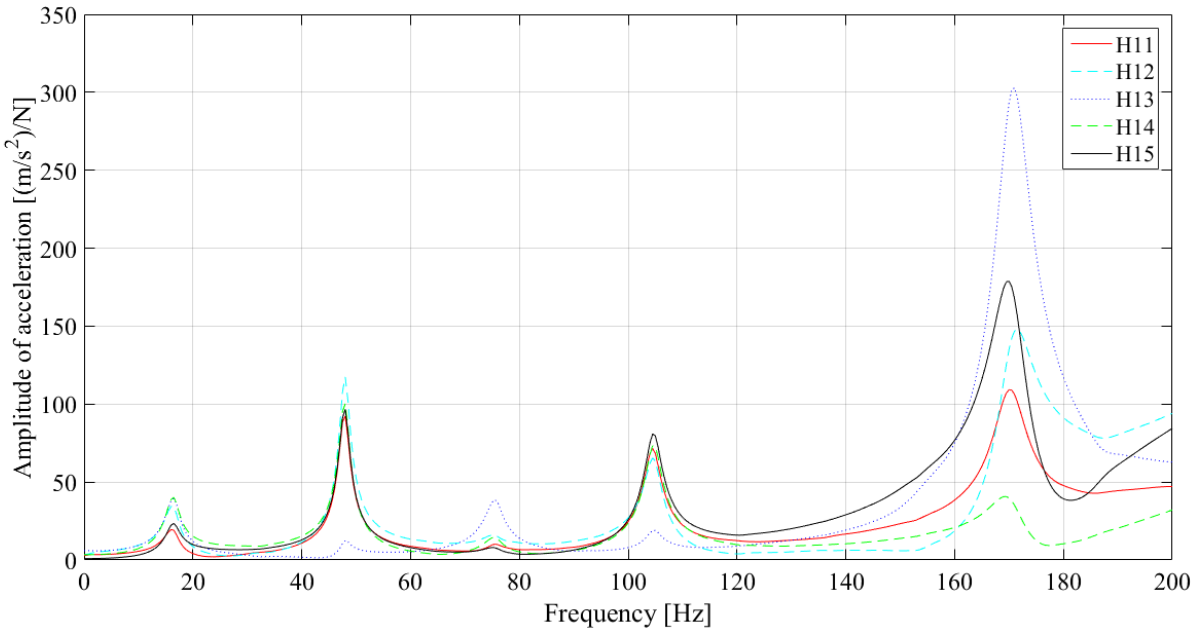

Figure 5.3: Frequency response of the beam given by 1st accelerometer — experimental analysis.

It can be observed that 5 eigenmodes were excited by hitting the beam in one point, over a frequency of 200 Hz.

The modes can be also identified in the deformed shape of the beam in the LabShop software, during the recordings. It can be observed in Figure 5.4 that the same behavior is provided by the software, for all modes.

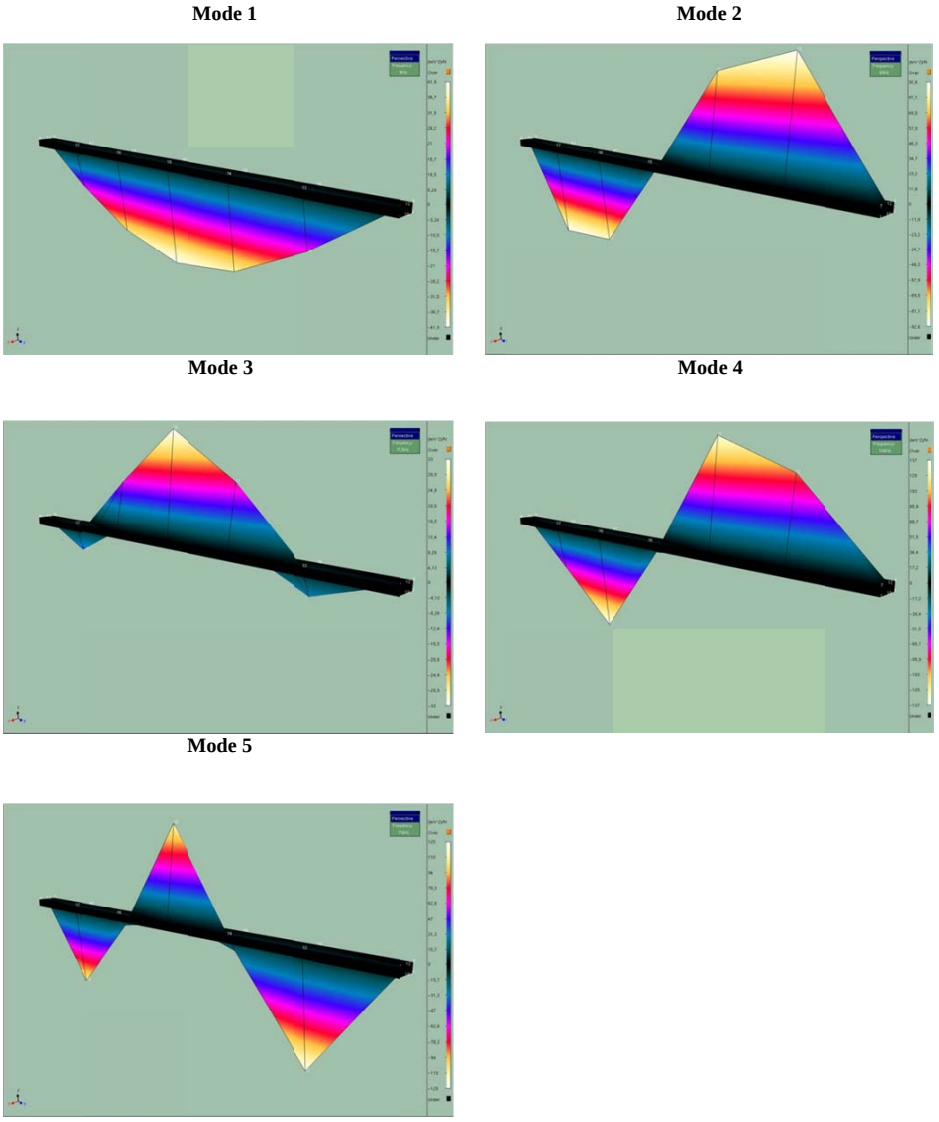

Figure 5.4: Deformed shape of the beam corresponding to each mode provided by LabShop software.

5.2 Numerical analysis of the simple beam

In the finite element program Abaqus CAE the exact model as in the experimental tests is reproduced. For reliable results and a fair comparison the exact same setup and properties has to be used.

In order to do that the same geometry was created, see Figure 5.5.

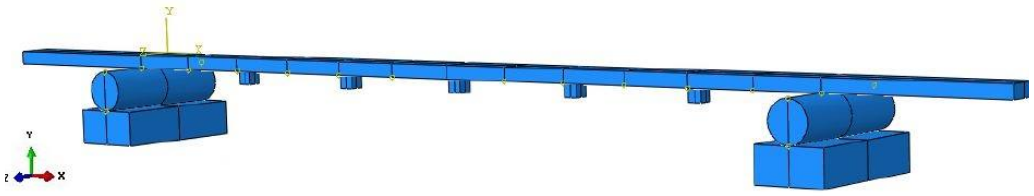

Figure 5.5: Model setup in the numerical program Abaqus.

The beam was connected to the cylinders with the tie constraint option by employing the master-slave surface definition in Abaqus. While the cylinder is fully coupled and being the slave, the beam is connected along a line to the cylinder, the beam being the master surface. The same connection exists between the cylinder and the metal plates, in this case the master surface is provided by the cylinder and the slave surface is provided by the line on the metal plates.

The beam's vertical and horizontal displacements (x-axis, y-axis and z-axis) and two rotations (x-axis and y-axis) were suppressed and the metal plates were encastrated at the bottom face. The accelerometers have been modeled as well because they influence the vibration propagation through the beam by adding extra mass to the system. They are connected to the beam with tie constraint option, having the beam's surface as a master and the accelerometer's surface as a slave.

In the numerical model the damping has to be introduced and it is the only unknown. Having a non-linear dynamic analysis the Rayleigh damping is used which is very suitable for an incremental approach to numerical solution. The damping matrix is proportional to the stiffness and the mass matrices and its formulation is given by Equation 5.2.

$$\mathbf{C} = \alpha \cdot \mathbf{M} + \beta \cdot \mathbf{K}. \tag{5.2}$$

Where α is the mass-proportional damping coefficient and β is the stiffness-proportional damping coefficient. The damping ratio at the circular frequency ω_n becomes:

$$\zeta_n = \frac{1}{2 \cdot \omega_n} \cdot \alpha + \frac{\omega_n}{2} \cdot \beta. \tag{5.3}$$

If two damping ratios are known, as ζ_i and ζ_j for two different modes, then α and β can be evaluated with Equation 5.4. In this case the damping ratios for mode 1 and 5 are used.

$$\begin{bmatrix} \zeta_1 \\ \zeta_5 \end{bmatrix} = \frac{1}{2} \cdot \begin{bmatrix} \frac{1}{\omega_1} & \omega_1 \\ \frac{1}{\omega_5} & \omega_5 \end{bmatrix} \cdot \begin{bmatrix} \alpha \\ \beta \end{bmatrix} . \tag{5.4}$$

In order to be able to evaluate α and β the damping ratio, ζ_1 and ζ_5 are found out performing a time series analysis in the experimental part. The beam has been left to vibrate freely after a forced displacement was introduced in the middle span of the beam. The data from one of the accelerometers, positioned in the middle of the beam, corresponding to the $1st$ mode, is presented in Figure 5.6 from which can be extracted the number of waves and to determine the amplitude at desired points.

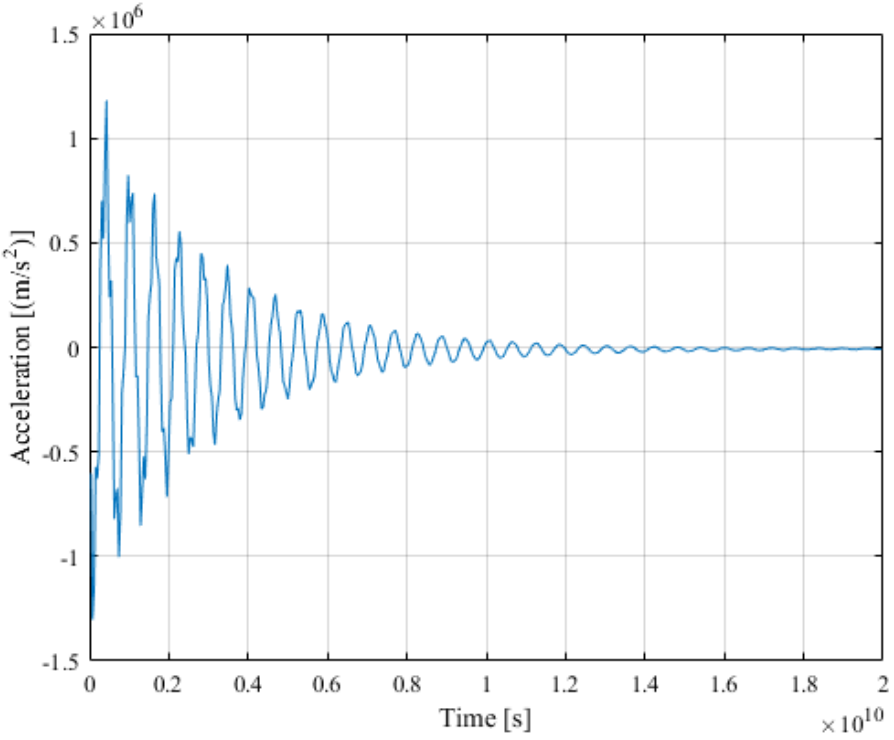

Figure 5.6: Time series for accelerations given by acc. 8.

Finding the starting amplitude A_0=149 300 m/s^2 and the amplitude for the nth wave A_n=74 440 m/s^2, where $n = 20$ the logarithmic decrement can be calculated as it follows:

$$\delta_i = \frac{1}{n} \cdot \log \frac{A_0}{A_n}. \tag{5.5}$$

Having δ_1 we can plug it in Equation 5.6 for calculating the damping ratio.

$$\zeta_1 = \frac{\frac{\delta_1}{2\phi}}{\sqrt{1 + (\frac{\delta_1}{2\phi})^2}}. \tag{5.6}$$

The same approach is done for ζ_5, which corresponds to the 5th mode.

ω_1 and ω_5 are known because the frequencies for the 1st and 5th modes are discovered with the analysis made in Section 5.1. The results for damping coefficients are presented in Table 5.2.

Table 5.2: Damping coefficients.

δ_1	ζ_1	ω_1	δ_5	ζ_5	ω_5	α	β
0.0348	0.0546	100.531	0.2207	0.3276	1068.81	9.272	$8.6347e^{-5}$

Having also the damping the model can be analyzed. Using a linear perturbation procedure and performing a frequency sweep over the same frequency range as in the experiment resulted the frequency response matrix of the system.

The results provided by first accelerometer are presented in Figure 5.7.

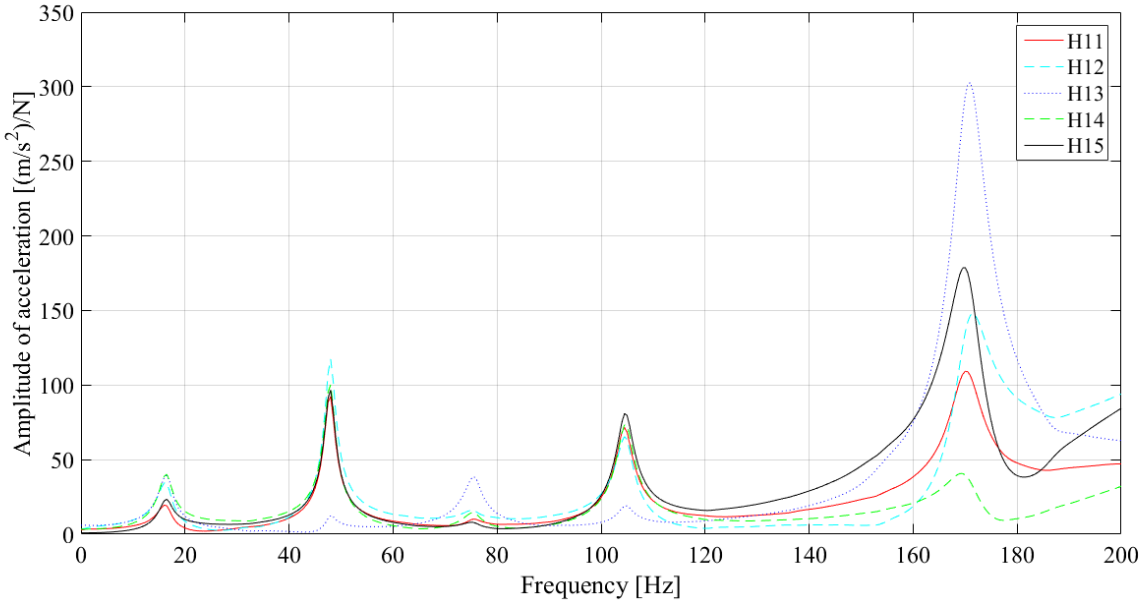

Figure 5.7: Frequency response of the beam given by 1st accelerometer — numerical analysis.

It is observed that the same number of peaks, approximately at the same position, results in both models with a small difference in the amplitudes. This could be caused by the material properties approximations, introduced in the numerical model. With these results, matching also the experimental ones it can be said that the equipment is well calibrated and a better understanding about the correlations between experimental and numerical models has been achieved.

In addition to Figure 5.7 and also to Figure 5.3 the deformed shapes of the beam in connection with each mode are presented in Figure 5.8, 5.9, 5.10, 5.11 and 5.12.

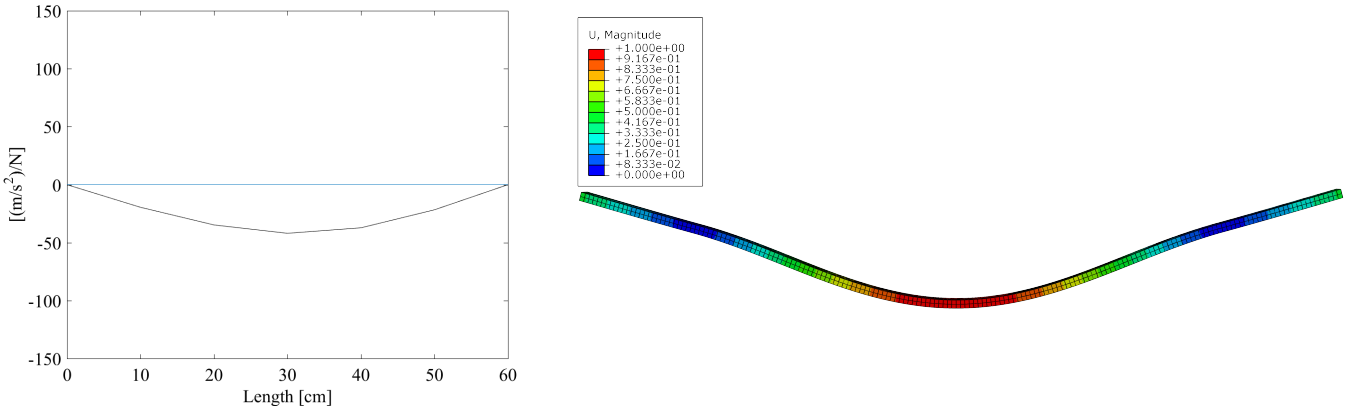

Figure 5.8: Deformed shapes of the beam for mode 1 provided by experimental (left) and numerical (right) analysis

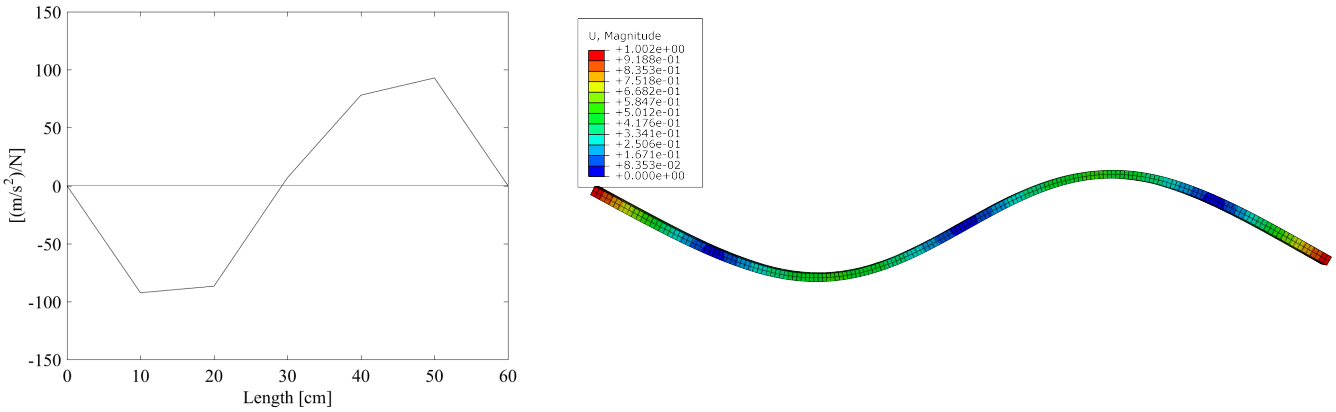

Figure 5.9: Deformed shapes of the beam for mode 2 provided by experimental (left) and numerical (right) analysis

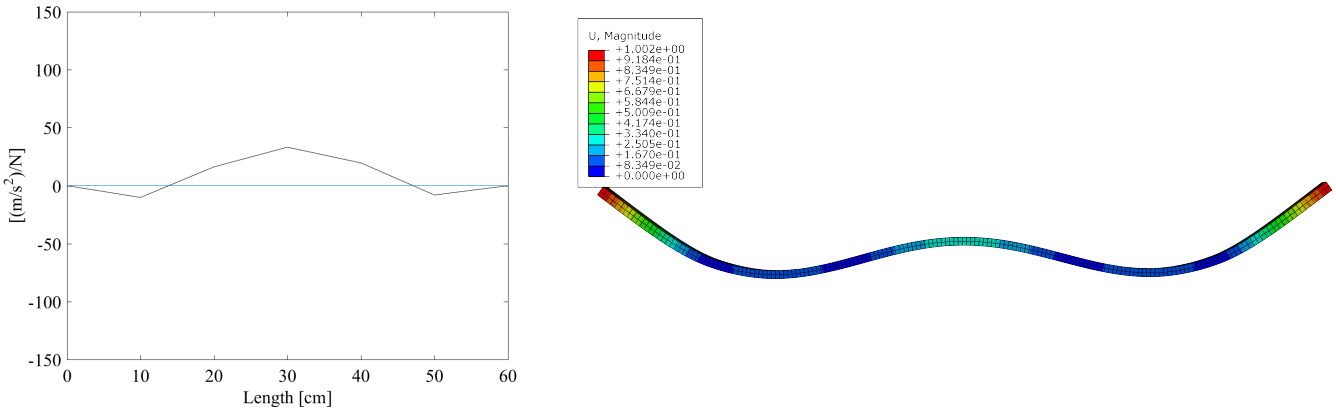

Figure 5.10: Deformed shapes of the beam for mode 3 provided by experimental (left) and numerical (right) analysis

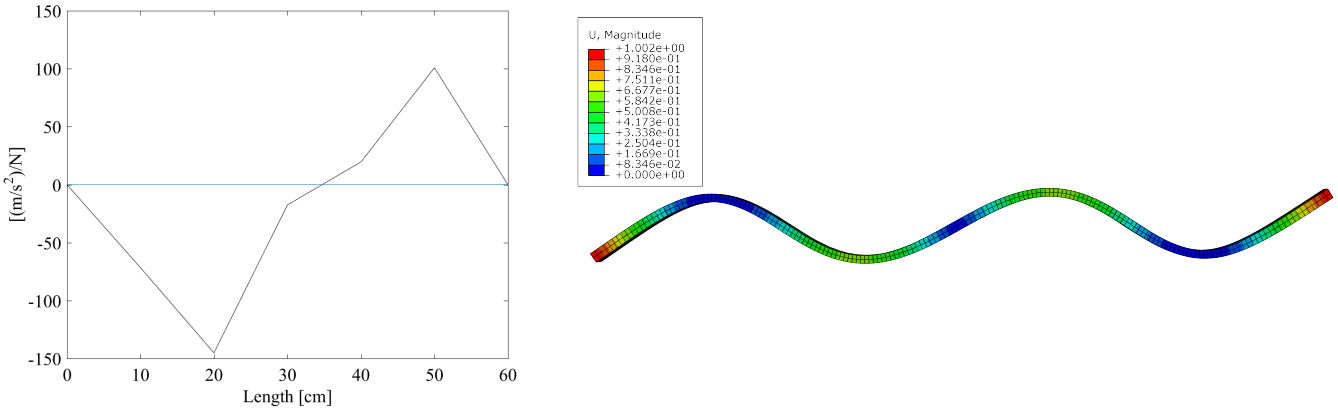

Figure 5.11: Deformed shapes of the beam for mode 4 provided by experimental (left) and numerical (right) analysis

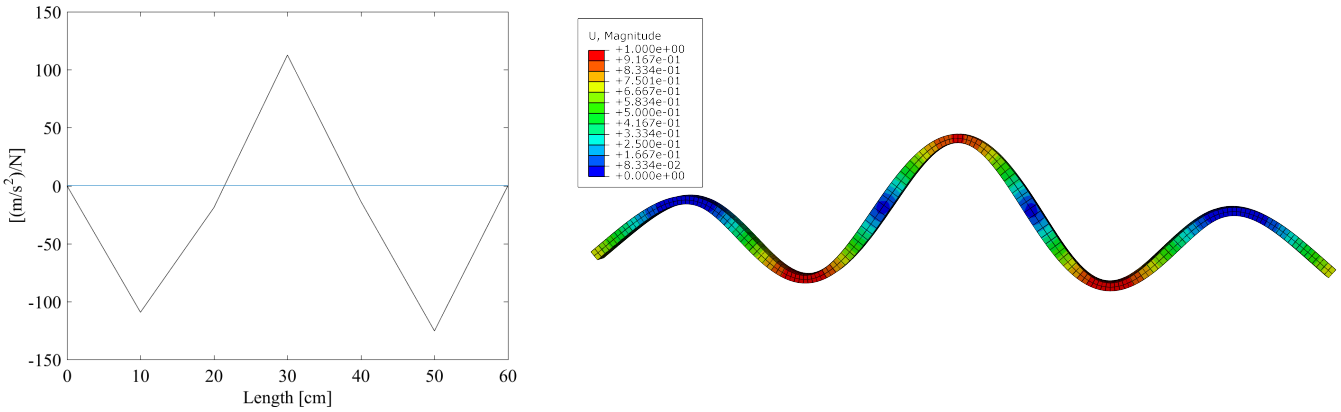

Figure 5.12: Deformed shapes of the beam for mode 5 provided by experimental (left) and numerical (right) analysis

At a first glance, in the experimental case, it can be observed that mode 2 and 4 and mode 3 and 5 have the same shape but different amplitudes, being caused by the fact that for the experimental analysis the data is recorded only in five points, enough data not being available in this case. This is why modes 2 and 4 and modes 3 and five have the same shape for the laboratory tests, having only the amplitudes different. The results match the modes provided by the LabShop software, see Figure 5.4. In the deformed shapes provided by the numerical analysis the modes are clear to be observed. It is easy to differentiate modes 2 from 4 and modes 3 from 5. Another important factor is given by the ends of the beam, because in the experimental results these are not available.

For a better comparison and a clear view over the results from the experimental and numerical models, the frequency response functions for both models are illustrated in Figure 5.13, recordings taken from the first accelerometer when the hit was applied in node 5.

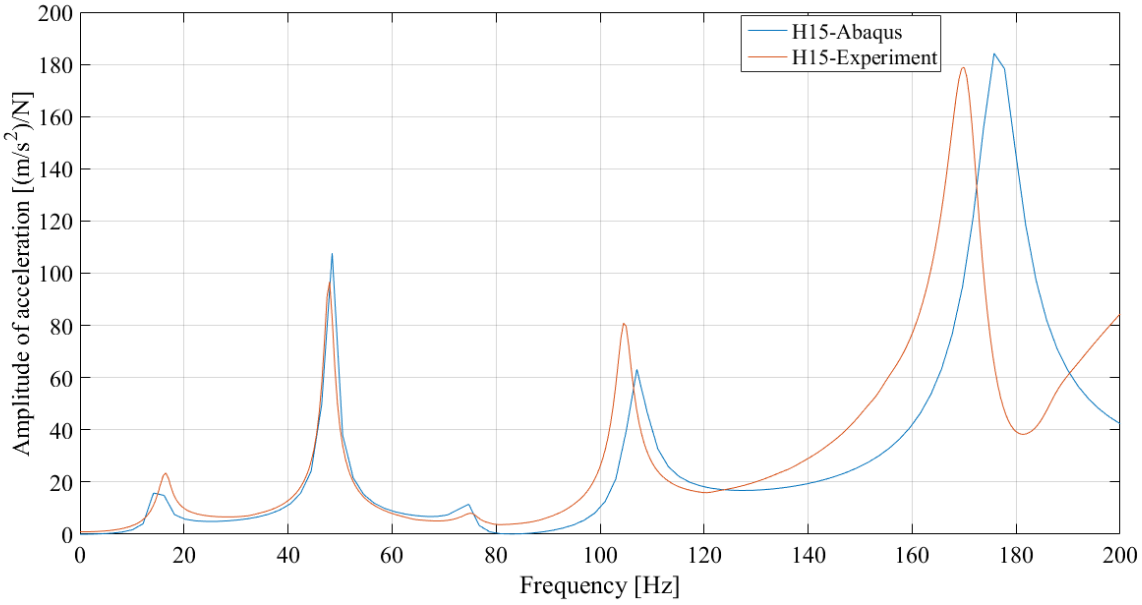

Figure 5.13: Frequency response results from both experimental and numerical models.

The results provided by the numerical analysis and experimental one matches almost perfectly, only the last peak from the experiment is reached at a lower frequency than the one given by Abaqus, meaning that the Abaqus model is slightly too stiff at higher frequencies than the experimental one. This error could be introduced by the fact that in reality the connection between the beam and the cylinder is not among a simple line. In laboratory the connection has been made on a small surface, on which the beam is glued to the cylinder, having bigger influence more for the higher frequencies. Another reason which could introduce this error is given by the suppressed horizontal displacement in the supports, because for higher modes, where is more rotation for the cross-section for higher modes than for the lower modes, the rotation is somehow prevented, creating stiffer model. Since the error is very small and the real connection is almost impossible to be reproduced in the numerical model, the results can be considered to be very precise and enough accurate.

5.3 Dry foam

5.3.1 Material properties

In order for a fair comparison to be made between the experimental and numerical results the material properties have to be determined. The material chosen to conduct the tests was a soft foam. Assuming linear viscoelastic material behavior the required properties are the density (ρ), Young's modulus (E), Shear modulus (G), and Poisson's ratio (ν).

Density determination

Firstly the density was determined. The dimensions of the foam mattress are 12 cm x 101.5 cm x 245 cm and the weight of the mattress is 11.35 kg. The density of the foam is given by Equation 5.7.

$$\rho = \frac{m}{V} \tag{5.7}$$

Shear modulus determination

The shear modulus is a mechanical property of the material that defines the ratio between the shear stress and the shear strain. Water cannot bear shear stress thus the shear modulus remains constant when transitioning from the dry to the soaked foam. Information regarding the shear modulus will later become important, because it will be used to determine Young's modulus for the soaked mattress. The shear modulus is determined using Equation 5.8.

$$G = \frac{E}{2(1-\nu)} \tag{5.8}$$

Poisson's ratio determination

Usually stretching a material in one direction produces a shrinkage in the other directions, rarely for some engineering designed materials expanding or contracting in both directions is observed, case in which the ratio takes values from -1 to 0.5 The Poisson's ratio theoretically takes values from 0 to 0.5 for natural, non-engineered materials. The determination of the Poisson's ratio for the foam was performed by following a similar procedure as in Subsection 5.3.1, correlating experimental and computational results. Two target points were followed in the two experimental tests. The same two points were studied in the Abaqus CAE model. See Figure 5.14.

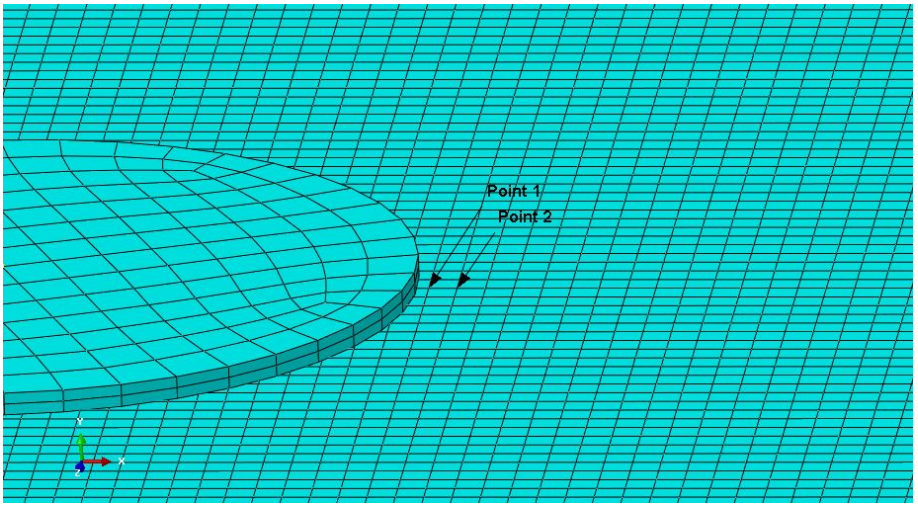

Figure 5.14: Observed points on the Abaqus CAE model-undeformed shape.

When the foam is loaded vertically, the material volume which presents deformations, is bigger than the actual surface under the plate. Using a visual inspection it was discovered that the influenced area was spread approximately 2 cm away from the plate edge. The points from this area presented a small vertical deformation, combined with a horizontal drag in the plate direction. This was observed in the numerical model as well, see Figure 5.15.

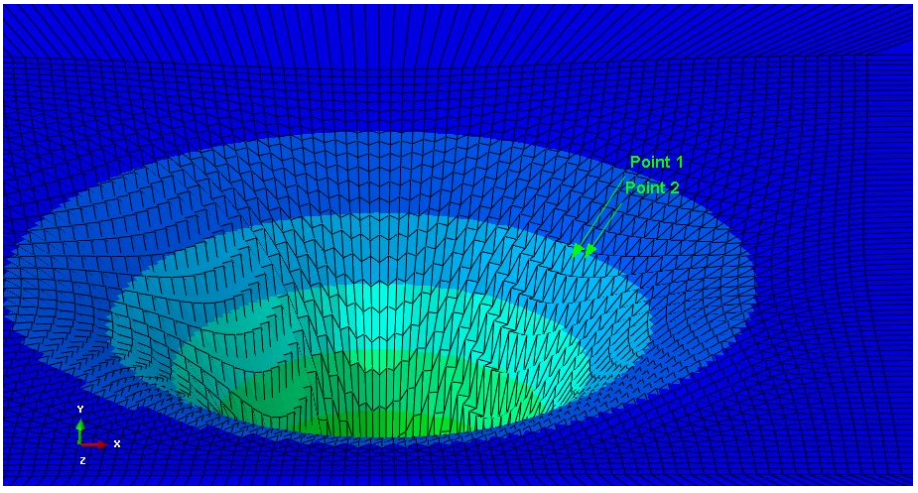

Figure 5.15: Observed points on the ABAQUS CAE model — deformed shape.

The displacement for each point recorded experimentally was matched with the value obtained in the numerical analysis, see Figure 5.16

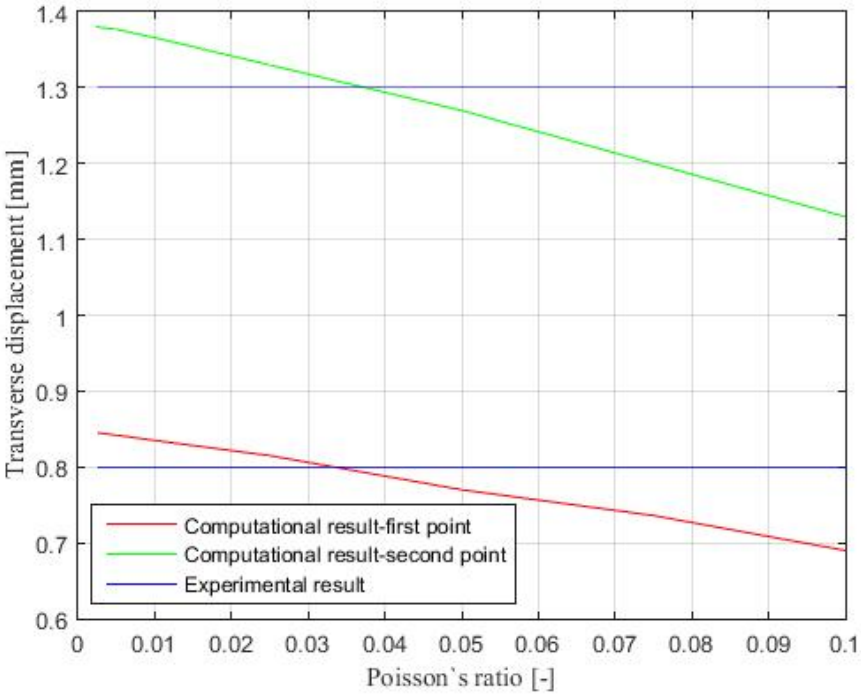

Figure 5.16: Determination of Poisson's ratio for Point 1 and 2

It was found that a good match for the horizontal displacements of the above illustrated points occurs when Poisson's ratio is set to be 0.035

Young's modulus determination

Young's modulus is related to the intrinsic mechanical properties of the material. Because of the nonlinear behavior of the foam and the lack of a sample of material the elastic properties are determined by conducting both a numerical and an experimental test. The results from both tests were used to determine the final value. Two experimental tests are made in the laboratory on the foam; the tests consisted in applying a compression force on a circular metal plate and measuring the displacement. Values for both tests are presented in Table 5.3

Table 5.3: Force and displacement values for the two tests.

Test 1 ϕ=7.3 cm		Test 2 ϕ=12.3 cm	
Force [kN]	Displacement [cm]	Force [kN]	Displacement [cm]
28.95	0.95	64.22	0.75

Further on a numerical model is created using Abaqus CAE software. The deformed shape

of one test can be seen in the Figure 5.17

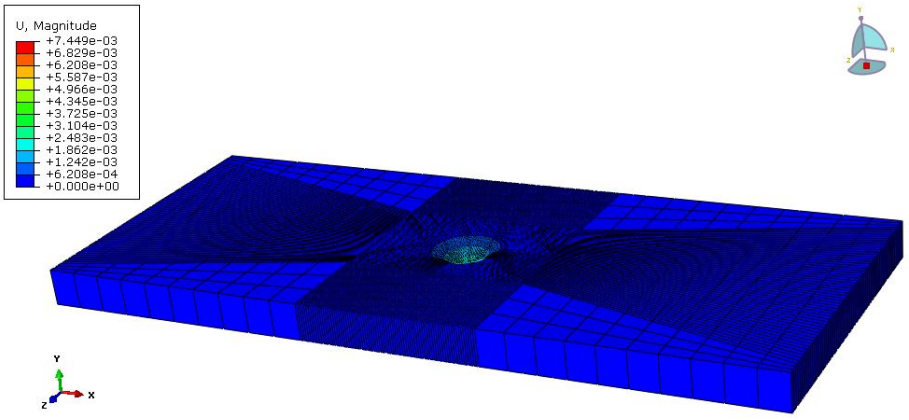

Figure 5.17: Deformed shape for the numerical model.

Unit values are inputted in the numerical model for the elastic modulus and load with the deformation being the desired output. Further on a relation between the load applied, material stiffness and deformation is formulated. Having a unit values for the elastic modulus and force, a relation is formulated between the experiment and FEM model. Equation 5.9 yields the value of Young's modulus of the foam.

$$E_e = \frac{u_c}{u_e} \cdot \frac{P_e}{P_c} \tag{5.9}$$

In Equation 5.9, the displacements are denoted with u and the forces with P while the index c and e stands for computational and experimental respectively. The equation above is valid only for unit values in the computational model.

Table 5.4 shows the calculated values for the density, Young's modulus, Shear modulus and Poisson's ratio.

Table 5.4: Plexiglas beam properties and dimensions.

ρ	E	G	ν
$[kg/m^3]$	[Pa]	[Pa]	[-]
37.43	2.51	86.55	206.37

5.3.2 Convergence study

In the following part a convergence study of the FEM model is made in order to observe, when increasing the number of elements in the model, has no longer an improving effect

on the result. The convergence is made for the 3D Hex elements with a quadratic hybrid formulation and full integration.

The study is performed using two approaches. The first approach involved running the same test on the FE model with the number of elements being the only variable. The mesh was gradually refined and values for the acceleration level corresponding to the first eigenmode documented. This study is presented in Figure 5.18

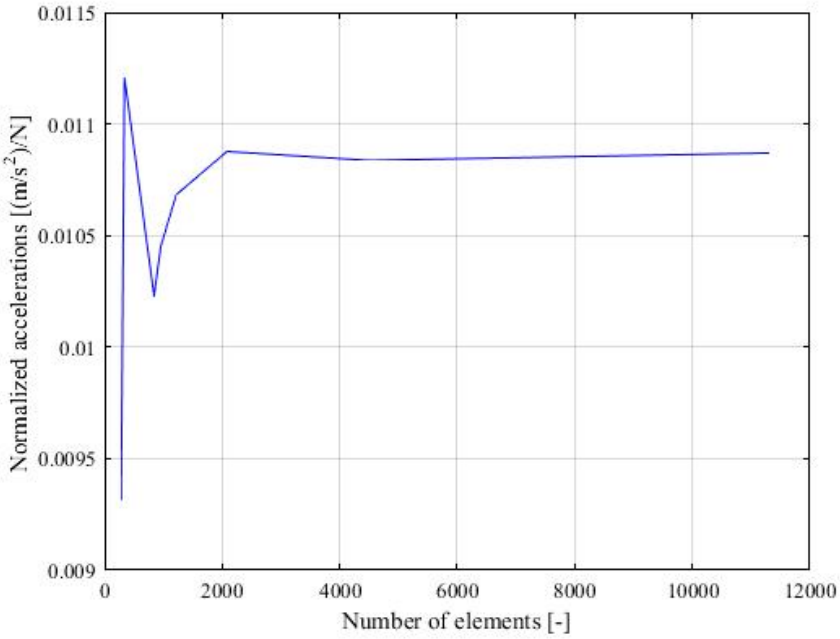

Figure 5.18: Convergence study of the acceleration values.

From Figure 5.18 it can be observed that the acceleration for the first eigenmode is converging at 2000 elements. From there on more refining of the mesh does not produce higher or lower amplitudes and would only make the FE model analysis less time effective.

The second approach involved studying the first ten eigenmodes and their corresponding frequency. Using a linear perturbation frequency analysis and the Lanczos eigensolver, the first ten modes of the system were found. For this approach observations were made regarding the eigenfrequency values for where the eigenmodes were found, the variable being again the number of elements of the model. The study is presented in Figure 5.19

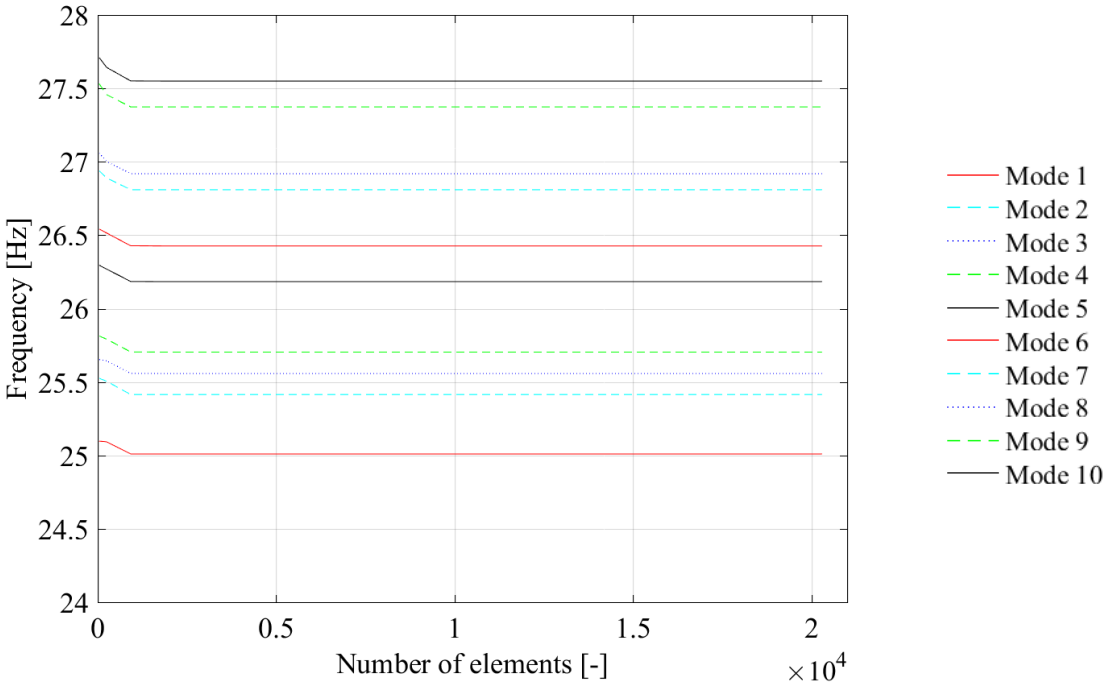

Figure 5.19: Convergence study of the first ten eigenmodes.

From Figure 5.19 it can be seen that all the modes are converging around 1000 elements. But given the observations found for the first approach and wanting to ensure a minimum of four elements per wavelength up to 100 Hz a mesh size of 49.8 mm is chosen which ensures over 2000 elements for the model.

5.3.3 Numerical vs. Experimental

An experimental and a numerical analysis were made on the dry foam on a the proposed setup. The purpose was to obtain frequency response functions of the system on a range of frequencies for both cases; and later compare them in between. In this way an observation could be made regarding the correlation accuracy between the FE model and the experimental study.

In process of setting up the proposed setup aspects as the material properties, boundary conditions, positions to apply the load and record the response had to be thoroughly considered in order for valid results and a good calibration between models.

The mattress was placed in an open on one side wooden box in order to replicate a free surface boundary condition on one side and suppressed degrees of freedom on the remaining five sides. Further on a frequency analysis of the system was made in the numerical model in order to identify the first ten natural modes of vibration of the system. Doing this and analyzing the mode shapes, the inflexion nodes were observed. With this in mind the grid

of accelerometers and the excitation points was created.

Figure 5.20 presents the proposed setup with the three places chosen for the excitation points.

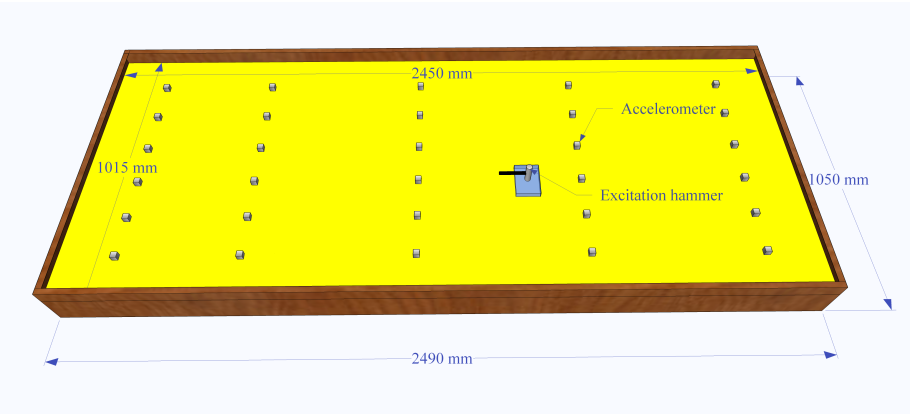

Figure 5.20: Proposed set up for testing the dry foam.

The excitation hammer was used to apply the load in various points, one position being represented in Figure 5.20. The accelerometers were used to record the normalized accelerations. The range of frequency chosen to study was 0 −200 Hz. The same operation was made the numerical model. Figure 5.21 presents the FRF of the system obtained in both models.

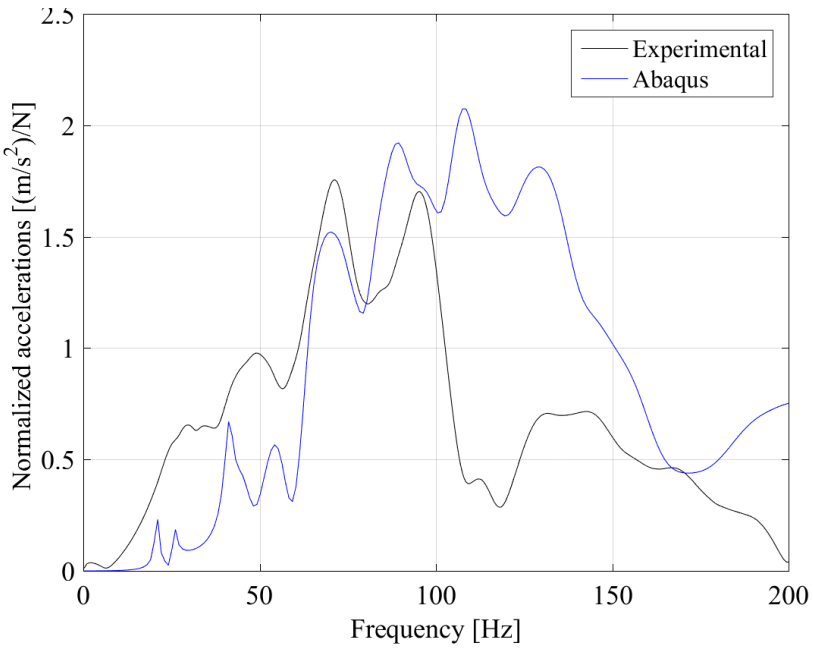

Figure 5.21: Experimental vs. Abaqus FRF for the dry foam.

As it can be observed the response of the numerical model is poorly correlated with the one obtained from the experimental study so a fair comparison is yet to be made. One of the factors that might lead to this poor correlation could be that the fixed boundary conditions replicated in the experiment are not set up well enough. To improve the BC the mattress was glued to the bottom of the box and wooden slabs were inserted on the sides of the box. Doing this tighter fixed BC were created and the same analysis described above was repeated. Figure 5.22 presents the FRF of the models.

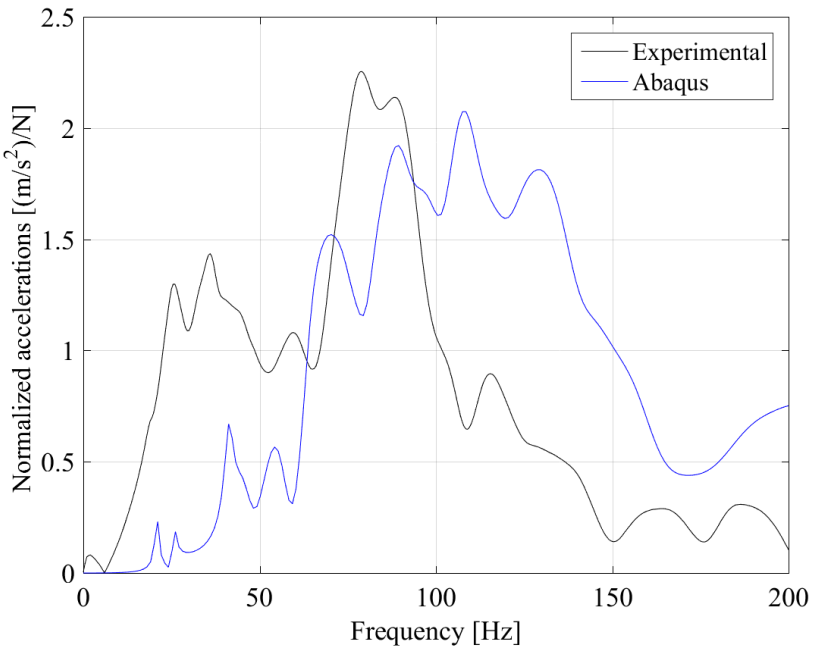

Figure 5.22: Experimental vs. Abaqus FRF for the dry foam with improved BC.

In spite of improving the boundary conditions a good correlation could not be made for the dry foam. Beside this the response presents a lot of fluctuations so also identifying the eigenfrequencies would be problematic. In addition, the response varied significantly between consecutive tests providing unstable results with a high degree of uncertainty. Instead of continuing to improve and run different analysis on the dry foam, it was chosen to saturate the foam with water. Increasing the inertia and the mass of the system is expected to lower the eigenfrequencies and provide a more stable response. The next subsection will present analysis employed on the saturated foam.

5.4 Wet foam

5.4.1 Material properties

Transitioning from the dry to the saturated foam changes the material properties. As described in Section 5.3 before conducting the experimental and the numerical analysis it is of great importance to find the correct material properties in order to correlate the FE model with the experiment.

The dry foam was fully saturated with water and first the new density was determined. The amount of water needed in order to soak the mattress was recorded and using Equation 5.7 the saturated density was determined to be around 980 kg/m^3. Because water is a nearly incompressible material, it is expected that the value for the undrained Poisson's ratio of the soaked mattress to be close to the upper limit of 0.5 Since water cannot bear shear stresses, the shear modulus G remains constant when transitioning from the dry to the soaked foam. With the shear modulus being determined in Subsection 5.3.1 next Young's modulus for the saturated foam is determined using Equation 5.10 and has a value around 45 kPa.

$$E = 2G(1 + \nu) \tag{5.10}$$

A further tuning of the material properties has been done by attempting to match the first few resonance frequencies and the associated modes, as well as the phase velocities of waves that can be detected on the surface of the foam. Initially, by using the previously determined value of Young's modulus 45 kPa, it was observed that the positions of the peaks in the frequency response spectrum for the accelerations were shifted towards lower frequencies. In order to solve this problem, Young's modulus was increased incrementally until the resonance frequencies replicated the experimental results, which occurred at a value of 60 kPa.

The second calibration performed using the phase velocities helped to tune the initial estimates of Poisson's ratio. A simple setup formed by an exciter and two receivers placed at 40 cm distance was used to determine the phase velocity from the experiment. A velocity of 5.7 m/s was determined by extracting the time interval between the first waves hitting the two separate receivers. This velocity was matched in Abaqus for a Poisson's ratio of 0.49 Having determined Young's modulus and Poisson's ratio, the final characteristic to match was the material damping. A Rayleigh damping model was adopted and the coefficients α and β for the mass and stiffness-proportional parts were determined iteratively. During this calibration it was observed to be necessary to further increase Poisson's ratio to a

value of 0.496 in order to match the response at the higher frequencies. The influence of the Poisson's ratio on the higher frequencies can be observed better in 5.23

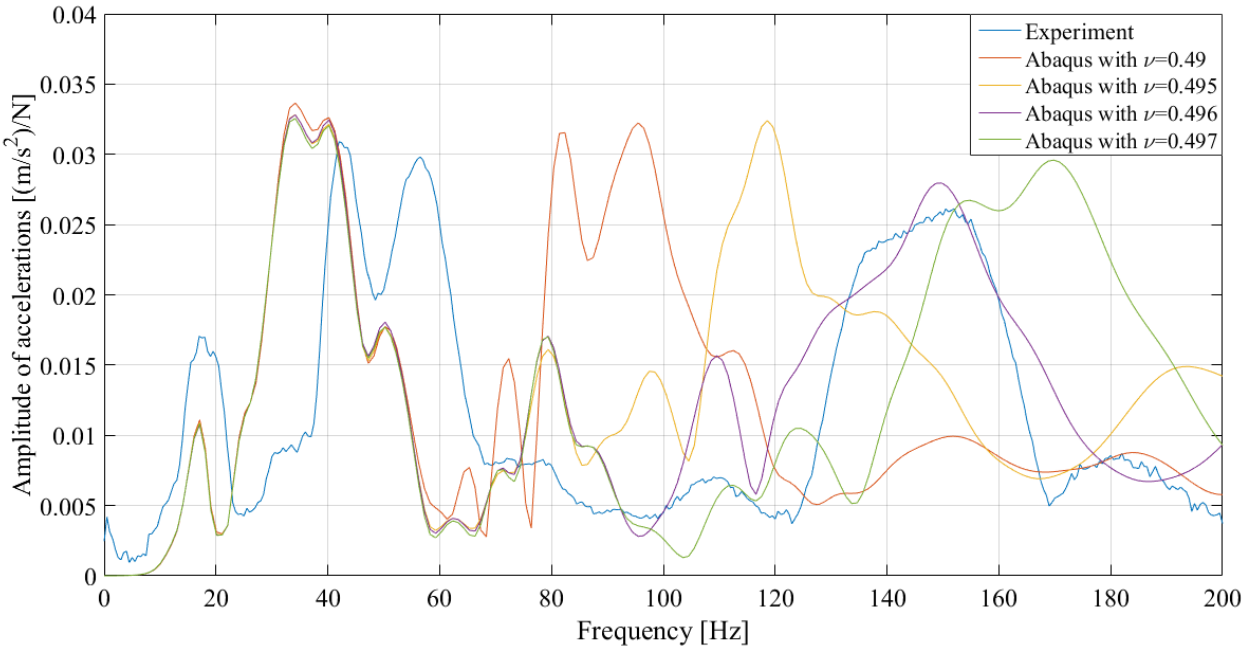

Figure 5.23: Influence of various values for Poisson's ratio on the FRFs.

It can be observed that by increasing the Poisson's ratio the response for the low frequencies are stable but the response for higher frequencies is shifted to the right. The peaks from the numerical an experimental analysis shared the same position for the Poisson's ratio, ν = 0.496.

Table 5.5 shows the values for the density, Young's modulus, Shear modulus and Poisson's ratio and α and β coefficients for the saturated foam.

Table 5.5: Material properties for the soaked foam.

ρ $[kg/m^3]$	E [Pa]	G [Pa]	ν [-]	α [-]	β [-]
980	60000	14976	0.496	31	9e-5

5.4.2 Numerical vs. Experimental

Exciter

Soaking the mattress, mass and implicitly inertia was added to the system. Doing this a more stable response was expected. The first analysis was performed exciting the mattress

in a chosen point using an exciter and a plate to introduce the load. Further the response was recorded using accelerometers attached to a receiver.

This analysis was done with the purpose of observing the dynamic behavior of the system and obtain a FRF on a sweep of frequencies. The range of the sweep was chosen to be from 0 to 200 Hz.

The sweep was manually made using a remote controller for the exciter. With the controller, a cyclic load of a frequency chosen by the user could be introduced and the normalized accelerations recorded using a program provided by the computer.

The setup for this experiment can be seen in Figure 5.24

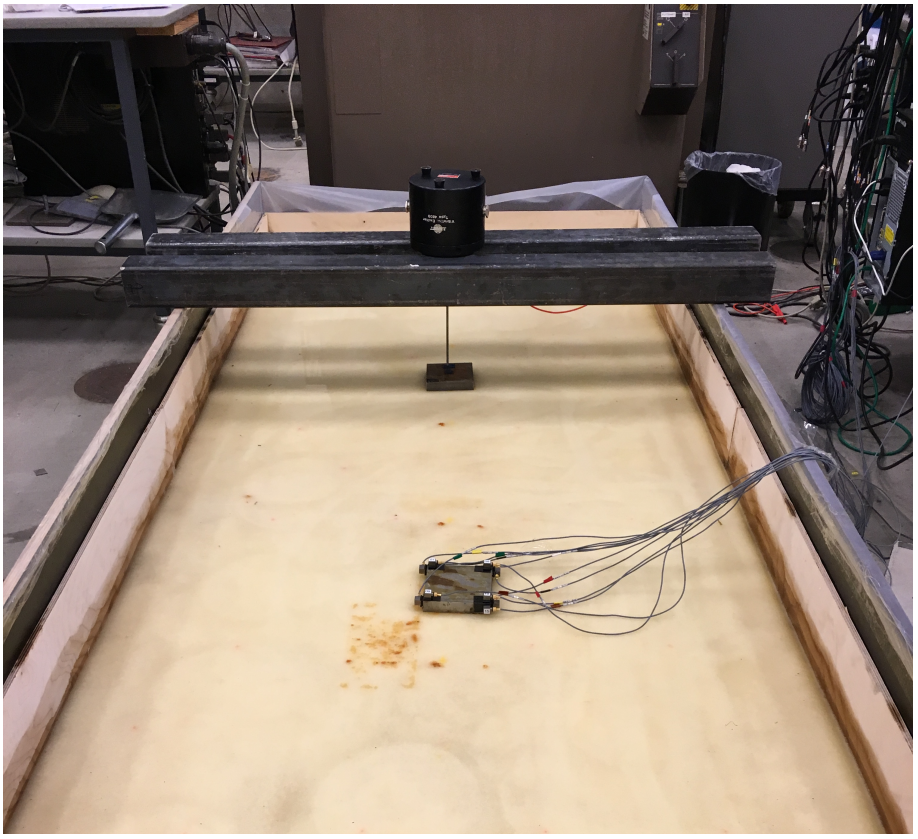

Figure 5.24: Vibrator machine experiment proposed set up

In parallel with this a FE model was setup in Abaqus. A linear perturbation frequency analysis was made on a setup that replicates the experiment. The Lanczos eigensolver was used to identify the natural frequencies that lie in the chosen range.

The FE model can be seen in Figure 5.25.

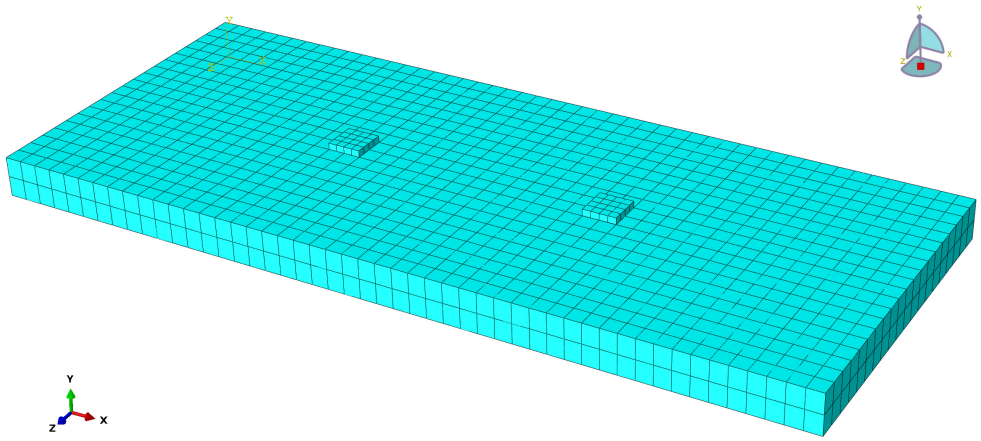

Figure 5.25: Vibrator machine FEM model

Running the numerical analysis a better overview of the modes of vibration and the values where resonance happens was obtained. In that way when doing the experiment sweep a more attentive look is at the resonance frequencies.

In the same time it was observed that the modes are not only vertical but as well transversal, so accelerometers were mounted on all three directions.

The FRF obtained is presented in the Figure 5.26.

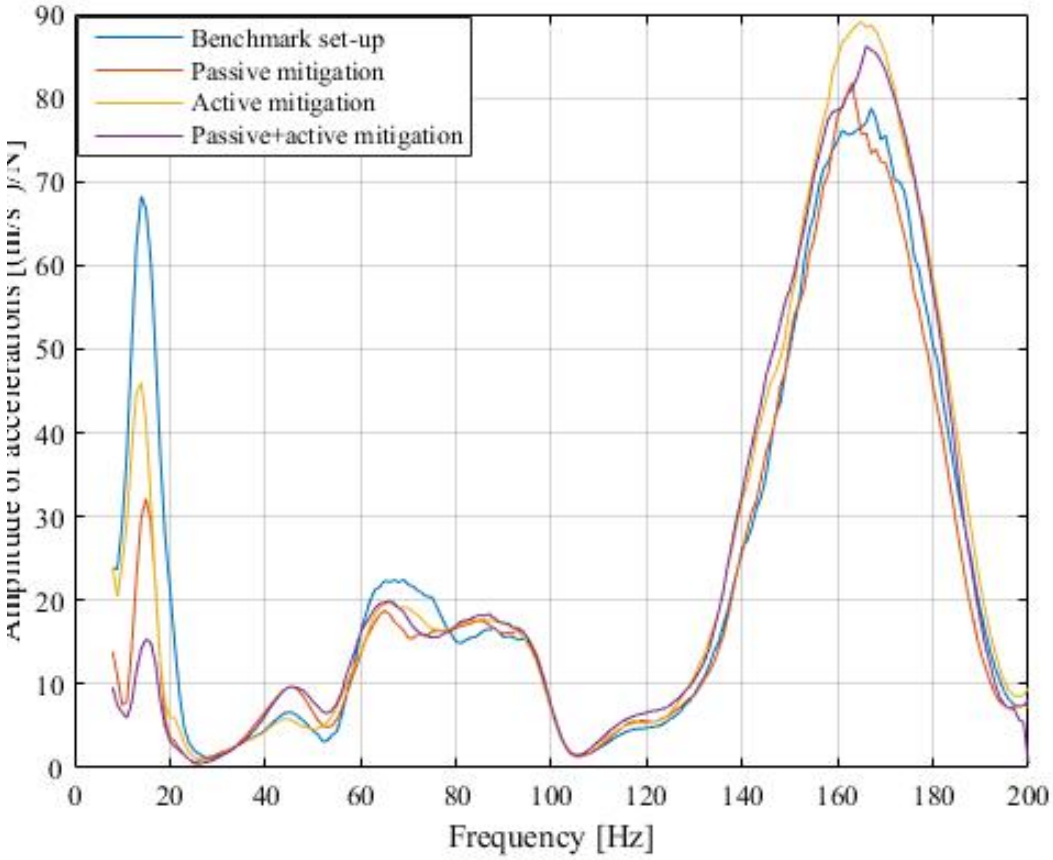

Figure 5.26: FRF obtained using the vibrating machine

It was concluded that this first experiment on the wet foam offers a good understanding of the phenomenon and it is a good exercise to see the response on the system. Implicitly it gives also a visual image of the modes that lie at low frequencies.

The downside of this exercise is however that it is very time consuming. A full sweep takes around four hours. Tests were made in several days to see if any difference appears in the values for the accelerations. It was observed that there are big fluctuations from one day to another, this might be caused by evaporated water or human errors since the response was recorded manually for each frequency increment.

As a conclusion using this method the response of the system can be observed providing a good representation. However due to multiple sources of errors mentioned above and the long time interval necessary to complete a single test, method was not chosen for further analysis.

Excitation hammer

The same analysis was made as described in Section 5.3.3.

A modular template was chosen, first a no mitigation test was conducted in order to have a reference point. Then several mitigation solution were studied placing mass on modular positions. A better insight of the chosen positions will be presented in Section 6.3.1.

The modular template chosen can be seen in Figure 5.27

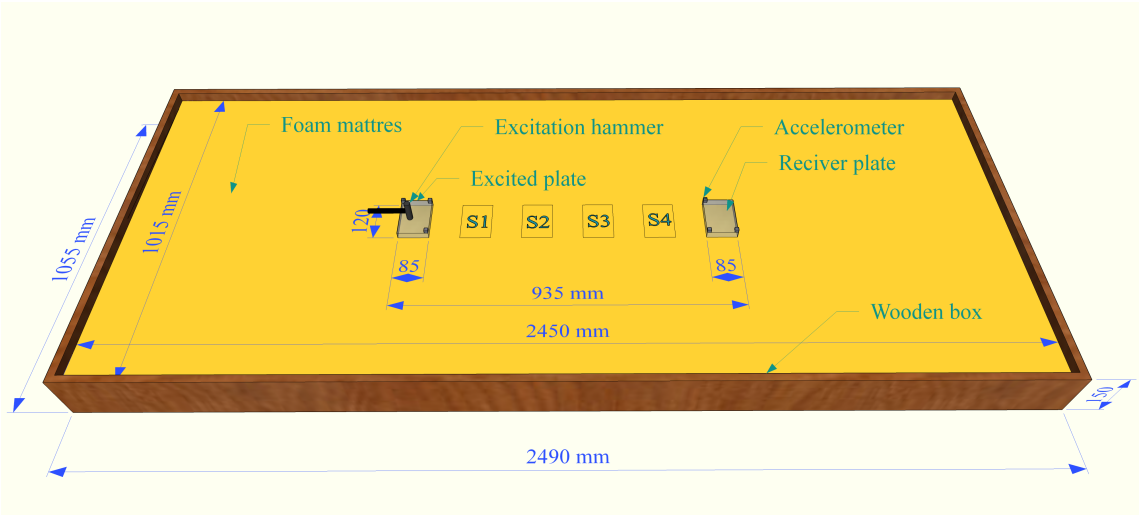

Figure 5.27: Modular setup with proposed mittigation solutions — experimental.

The same modular setup was also used in the numerical analysis as it can be seen in Figure 5.28

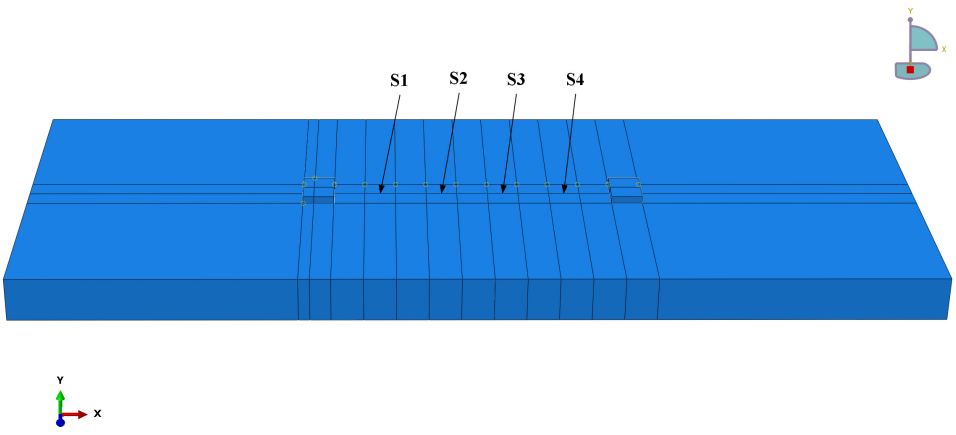

Figure 5.28: Modular setup with proposed mittigation solutions — numerical.

Frequency response functions were then set up for both cases and compared in order to observe the correlation between the models.

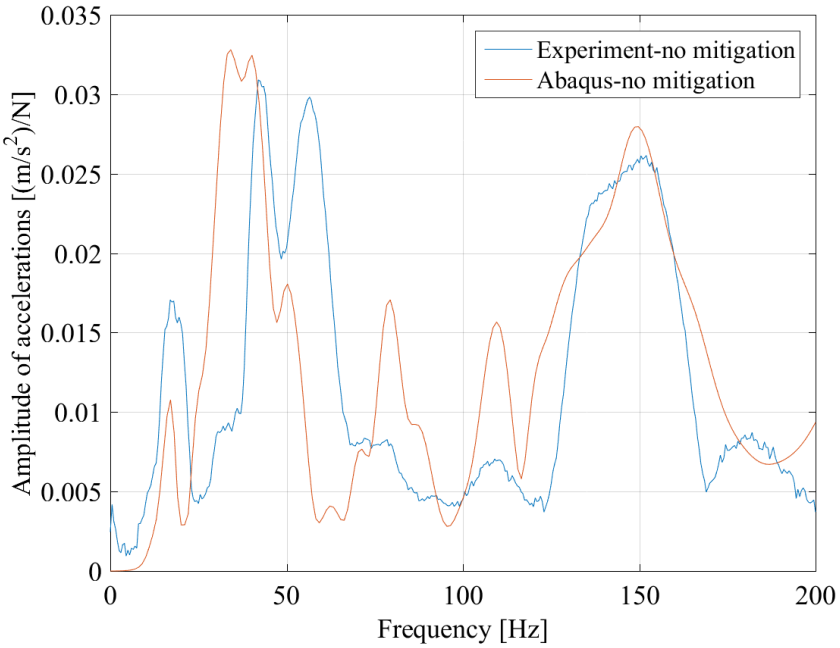

Figure 5.29: FRF for no mitigation.

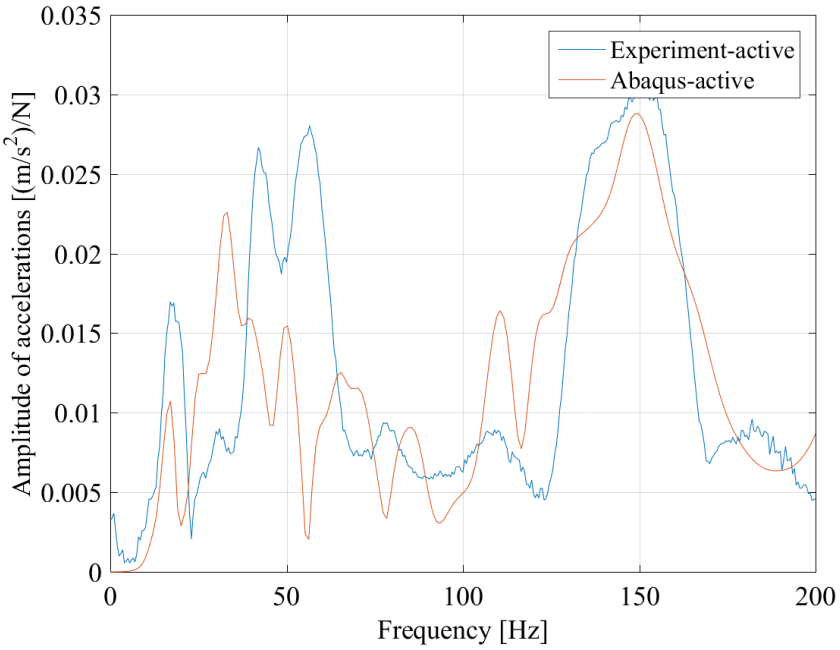

Figure 5.30: FRF for active mitigation.

As it can be seen in Figure 5.29 for the no mitigation case and in Figure 5.30 for the active mitigation case a fair correlation is obtained between the models. With this in mind this exercise is chosen to be the way to conduct all further studies. The final results and conclusions will be presented in the next chapter.

Chapter 6

Vibration mitigation analysis

In this chapter the mitigation vibration study is presented. First a model represented by one layer of material and the influence of masses placed on the surface is studied. A second model is then developed by adding one more layer of foam and studying the influence of embedded masses. Moreover an additional study of a vertical barrier width influence regarding the screening efficiency is performed. Having well defined test configurations and employing both a numerical and an experimental analysis the responses were recorded, interpreted and compared.

6.1 Introduction

As an alternative to barriers in soil, masses can be added on the ground between the source and the receiver in order to mitigate the vibrations. Applying these masses and increasing the stiffness creates stop bands in the frequency domain. The behavior of transient loads within such stop bands is less well defined, but some mitigation may occur. In this final chapter, conclusions of the behavior of the vibrations under the influence of added masses nearby the receiver footing, the source or in between the path of the two, in various ways are presented.

To quantify the mitigation effect of adding mass to the ground surface two approaches were used. A small scale laboratory model and a 3D finite-element model. A comparison between the models was made which lead to an assessment of the mitigation that can be expected in a real project compared to the mitigation predicted by a numerical model.

6.2 Data processing

Accelerometers were mounted on both the source and receiver footing and vertical accelerations were measured in the pre-determined positions. Based on these measurements, frequency response functions (FRF) defining the acceleration output were derived with the use of PULSE program.

In the FE model, unit-amplitude harmonic loads have been applied, using a steady state dynamic analysis, and the acceleration output measured in the same places as in the experiment. The acceleration levels at the surveyed points in the numerical model can be

compared directly to the FRFs from the experiment for each frequency within the steady state because unit forces have been applied and the results from PULSE are normalized.

The results will be presented for a better understanding in two ways. Firstly FRFs of the no mitigation case vs. a mitigation solution will be presented. This will be done in decibel dB relative to the acceleration per unit force $1\,\mu\text{m/s}^2/\text{N}$. This is done using Equation 6.1.

$$FRF_{db} = 20\log_{10}\frac{FRF}{FRF_{ref}}, \quad \text{where} \quad FRF_{ref} = 1\,\mu\text{m/s}^2/\text{N} \tag{6.1}$$

Further to quantify the effect of placing additional masses in one or more positions, insertion loss (IL) graphs had been created using Equation 6.2.

$$IL_{db} = 20\log_{10}\frac{FRF_0}{FRF_{ref}} - 20\log_{10}\frac{FRF_k}{FRF_{ref}} = 20\log_{10}\frac{FRF_0}{FRF_k} \tag{6.2}$$

Where subscript 0 indicates the no mitigation case, while the subscript k indicates one of the chosen mitigation solutions. Here the IL is calculated in all cases relatively to the same reference.

6.3 One layer mattress

As it was presented earlier, in Section 5.4, a numerical and experimental model has been created for the one layered mattress. The results provided by the FRF analysis are accurate and the analysis can proceed. The problem concerns now on how to mitigate the vibrations by positioning the weights directly on the ground surface, between the source and the receiver

6.3.1 Position of the weights

The influence of added mass on the ground surface is studied by creating a modular grid between the exciter and the receiver. In this way the additional masses were introduced in prescribed positions, the response was recorded and compared with the response where no additional masses were introduced. In Figure 6.1 is noticed that four slots are available for the masses between the source and the receiver. The possible positions for additional masses are marked as S1, S2, S3 and S4 with red color.

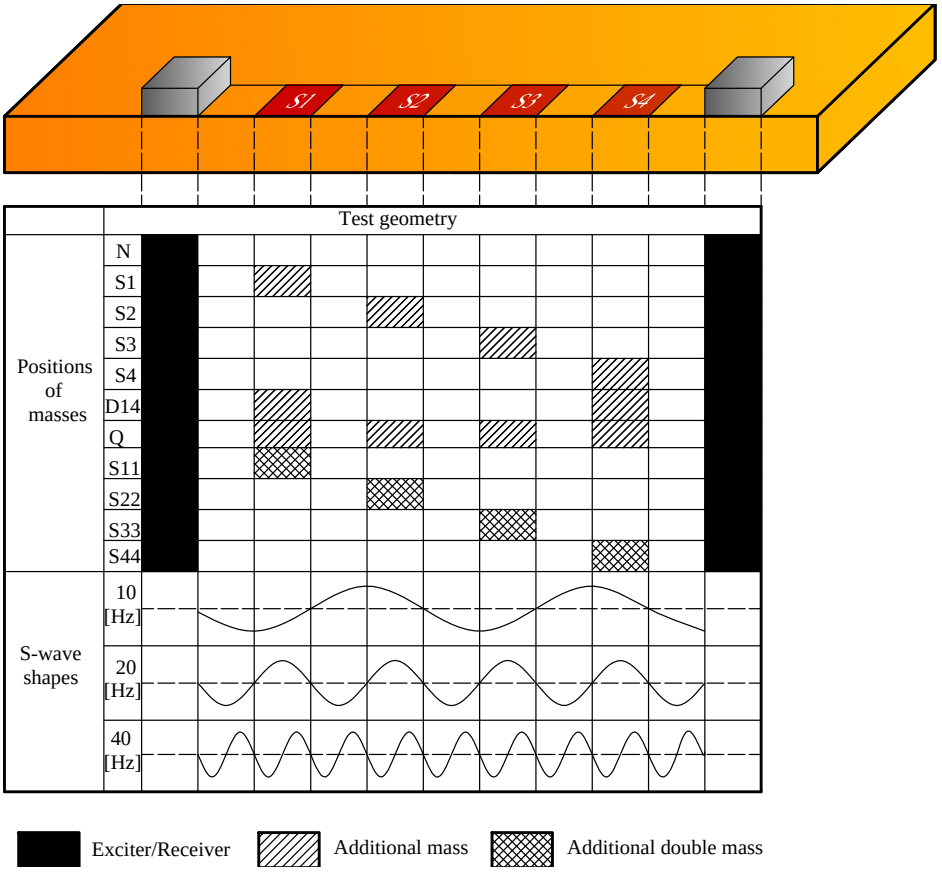

Figure 6.1: Tests configurations with single masses and double masses added on the ground surface.

In Figure 6.1 a total of ten different configurations are presented. As it can be observed, test geometry N represents the original setup while setups called S1 to S4 are related to single masses added in one of the slots. The test geometries S1 and S4 simulate active and passive mitigation respectively, and the setups S2 and S3 are intermediate possibilities of the previously mentioned solutions.

A secondary approach was by introducing multiple masses, meaning that configuration D14 (D for double) concerns adding masses in slots S1 and S4, being a combination between active and passive mitigation. The one with masses in all four slots is called Q (Q for quadruple), simulating a periodic positioning of the masses. Furthermore another four configurations are tested, called S11 to S44, studying the influence of increasing the mass of the previously discussed geometries. The mass was doubled by placing two masses on top of each other in one position.

In the bottom of the Figure 6.1 the shapes of three S waves are represented for three frequencies. The lengths have been calculated for these frequencies, in the considered frequency range, so at 10 Hz each mass covers about one quarter of the wavelength, at 20

Hz it covers one half, and at 40 Hz it covers a full wavelength.

6.3.2 Comparing results

In the following part the results from experimental and numerical FE models are presented and compared in between. The results are presented in dB as it was presented in Section 6.2.

Figure 6.2 provides the results for the reference case with no mass, the results being presented for both the source and receiver.

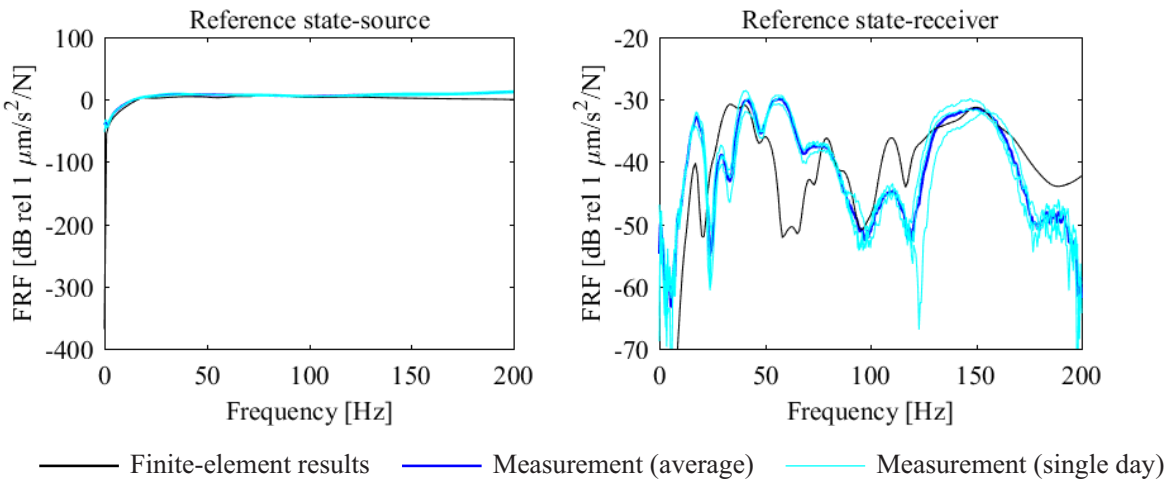

Figure 6.2: The reference case with no added masses — single layer foam.

As it can be observed in Figure 6.2, the experiment was repeated in three consecutive days within an error of few dB for most of the frequencies. It is concluded that the mattress was fully saturated in all three days, such that no changes in the mass density or stiffness occurred and the results are representative for the geometry. In the left side, for the source response, it is noticed that the response starts with a value around $-200\,1\mu/\mathrm{s}^2/\mathrm{N}$ and around 50 Hz it becomes constant. This is caused by the impact hammer which is applied once on the Plexiglas footing.

It is clear that there are differences between the experimental and the numerical models at some frequencies, in especially in the interval of 50 Hz to 70 Hz but some of the peaks match perfectly regarding their position and as well magnitude. This is due to the fact that it was not possible to calibrate the FE model to match the results provided by the experimental analysis.

One of the most influential factor was the boundary conditions, except for the free surface, the other surfaces were assumed to be fully fixed in the numerical model created in Abaqus. In the laboratory some sliding could occur for the fixed surfaces, introducing

errors, furthermore the box itself may not be completely rigid.

In Figure 6.3 the results for the tests with single masses placed in one of the four slots are presented. The figure contains the results measured in all three days but also an average of the measurements being compared with the results provided by the FE software. On the left side are presented the FRFs for all setups from both experimental and numerical models and on the right side are presented the insertion loss (IL) for both models as well.

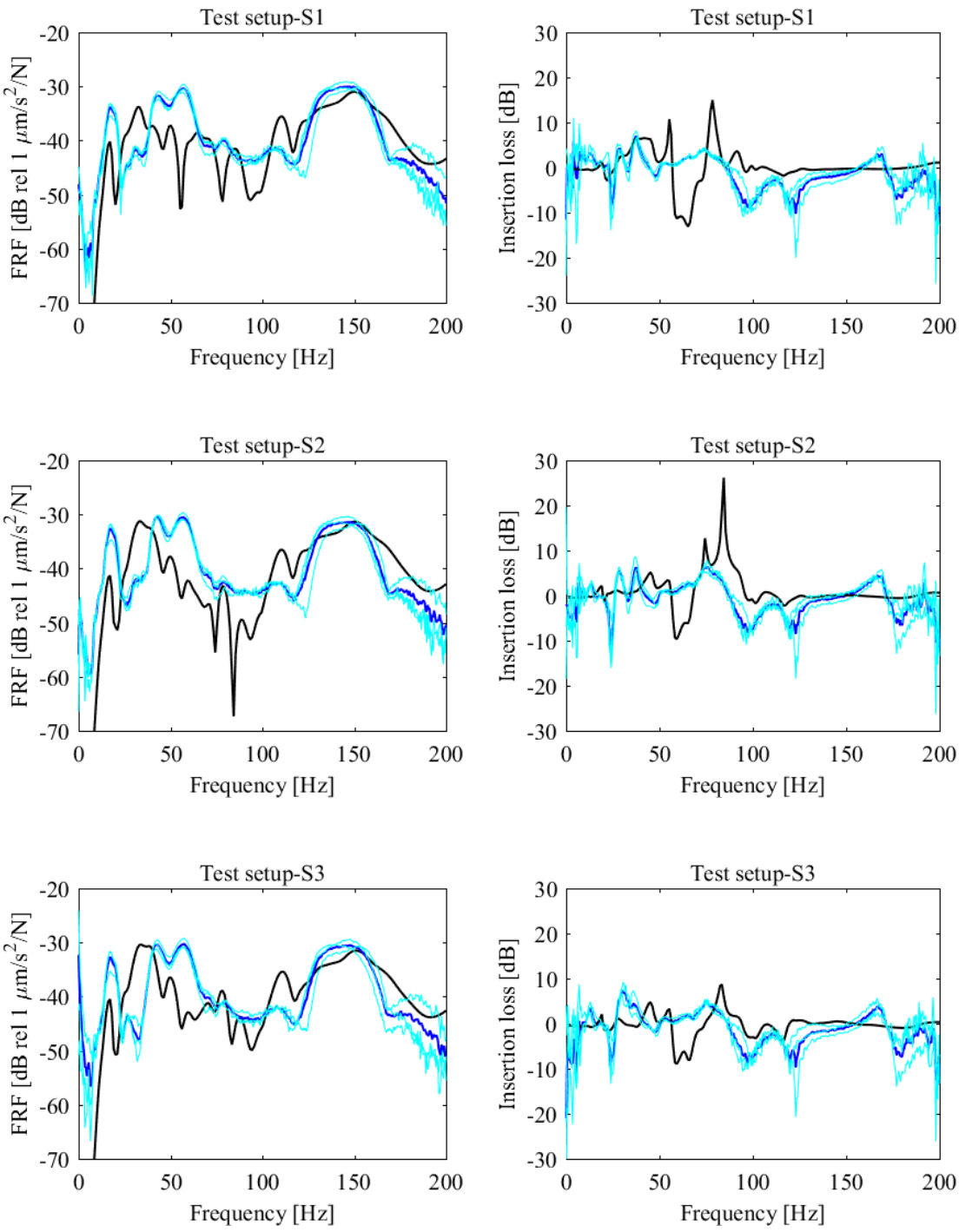

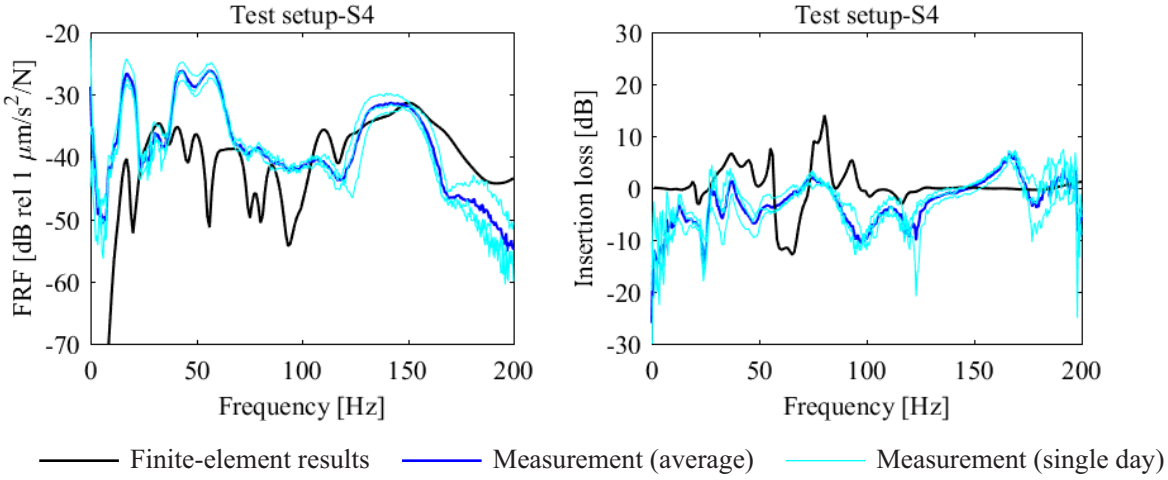

Figure 6.3: Results for single masses placed between source and receiver.

At a first inspection the results provided by the experimental analysis do not differ too much between the various configurations of added masses. The differences, as it can be seen, given as IL are generally within the range of $-10\,\mathrm{dB}$ to $10\,\mathrm{dB}$. The FE results do not match well the experimental results, the differences being larger in the range of $50\,\mathrm{Hz}$ to $70\,\mathrm{Hz}$, as it was expected.

The results for the double masses are presented in Figure 6.4.

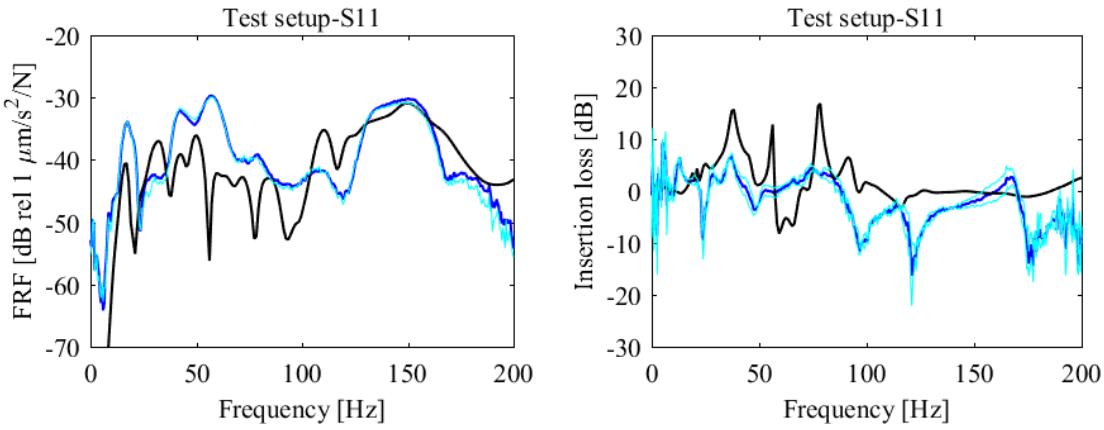

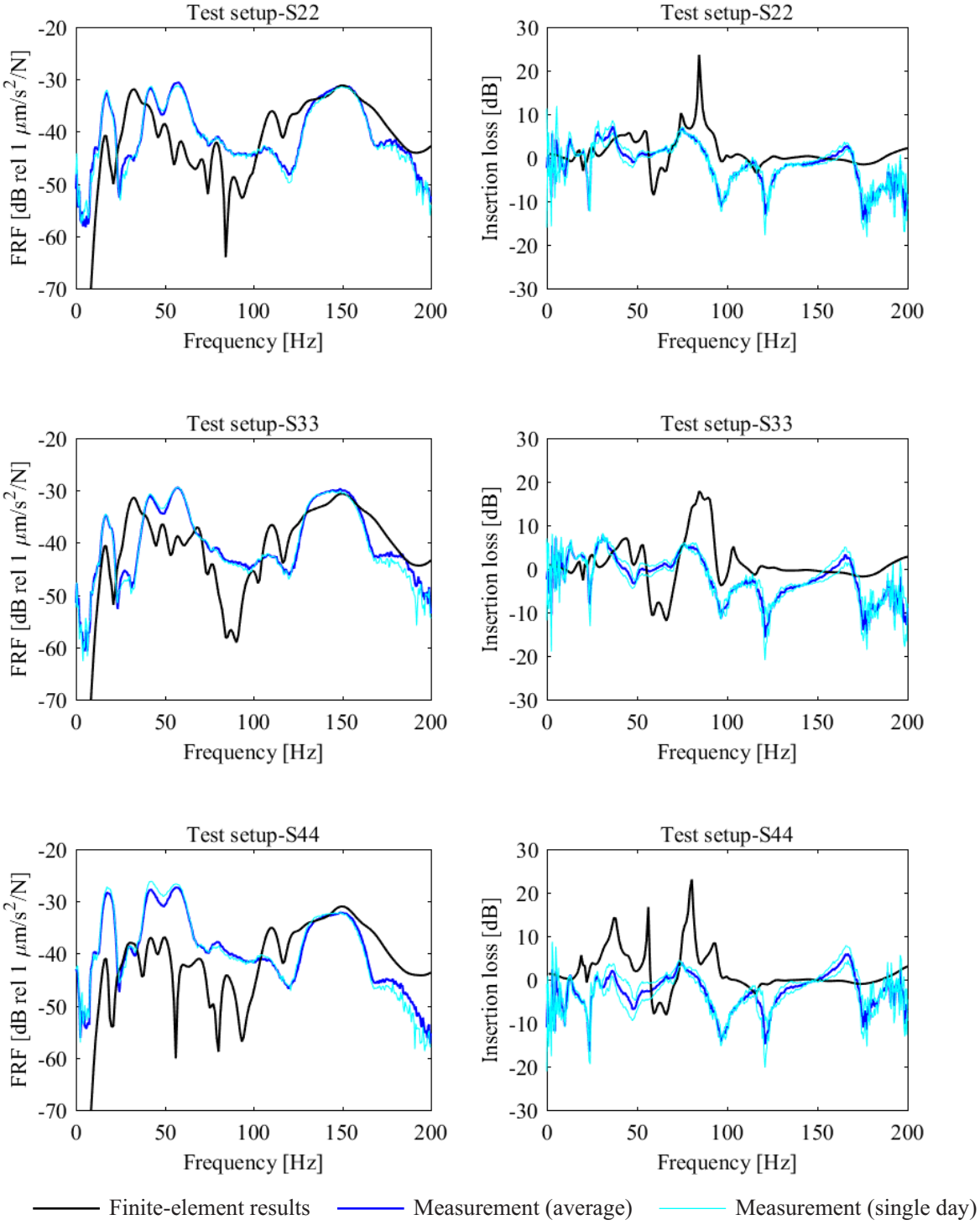

Figure 6.4: Results for double masses placed between source and receiver.

In Figure 6.3 the experimental results show that for the low-frequency range, S1 and S2 are giving better results than S3 and S4. For S1 and S2 setups only about $-10\,\mathrm{dB}$ are observed, while the S3 and S4 setups provide an IL of $-20\,\mathrm{dB}$, which means more vibrations introduced in the system. For the cases with the double masses, in Figure 6.4,

the difference is not that pronounced. In the frequency range of 30 Hz to 40 Hz the S3 configuration provides the highest IL, while the single mass added in S4 provides a smaller IL in the same range. Same observation is made when the double masses are added in the same slots, see Figure 6.4.

At frequencies near 60 Hz to 70 Hz, Figure 6.3 shows that the S2 configuration provides a higher IL than the other configurations, setup S4 providing the same low or negative IL. A similar effect is observed in Figure 6.4 for the double masses. This could lead to a conclusion that placing a mass close to the receiver could be a direct disadvantage.

Figure 6.3 and 6.4 proves that for a frequency range of 100 Hz to 200 Hz, the IL for the single or double masses in single slots are generally negative. Two particular peaks occur around 95 Hz and 120 Hz, which could be due to resonance of the inserted masses leading to additional wave scattering. In support of this assumption, the frequencies at which the peaks occur shift to lower values and the IL becomes 5 dB more negative when double masses are present instead of the single ones.

The FE models, compared to the experimental ones, provide more variations in the IL. Figure 6.3 proves that configuration S2, when single masses are present, exceeds the other configurations at certain frequencies. However the peaks around 60 Hz to 70 Hz moves to around 70 Hz to 80 Hz for the FE model, a similar pattern being noticed for the double masses. Around 80 Hz it is noticed that configuration S44 performs well, see Figure 6.4. Also configurations S11 and S44 show a bigger IL around 35 Hz than in the others configurations with single or double masses. Another observations is that the position and the size of the masses for the FE model have a slightly more influence compared to the experimental results.

In Figure 6.17 are presented the results for more masses added in different positions.

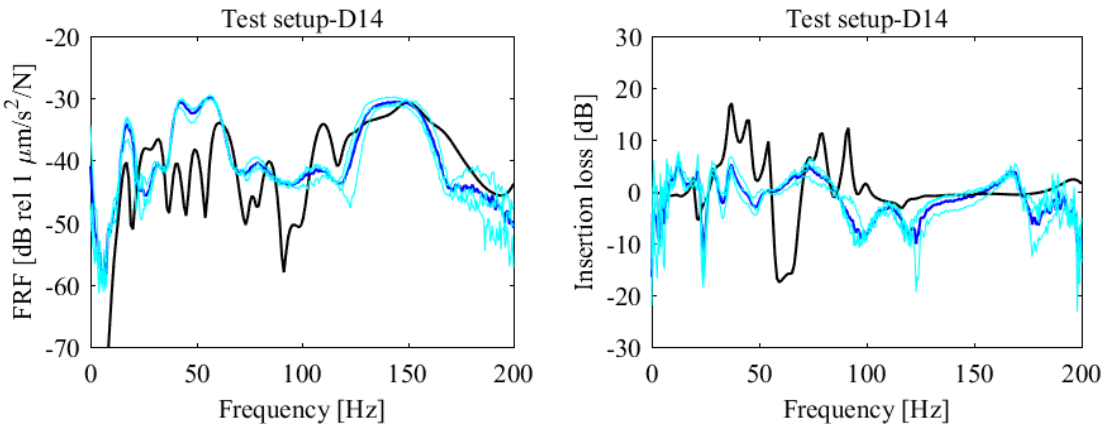

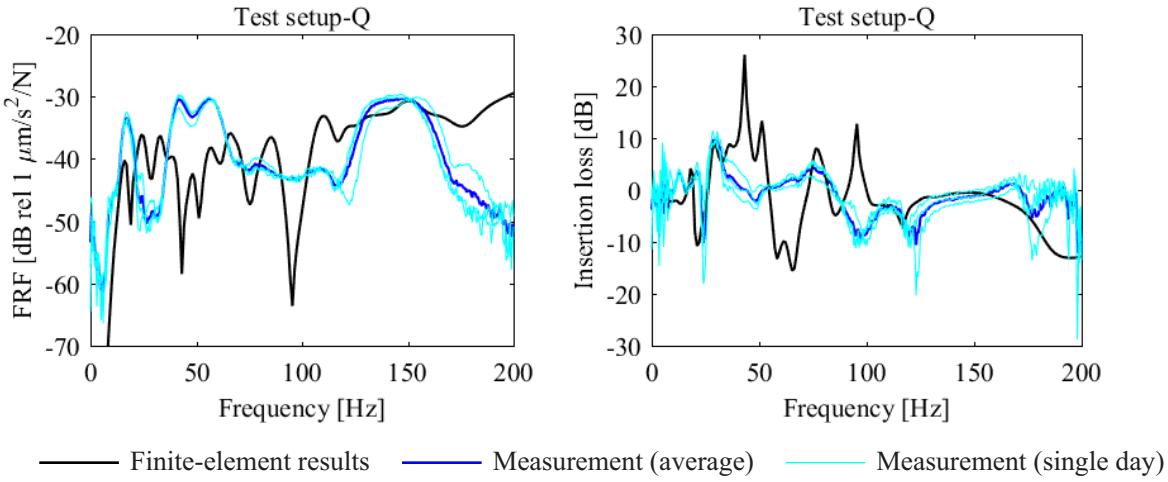

Figure 6.5: Results for multiple masses placed between source and receiver.

Configurations D14 and Q indicate the same trend in response as for the single and double masses. Test setup Q, with the masses placed in all slots, performs quite well around 30 Hz providing the highest IL recorded for any configurations. This phenomenon could be caused by the periodic masses added and the frequency range of 30 Hz being regarded as a stop band. Although the FE results do not match too well the experimental results, it replicates the same peak in the IL.

Finally, configurations D14 and Q provide a mitigation in the frequency range of 40 Hz to 50 Hz. The IL, comparing the Figures 6.3, 6.4 and 6.17, is observed to be stronger for configurations D14 and Q than any other cases. Also the peak around 45 Hz is not very pronounced for single and double masses. For the configuration D14 it reaches a value of 12 dB and for configuration Q a value of 25 dB. This could be the result of a stop band forming in the FE model but not being present in the experimental one. An observation to this is that the identification of stop bands for nearly periodic structures may be difficult. Another observation is that computational models could be inadequate for design purpose if the stop bands are narrow and mitigation of vibration from sources with specific frequencies must be achieved.

As a conclusion for the experimental tests, by introducing masses directly on the ground surface, the insertion losses (ILs) in the frequency-response functions (FRFs) were mostly in the range of -10 to +10 dB rel to 1 µm/s^2. The more favorable solution was to introduce the masses near the source footing and not placing them close to the receiver footing. Moreover at frequencies identified as resonance frequencies of the masses placed on the ground, an increased response is observed for the additional masses. A peak in the IL is identified for the case with nearly periodic masses added on the ground due to result of a stop band. The FE reproduces the same peak witch in addition to this, is producing a second one as a result of placing masses nearly periodically.

6.4 Two-layers mattress: Experiment

A similar study with the one presented in the previous section is performed but in this case the mitigation effects of buried masses are studied. For this to be studied the setup was changed by adding another foam layer. Following the same practice the second layer is soaked having the same material properties and the same thickness of 12 cm. Since the density of the soaked material is lower then the water density, in order to avoid buoyancy effects the two layers were attached together using silicon as adhesive. The external masses are going to be placed in between the foam layers, more exactly on the top of the first foam layer.

6.4.1 Position of the weights

The same modular grid as presented in Section 6.3 and the same Plexiglas blocks were used as additional masses. In this case, however, the four possible mass positions were cut out from the top layer resulting of four hexahedral foam pieces, see Figure 6.6.

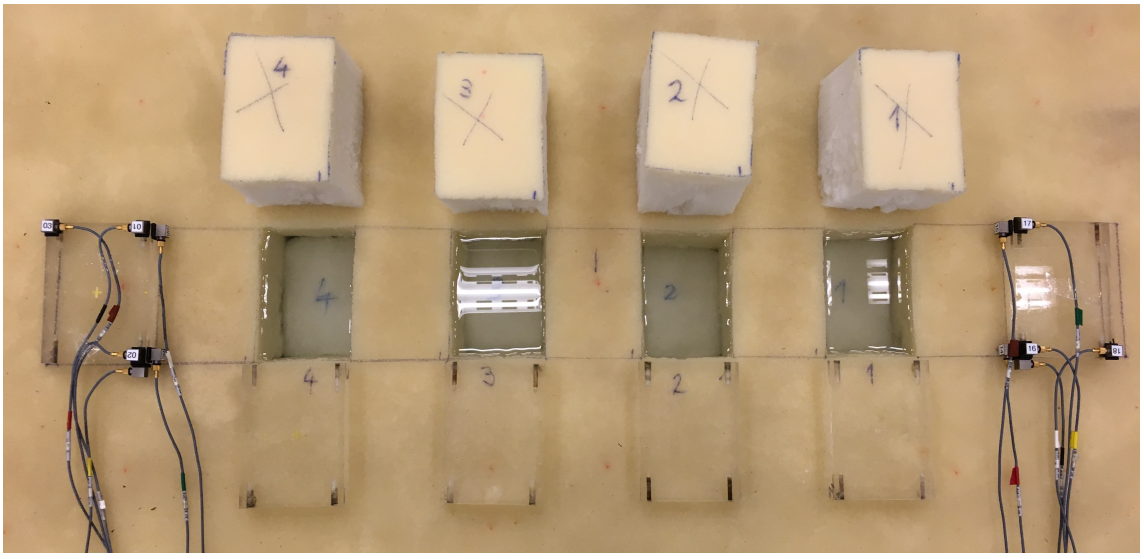

Figure 6.6: Detail with the parts used for the two layers test setup.

Furthermore this small pieces were each subjected to an extra cut of the dimension of one Plexiglas block in order to maintain the foam density above the additional masses. A total number of seven different layouts were analyzed as seen in Figure 6.7.

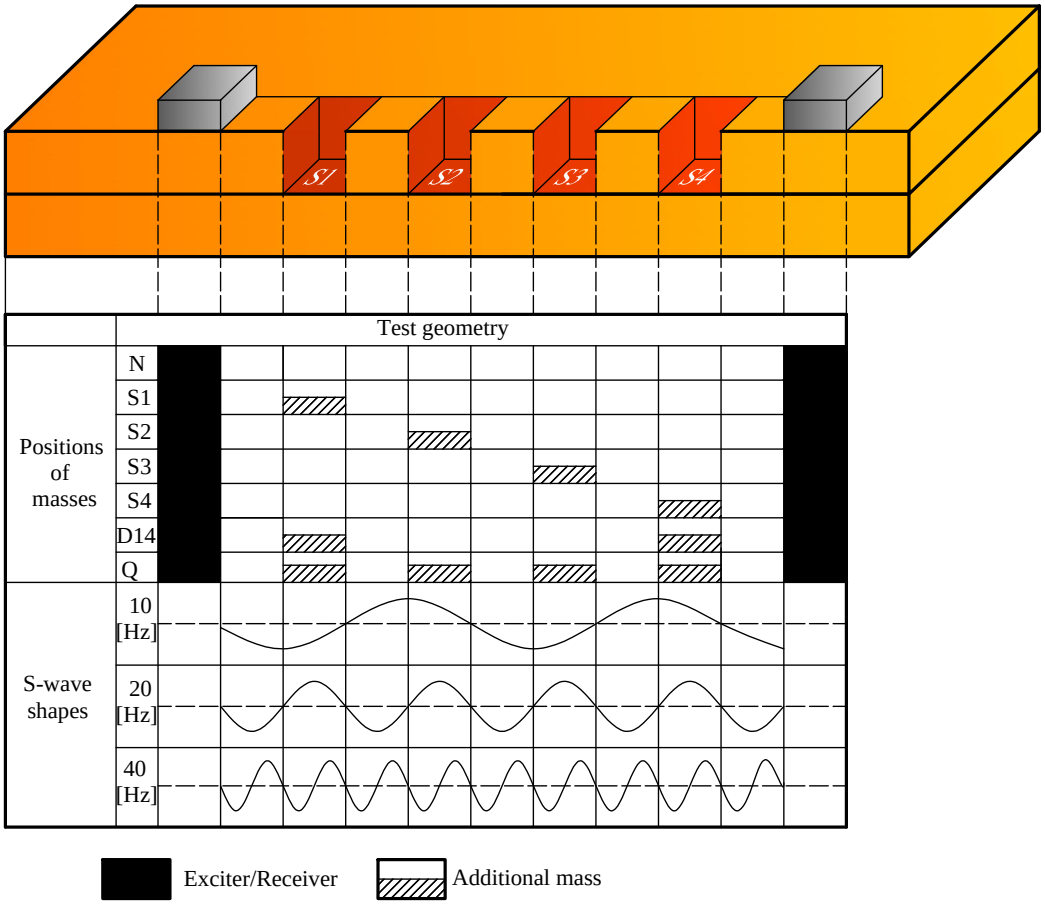

Figure 6.7: Tests configurations on the two-layers foam.

Here beside the fact that the masses are buried between the layers, the tests have the same configurations as for the one-layer test setup. The undisturbed/no mitigation setup is denoted as N and when singular masses are added, the setups become S1, S2, S3, or S4, where S1 simulates active mitigation, S4 passive mitigation while S2, S3 are intermediate positioning possibilities. The active and passive mitigation is then combined in the test D14 and finally the periodicity effects are tested in the test geometry Q. The S-wave shapes are as well plotted for 10 Hz, 20 Hz and 40 Hz to observe the similarity between the dimensions of the external masses and the wavelengths.

6.4.2 Results and interpretation

Ideally the results should be presented in the same format as for the one-layer mattress i.e. experimental versus numerical results. However, since the numerical model could not provide a good match, the experimental work was chosen to be presented separately and

leave the comparisons and final discussions at the end of this section.

To start with, the reference states for both the exciter and receiver are presented in Figure 6.8. The response is presented in decibels relative to the reference acceleration of $1\,\mu\text{m/s}^2/\text{N}$.

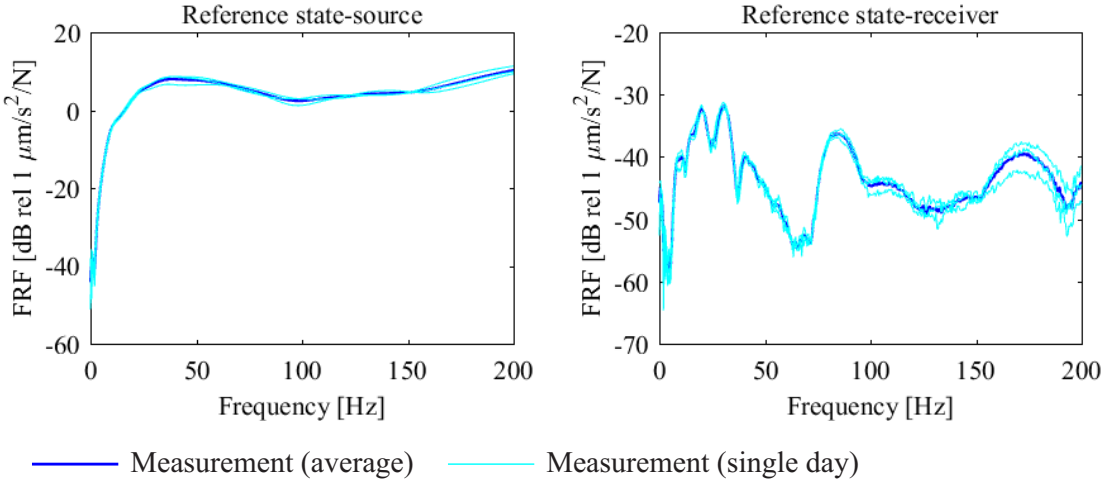

Figure 6.8: The reference state with no added masses — two layers foam.

As expected the accelerations amplitude at the exciter are considerably higher in comparison with the receiver. Similar with the studies on the single foam layer the response of the exciter is close to 0 dB and has no obvious peaks. On the other hand the response of the receiver presents some differences which confirms the dissipation phenomenon as well as wave reflections and other interactions. The results of the all mitigation test-setups are presented in Figures 6.9, 6.10 and 6.11. The responses are presented side by side, the FRF to the left and the insertion loss (IL) to the right.

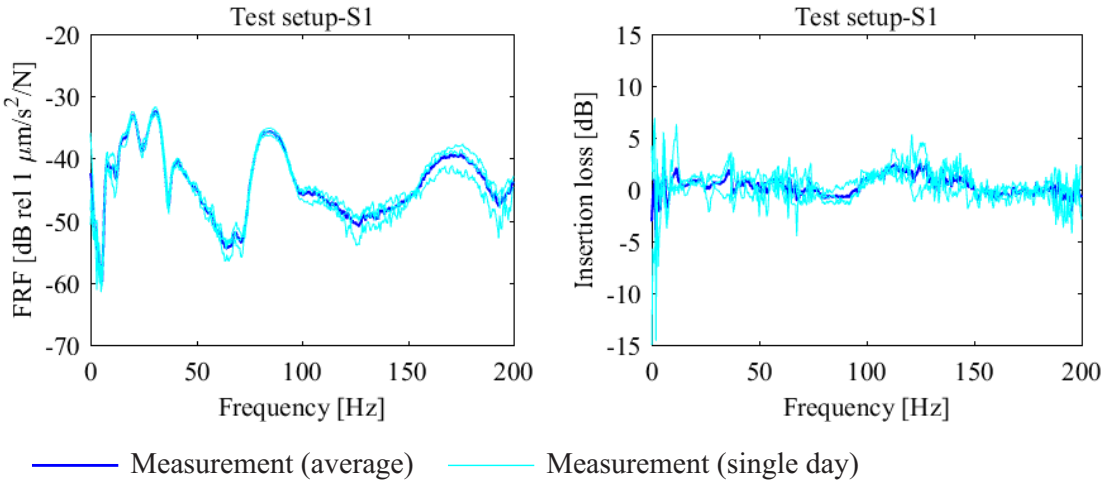

Figure 6.9: Results for configuration S1 of the masses placed in the ground surface.

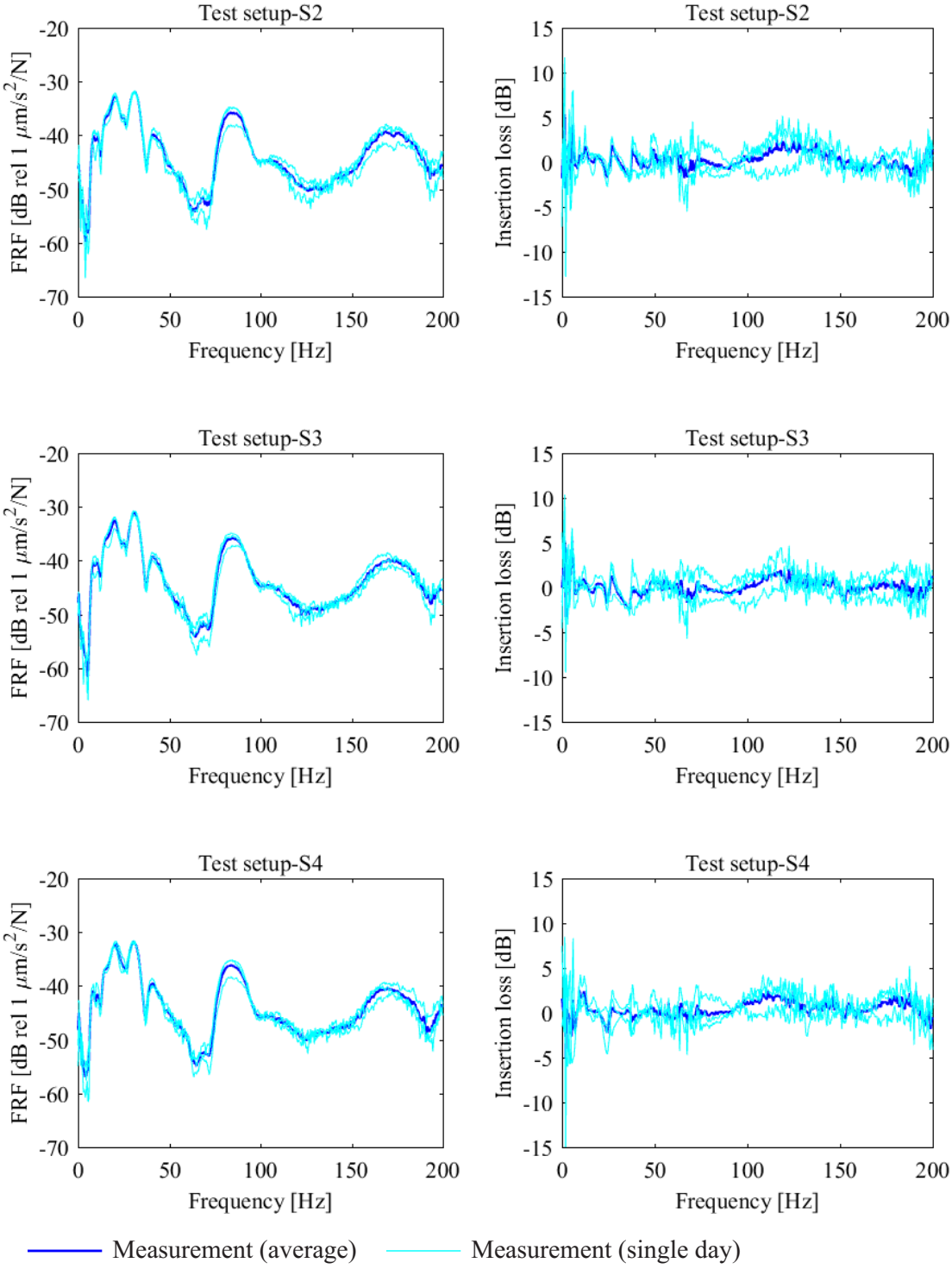

Figure 6.10: Results for configurations S2, S3, S4 of the masses placed in the ground surface.

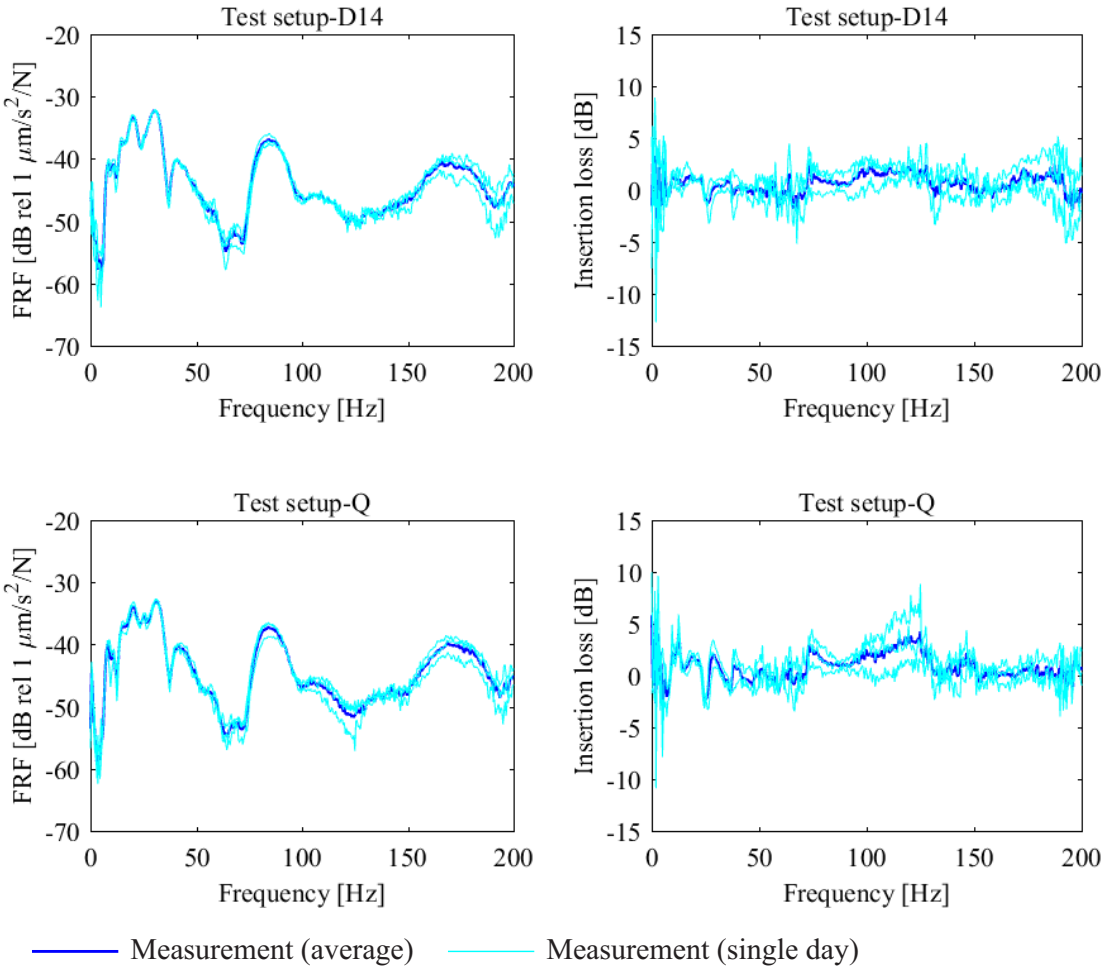

Figure 6.11: Results for configurations D14 and Q of the masses placed in the ground surface.

There are no significant changes in the responses independently of the test geometry. The frequencies response functions illustrate the peaks with the same amplitude and the same positions while the insertion loss varies from -5 to 5 dB. Hence it can be concluded that the Plexiglas blocks buried in the soaked foam has lower influence on the response compared with the test setups with a single foam layer. As a general observation it can be pointed out that the responses in the third day are lower than the previous two days for frequencies higher than 60 Hz. This deviation can be seen on the both graph types, FFR and IL. The deviation is approximately of 3 dB which is quite significant for these sets of results and it might be caused by the effects of evaporation leading to a decrease of Young modulus. Another general characteristic is that from 0 to 5 Hz the response is not stable, as it can be deducted from the individual day plots and as a consequence is disregarded from the analysis.

When looking separately to model setup S1, see Figure 6.9, some mitigation trends are observed at a frequency of 12 Hz and 35 Hz. The IL for both positions are about 2 dB.

Next the model geometry S2 presents a rapid change in response from an approximately IL of −2 dB to 2 dB at a frequency of 25 Hz and 27 Hz respectively. For higher frequencies, the IL fluctuates around the value 0 dB and considering the variation between the single-day recordings, no significant mitigation or amplification of the accelerations can be interpreted. The same pattern is observed for S3 and S4 test setups. Furthermore a similar jump in the IL is observed at 25, 27 Hz. By introducing two or more masses in the system some deviations in the IL occur at higher frequencies, see Figure 6.11. For instance for both test setups D14 and Q positive values of 2.5 dB occur at 75 Hz. Moreover the Q test layout shows an IL of 4.3 dB at a frequency of 125 Hz with the observation that the single day recordings presents variations around that frequency.

To conclude, rapid variations around 25 Hz were observed for all test configurations and when more masses were introduced in the system a positive response is recorded at higher frequencies. However since the added masses induces an IL with an average magnitude of 2 dB the effect of embedding masses in the material volume has a small influence on the receiver response.

6.5 Two-layers mattress: Numerical model

This section focuses the numerical analysis of the two-layers mattress. As it was observed in Section 6.4, the results provided by the experimental and numerical analysis do not match, the analyses being treated separately.

6.5.1 Model setup

The setup of the model follows the same steps as for the one layer mattress. The only differences are given by the masses which, for this case, are not longer positioned on the surface but they are embedded inside the mattress.

To reproduce the laboratory setup as close as possible and to reduce the resources used for the analyze, the boundary conditions and the connections between the elements presents a high importance factor.

The approach used for creating this model was to create only one single part, regarding the two-layers mattress and the weights inserted instead of creating each part individually and to connect the parts using different types of connections. This would lead to a longer time and computational resources needed for the analyses. Moreover the uncertainties are being introduced among these connections and the results will be affected.

The Plexiglas blocks are modeled by cutting the part, providing the exact locations of the blocks. Further, the material is assigned to the individual sections, the entire part was designed as foam with the exception of the inserted blocks. The setup can be seen in

Figure 6.12, where it can be observed that the mattress is cut as well, reproducing the real model and being an important factor when meshing the model.

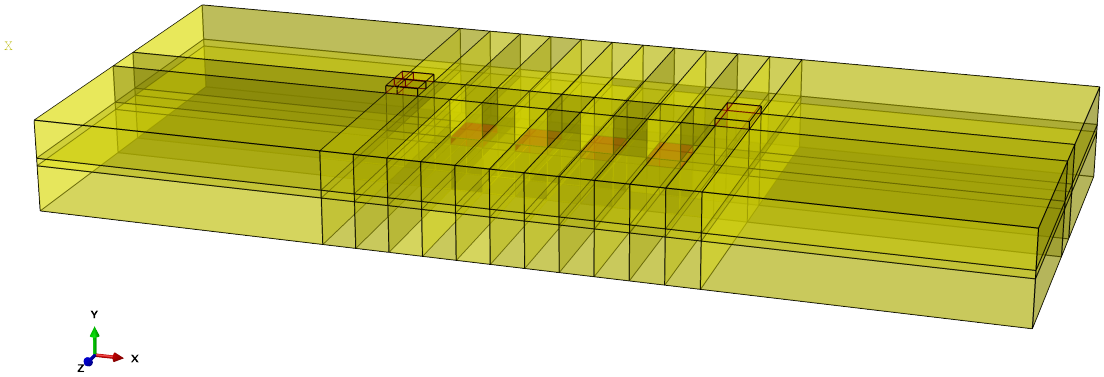

Figure 6.12: Detail with the parts used for the two layers test setup.

The boundary conditions and the connection between the surface footings and the mattress follows the exact same procedure as for the one-layer mattress model.

6.5.2 Results and interpretation

As in the previous Section 6.4 the reference states for both the exciter and receiver are presented in Figure 6.13.

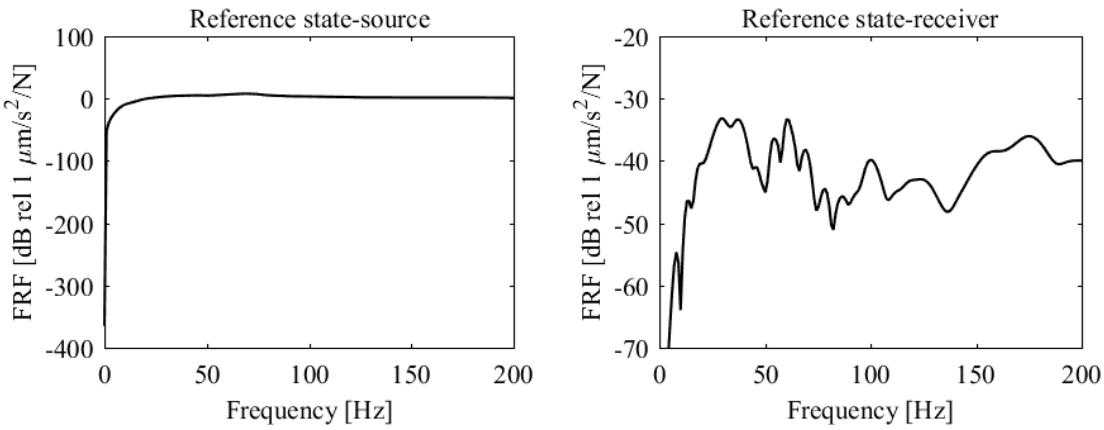

Figure 6.13: The reference case with no masses.

For the source case, as it was expected, the numerical model matches the experimental one, but for the receiver case, it can be seen that the results do not match, even though the magnitude of the amplitudes are similar, still considerable differences could be observed, this being the reason why the numerical model is treated separately from the experimental model.

The results of the all mitigation test setups are presented in Figure 6.14.

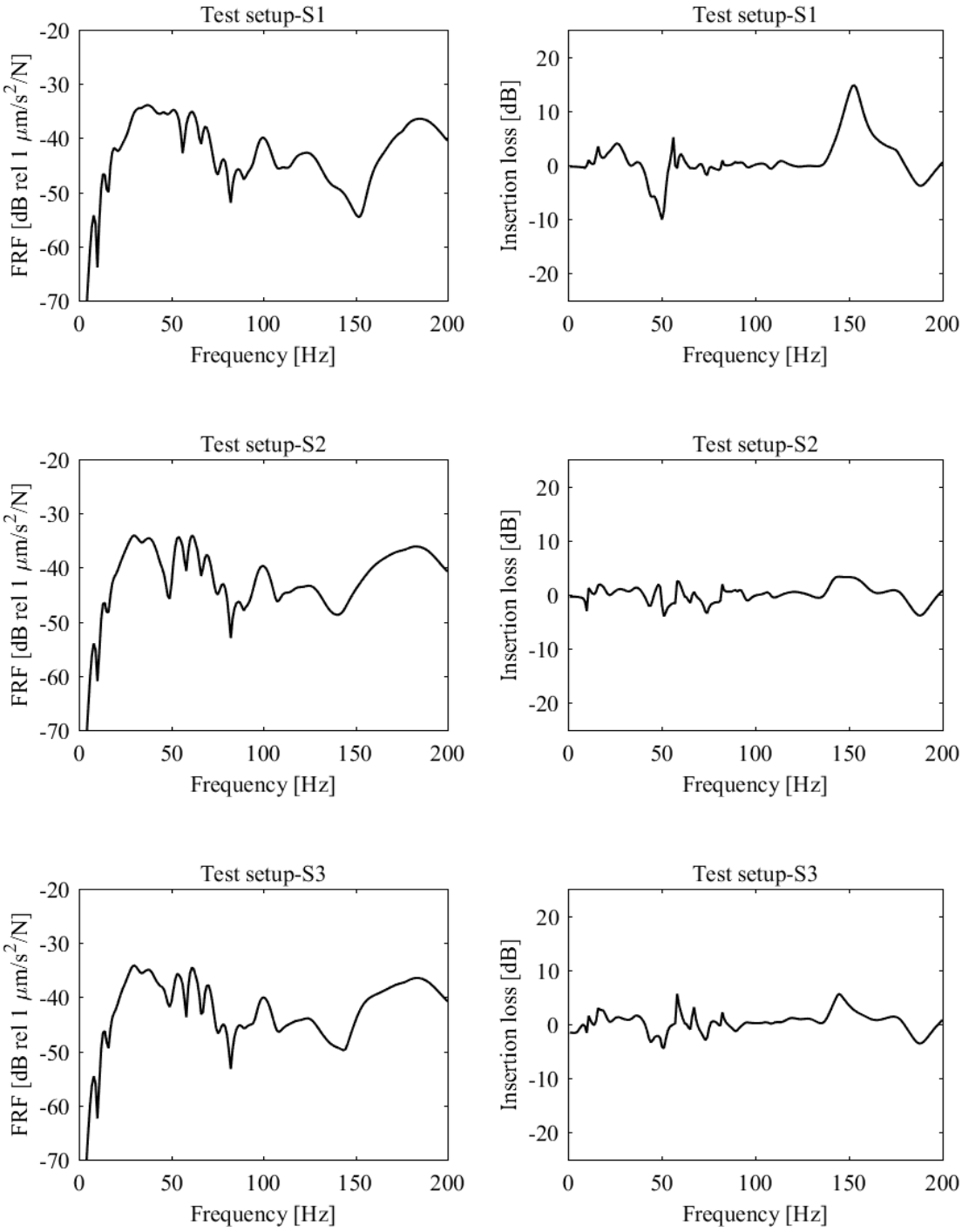

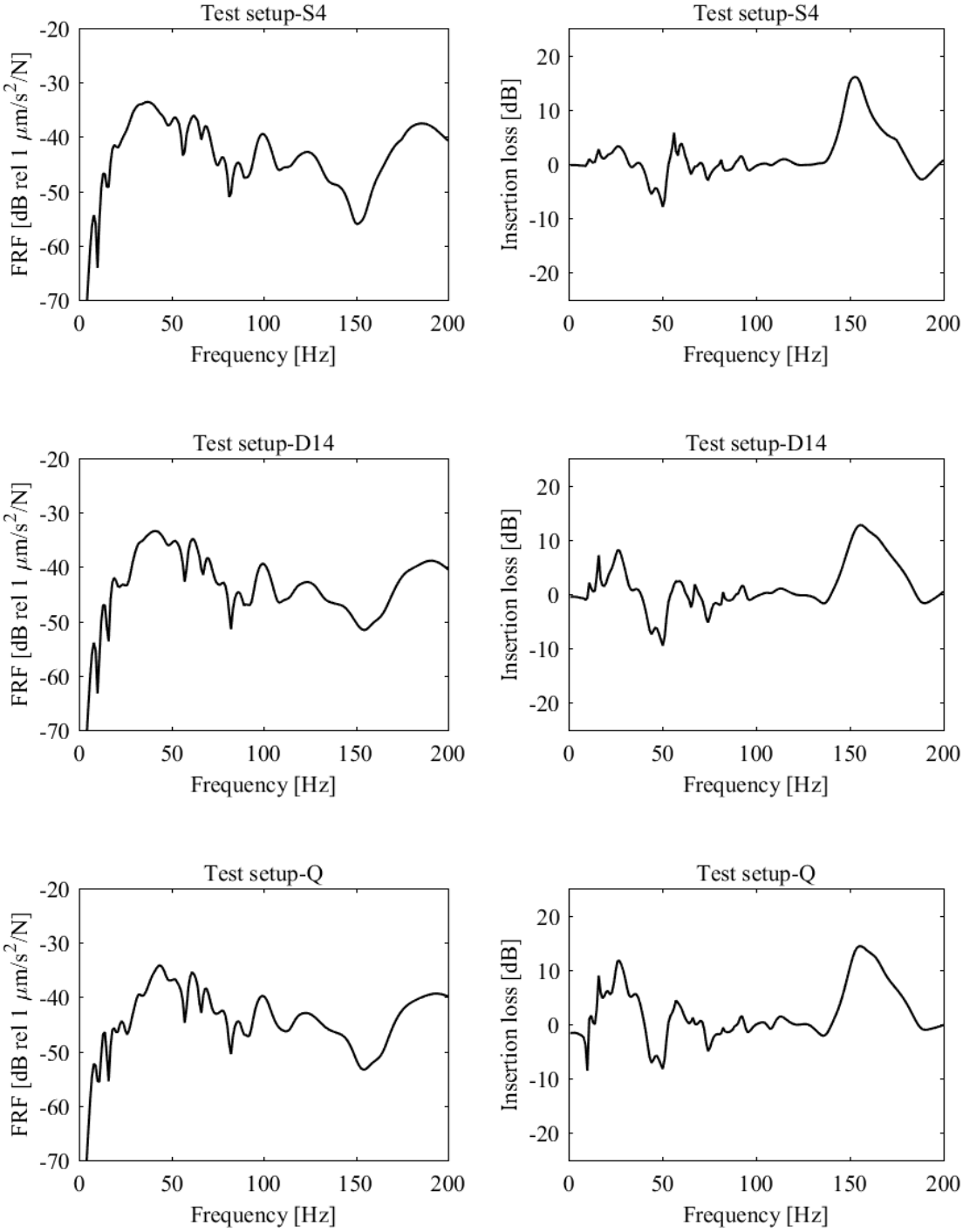

Figure 6.14: Mitigation results provided by numerical analysis — two layers foam.

In contrast with the results presented in the above section, results provided by the experimental analysis, see Figure 6.4.2 presents a quite higher variation of the IL. As for the experimental results provide a variation between -5 to 5 dB for the entire range of 200 Hz, here it is clearly to observe that the differences are between -10 to 15 dB. Hence it can be concluded that the Plexiglas blocks embedded in the soaked foam has a higher influence

on the response compared with the experimental setup for the two layer mattress.

The same seven configurations were studied as in the laboratory setup for the foam composed by two layers. In Figure 6.14, the first four configurations are the ones with the mass added in one of the slots, called S1 to S4. A closer inspection of these configurations shows that test setup S1 and S4 provides better results than setup S2 and S3. This can be observed at low frequencies, where around 10 to 20 Hz and 50 to 70 Hz these two configurations provide a higher IL than configurations S2 and S3 with around 3 to 5 dB. Similar behavior is observed also at higher frequencies with an increased IL of 10 to 12 dB for test setup S1 and S4. A downside of these setups represents the dips occurred at around 50 Hz being more negative with a value around −5 dB. The mass added in slots S2 and S3 seems to not influence the results, being neither an advantage nor a disadvantage.

The last two configurations that can be observed in Figure 6.14 regards the masses added in slots S1 and S4 for one configuration and with the masses added in all the available slots in the other one. Both configurations provide around the same values of IL, but it is observed that the test setup Q provides slightly higher values. It is observed that the peaks and dips are in the same frequency range for both setups. At frequencies 10 to 30 Hz, test setup Q, provides an IL with a value of 13 dB being higher than the one provided by setup D14, which provides a value only of 8 dB. At higher frequencies, around 140 to 170 Hz the difference between these two setups is only of 3 dB. The dips are of the same value of 8 to 10 dB at frequencies from 40 to 50 Hz. At 4 Hz an extra dip is present for Q configuration.

Configurations S1, S4, Q and D14 provide the same variation of IL for the range of 200 Hz. Configurations S2 and S3 are the ones that perform poorly than any others, providing no concludent peaks or dips. As for the single layer mattress, test setup Q is providing the highest IL for both lower and higher frequencies. This may be again the result of a stop band forming in the FE model.

6.5.3 Roots of numerical vs. experimental inaccuracies

The significant deviations between the responses observed from the experimental and numerical analysis might be caused by a series of factors which will be presented in order of their impact on the response in the following.

The main factor is the physical impossibility of reproducing the exact boundary conditions. In the numerical model the assembly of foam and embedded Plexiglas blocks were modeled as a single part while the experimental setup was built by putting together the two layers of foam, the Plexiglas blocks and the corresponding covering hexahedral foam parts. In between these parts sliding may have occurred as well as air bubbles filling the gaps. Moreover a visual inspection during the experiments indicated a loss of contact in of the

corners between the two foam layers.

Another factor that could have introduced errors is the approximation of the material properties and especially the difficulty of matching the exact damping. In addition the material was considered as one phase material, observation made at frequencies higher than 5 Hz but this might not fit the exact behavior of the material.

In the future, these errors could be reduced by finding a better way of assembling the experiment components and by this reducing the sliding and the contact imperfections. Furthermore using poroelastic elements in the FE model is recommended, since they reproduce better the foam material compared with the solid elements.

6.6 Vibration screen influence

As a final test, an experiment was made in order to study the screening effect of vibrations when placing trenches between the source and the receiver. The trenches are filled with Plexiglas with the same characteristics as presented in the previous chapters. Two different types of tests were made, an active respectively a passive test.

One test setup can be seen in Figure 6.15

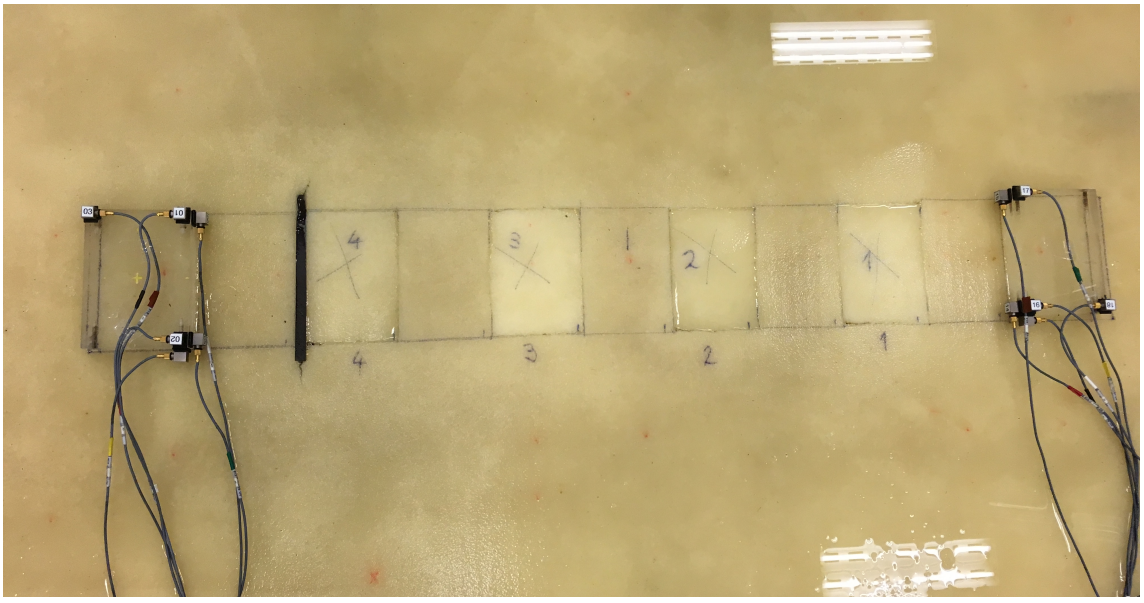

Figure 6.15: Active mitigation setup with a 15 cm screening barrier

The width of the barriers was changed in order to study its influence on the vibration mitigation. Three widths were used: 15 cm, 20 cm, 35 cm. Each test was repeated 3 times in order to obtain stable and trustworthy results.

The results of all mitigation test setups are presented in Figure 6.6. The responses are presented side by side, the FRF to the left and the insertion loss (IL) to the right.

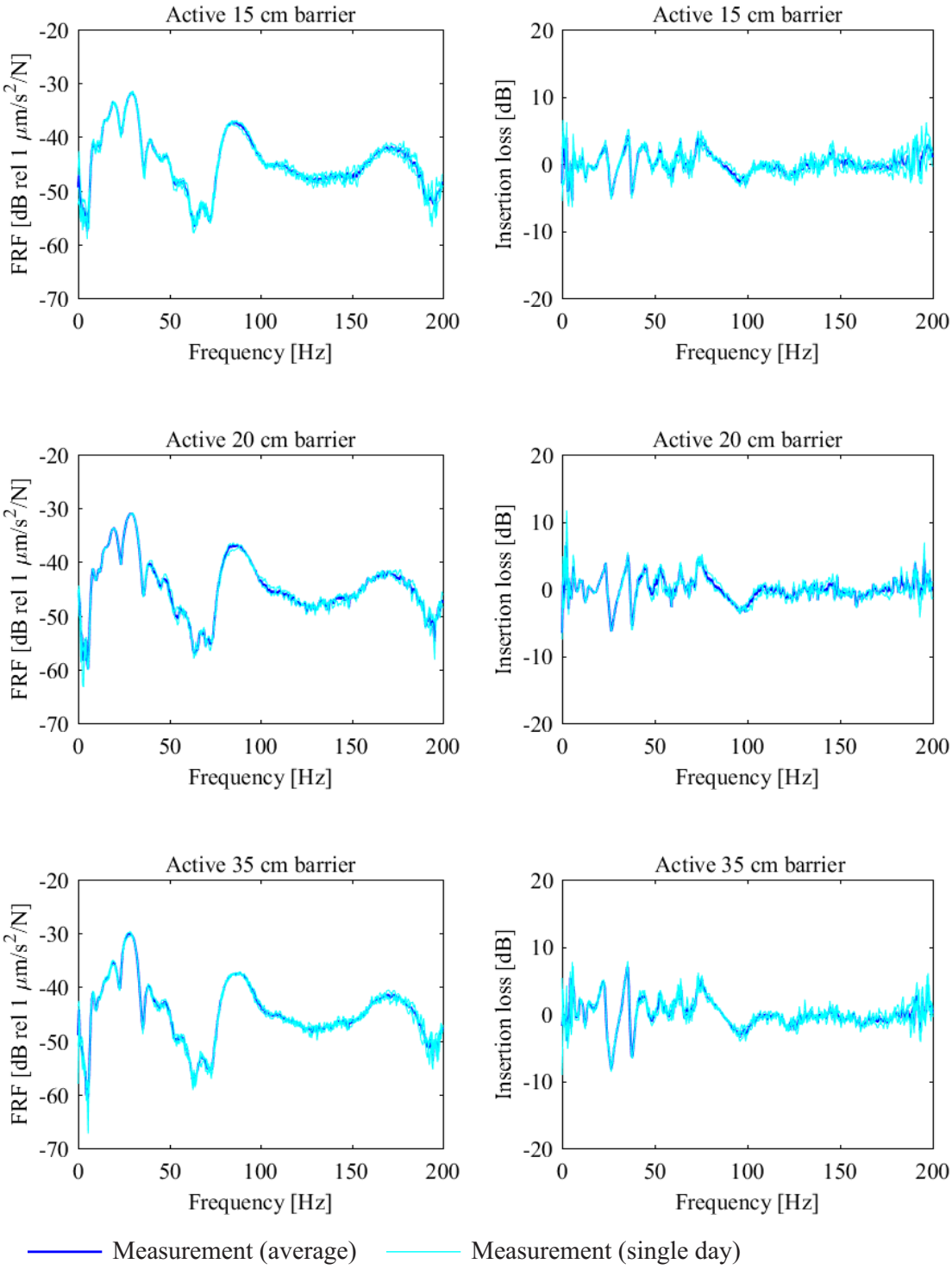

Figure 6.16: Results for vibration screen influence-active tests.

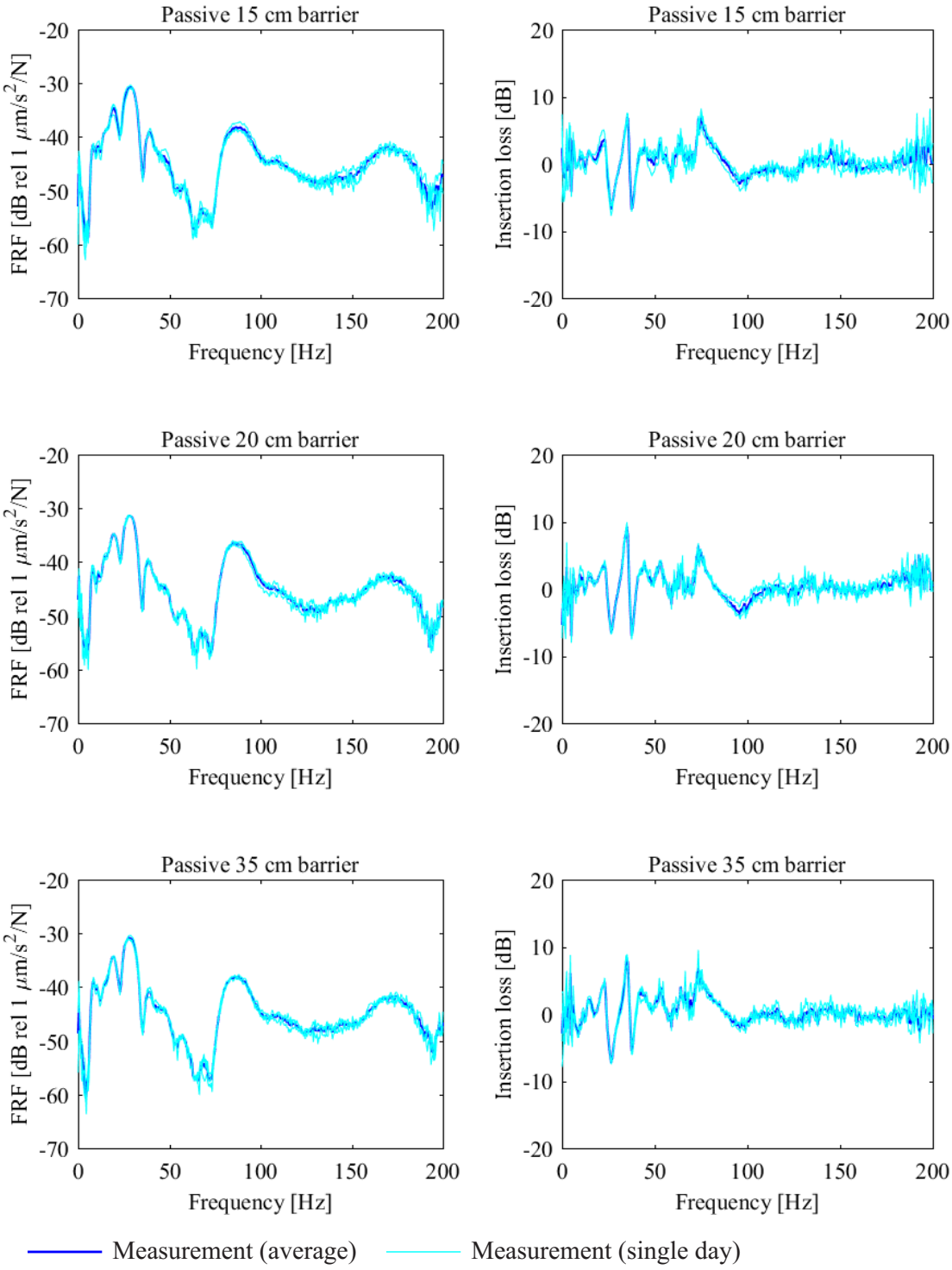

Figure 6.17: Results for vibration screen influence-passive tests

As it can be seen, positioning trenches in front of the source or in front of the receiver has an effect on the vibration. The effect is mostly a function of the exciting frequency. Depending on it, the barrier can act as attenuator or as amplifier on the vibration.

But this study was made in order to observe if the width barrier has an influence over the vibrations.

In figure 6.18 and 6.19 the IL for the active, respectively passive setup tests is presented, with variation in the width dimension.

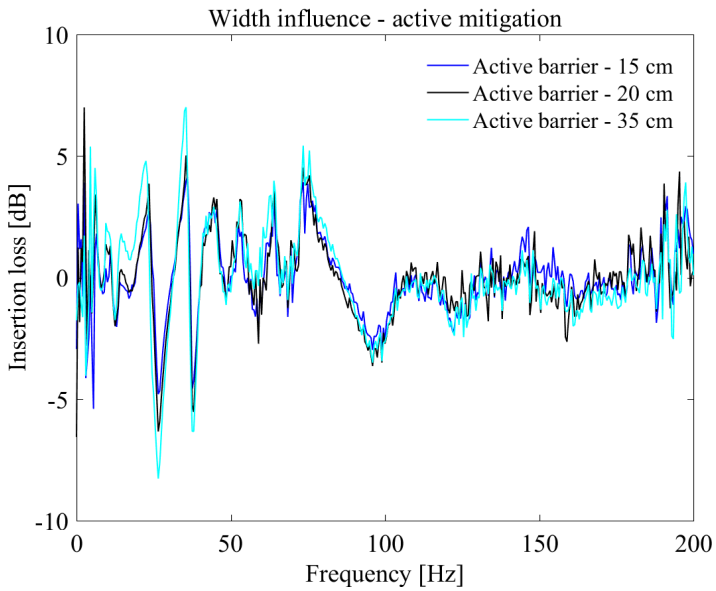

Figure 6.18: Active mitigation with width variation

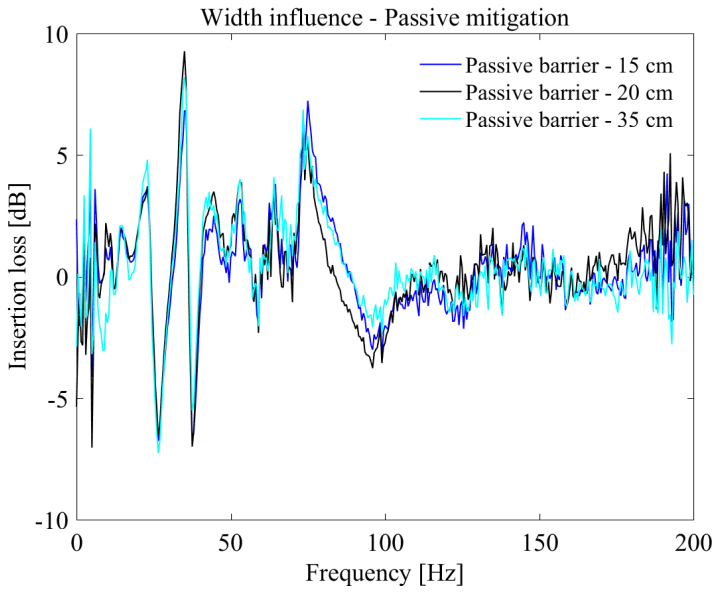

Figure 6.19: Passive mitigation with width variation

It can be seen from Figure 6.18 that in the active mitigation setup the barrier width has an effect on the vibrations. Better mitigation occurs by increasing the width of the trench. At the same time this trend is also present for the frequencies where the vibrations are amplified.

Furthermore, from Figure 6.19 it can be observed that a wider barrier does not produce a better screening effect for the passive-case setup.

Even though the width of the barrier has an effect on the vibrations in the active-case setup, this effect is small, so in conclusion the width is not so important when the vibration mitigation problem is the concern. In contrast to this previous studies have shown the depth is of great importance especially for the Rayleigh waves.

Chapter 7

Conclusion

In the present project the influence of masses placed on the ground or embedded in the soil, together with a study regarding the trench-width influence, was studied. The analyses were performed in the frequency range of 0 to 200 Hz on a small-scale laboratory experiment as well as on similar numerical models.

The design of the experiment represented a challenging exercise for this research and it consisted in scaling the real in situ conditions of vibrations to a small-scale laboratory model. The model design started with a study on the vibration frequencies and wavelengths in real soil together with setting up the rules for the design of the model. Based on this the geometry dimensions and suitable materials were found. Extensive problems occurred while testing the dry foam, resulting in unstable results. The problem was solved by saturating the foam with water, thus increasing the mass and in the same time the inertia, stabilizing the results. In the future it is recommended to start from the beginning with a material characterized by more inertia. Another time-consuming process represented the determination of the correct material properties since they were unknown. To solve this, a method using both numerical and experimental results was implemented from which suitable results were obtained. It has been observed as well that an important factor that has an impact on the results was maintaining constant conditions regarding the water saturation level in the mattress and necessary measures were taken to in order to avoid water evaporation.

With the material properties determined and stable, the next step consisted of test planning. This resulted in a modular grid with a clear configuration which could be used both for one and two-layer models. For the various configurations, frequency-response functions (FRFs) were recorded using accelerometers to measure the accelerations in the vertical direction on the source respectively on the receiver footing, by exciting the source foundation with an impulse hammer.

A second approach of the problem involved using the commercial software Abaqus CAE and developing numerical models with the same characteristics as the small-scale laboratory experiment. In this part, a first challenge was to match the boundary conditions but an even more difficult problem was the calibration of the model by means of stiffness and damping. The Rayleigh damping model was used for the models and the coefficients α and β were determined iteratively. This damping model was found to be an adequate choice

since it gives the user the means of tuning damping separately to low and high frequencies by adjusting the coefficients. Another special characteristic of the numerical model was selecting the hybrid formulation for its elements. This option allowed a calibration of the Poisson's ratio value close to 0.5 and still returning accurate results.

Single-layer foam

The one layer experimental setup results proved that the presence of the masses positioned on the ground surface has an influence on the receiving response. It was discovered that by using a S1 and S2 configuration beneficial results were obtained in the frequency range between 30 to 40 Hz and 70 to 100 Hz with an IL of 8 dB. On the other hand, using configurations S3 and S4, an important negative influence of −10 dB was observed, which increased the response significantly. When positioning between the source and receiver multiple masses (D14 and Q setups) positive effects were as well recorded. For the D14 configuration a peak of 7 dB was observed at frequencies between 30 to 40 Hz and 70 to 100 Hz. However the periodic placing of the masses, test configuration Q, provided the highest positive IL with values of 12 dB at 45 Hz. A similar pattern is observed when increasing the added mass to double for the single-slot test configurations. The numerical model of this experiment did not match perfectly the laboratory results but in some frequency ranges the two approaches present a good correlation. Similar with the experimental results, configurations S1 and S2 performs well compared with S3 and S4 test layouts, with the observation that for the Abaqus models the magnitudes of IL was higher. Again the periodic configuration Q returned the highest positive result in terms of IL.

Two-layers foam

The two-layers experimental setup, in contradiction to its one-layer equivalent, could not be matched with the numerical model. This was caused mainly by the inaccuracy of the boundary conditions and the lack of contact between the two layers of foam in the small scaled laboratory experiment. In future tests this should be avoided by using a thicker foam layer instead of an assembly of two separate pieces.

The results of the experimental analysis using embedded masses between the two layers of foam were more significantly lower compared with the masses placed on the surface. However an interesting discovery was that by introducing multiple masses (D14 and Q) mitigation influence was observed at higher frequencies (75 and 125 Hz). The results provided by the numerical analysis are in a strong contradiction with the experimental results, actually presenting more similarities with the results from the single layer.

Taking into consideration that the results from the experimental analysis showed little influence of the embedded masses, it can be concluded that the solution of burring masses into the ground does not result in reduction of vibrations. However, this result is meaningful

for real situations where the influence of vibrations has to be evaluated for existing buildings surrounded by buried elements of old constructions such as foundations or tanks. With the results above in mind, a numerical model designed to predict the effects of the vibrations on a studied building the focus of the model should not be on the buried masses.

Barrier width influence

The influence of the barrier width on vibration screening was studied in the end of the experimental work using both active and passive configurations.

For the active configuration it was discovered that the increased width has an influence on the response, while for the passive configuration insignificant influence was observed. Therefore it can be concluded if mitigation measures are taken by positioning an active barrier, then the width is one of the important parameters.

Conclusion

In the present project the effects of placing masses on or in the ground were observed. The overall influence on the response was around 10 dB for setups where masses were placed on the surface, and approximately 4 dB for setups where the plates were buried in the ground. Judging that the experiments presented uncertainties of around 3 dB, the influence on the receiver response, for the embedded mass cases, is low. From the configurations with the masses placed on the surface it was observed that the periodic setup yields a significant influence on the response of around 15 dB. Hence this configuration could be used for real projects to mitigate vibrations at a relative low frequencies, while the vertical barriers seem to perform better for higher frequencies. The distance and the masses of the inserted blocks can be approximated by use of the numerical model. This solution allows a further tuning directly on the site by adjusting the blocks's position.

It was also discovered that even though it was possible to calibrate the numerical model of the no mitigation test setup with its experimental equivalent, for the other configurations the numerical results presented significant deviations. Therefore, in the future the reliability of a prediction given by a numerical model has to be tested before is validated for use. It also has to be mentioned that for real case conditions a numerical model is expected to perform better since the numerous boundary conditions and contact problems introduced by the experimental model would not be present.

Acknowledgments

First of all, we would like to thank our supervisor, Lars Vabbersgaard Andersen, for all the work and time dedicated to this project and for all the productive meetings which combined good ideas together with some classic danish humor. Furthermore we are grateful to the

PhD candidate Paulius Bucinskas and the staff from Aalborg University laboratory who offered their assistance with various tasks. We also express our gratitude to Brüel & Kjær for kindly offering the authors free use of the PULSE front-end and LabShop.

Chapter 8

Bibliography

Andersen, 2006. Lars V. Andersen, *Linear Elastodynamic Analysis*,ISSN 1901-7286 DCE Lecture Notes No. 3, 2006

Wilkinson, 1965. Wilkinson, J. H., *The Algebraic Eigenvalue Problem*, Oxford University Press, Oxford, 1965

Ramaswami, 1979, Ramaswami S., *Towards Optimal Solution Techniques for Large Eigenproblems in Structural Mechanics*, Ph.D. Thesis, MIT, 1979.

P. Coulier, G. Degrande, A. Dijckmans, J. Houbrechts, G. Lombaert, W. Rucker, L. Auersch, M. R. Plaza, V. Cuellar, D. Thompson, A. Ekblad, and A. Smekal, "RIVAS WP4.1 Scope of the parametric study on mitigation measures on the transmission path," 7th European Framework Programme (2011), pp. 1–90.

Woods, 1968, Woods J. D. Woods, *Wave-induced shear instability in the summer thermocline*, J. Fluid Mech. 32, 791–800, 1968.

R. D. Woods, R. D. Woods, *Screening of elastic surface waves by trenches*, Ph.D. thesis, University of Michigan, 1967.

6B. Dasgupta, D. E. Beskos, and I. G. Vardoulakis, "Soil, vibration isolation using open or filled trenches. Part 2: 3D homogeneous," Comput. Mech. 6, 129–142, 1990.

P. Coulier,G. Degrande, 2015, P. Coulier, V. Cuellar, G. Degrande, and G. Lombaert, *Experimental and numerical evaluation of the effectiveness of a stiff wave barrier in the soil*, Soil Dyn. Earthquake Eng. 77, 238–253, 2015.

L. Grau and B Laulagnet, L. Grau and B Laulagnet, *Effect of horizontal wave barriers on ground vibration propagation*, Departement Genie Mecanique et Conception, Laboratoire Vibrations et Acoustique, Institut National des Sciences Appliqutees Lyon, 25 bis av. Jean Capelle, 69100, Villeurbanne, France

Woods, R.D., N.E. Barnett and R. Sagesser, 1974, Woods, R.D., N.E. Barnett and R. Sagesser, *Holography, a new tool for soil dynamics.*, J. Geotech. Eng., 100: 31-47.

S. Liao and D. A. Sangrey, 1978, S. Liao and D. A. Sangrey, *Use of piles as isolation barriers*, Journal of the Geotechnical Engineering Division, vol. 104, no. 9, pp. 1139–1152,

1978.

Massarsch, K. R. and Ersson, 1985, Massarsch, K. R. and Ersson, *Vibration Isolation in Soils*, Royal Institute of Technology (KTH), Stockholm, Job Report No. 20, 32 p.

Ashref Mohamed A. Alzawi , M. Hesham El Naggar, 2011, Ashref Mohamed A. Alzawi, M. Hesham El Naggar, *Vibration Isolation Using In-filled Geofoam Trench Barriers*, The School of Graduate and Postdoctoral Studies The University of Western Ontario London, Ontario, Canada

W. A. Haupt, 1981, W. A. Haupt *Model test on screening of surface waves*, Proceedings of the 10th International Conference on Soil Mechanics and Foundation Engineering, vol. 3, pp. 215–222, Stockholm, Sweden, 1981

Dooling 1970, Dooling, *Filed tests on in filled trenches*

D. D. Barkan,1962, D. D. Barkan, *Dynamics of Bases and Foundations*

Abaqus 6.14. Dassault Systèmes Simulia Corp., Providence, RI, USA: Dassault Systèmes; 2014.

List of Figures

2.1 Mitigation types depending on the barrier position: a) active mitigation, b) passive mitigation. 6
2.2 Components of the displacement field in a plane elastic wave. 7
2.3 Soil deformation subjected to wave type vibrations [L.A-2006]. 7
2.4 Rayleigh wave. 10
2.5 Rayleigh wave. Amplitude variation with depth. 11
2.6 Relative wave velocities. 12
2.7 Example of trench. 14
2.8 Active trench a), passive trench b). 15
2.9 Example of added mass. 15

3.1 Static scheme for the main model. 19
3.2 Benchmark setup 21
3.3 Modular set up with proposed mittigation solutions 22

4.1 Impact hammer type 8202. 23
4.2 Impact hammer tips. 23
4.3 Accelerometer type 4507 Bx. 24
4.4 Impact hammer type 8202. 24
4.5 TCELLNER Function Generator. 24
4.6 Amplifier Type 2692-C. 25
4.7 Front-end, type 3560 D. 25
4.8 Hardware setup window. 26
4.9 Geometry Basis window. 27
4.10 Geometry Measurement Points window. 28
4.11 Analysis Setup window. 29
4.12 Hammer Trigger window. 29
4.13 Hammer Weighting Setup window. 30
4.14 Response Weighting Setup window. 31
4.15 Measurements tab, Level Meter, Analyzer Status, Average Counter, Double Hit Detector and Measurement Displays. 32
4.16 FRF validation window with frequency response functions (right) and deformed animated geometry (left). 33

4.17 First order versus second order elements 34
4.18 1D model in MATLAB 37
4.19 1D model in Abaqus 37
4.20 MATLAB (left) and Abaqus (right) results for 1D model at t=5 sec. 39

5.1 Static scheme for the simple beam. 42
5.2 Model setup. 42
5.3 Frequency response of the beam given by 1st accelerometer — experimental analysis. 43
5.4 Deformed shape of the beam corresponding to each mode provided by LabShop software. 44
5.5 Model setup in the numerical program Abaqus. 45
5.6 Time series for accelerations given by acc. 8. 46
5.7 Frequency response of the beam given by 1st accelerometer — numerical analysis. 48
5.8 Deformed shapes of the beam for mode 1 provided by experimental (left) and numerical (right) analysis 49
5.9 Deformed shapes of the beam for mode 2 provided by experimental (left) and numerical (right) analysis 49
5.10 Deformed shapes of the beam for mode 3 provided by experimental (left) and numerical (right) analysis 49
5.11 Deformed shapes of the beam for mode 4 provided by experimental (left) and numerical (right) analysis 50
5.12 Deformed shapes of the beam for mode 5 provided by experimental (left) and numerical (right) analysis 50
5.13 Frequency response results from both experimental and numerical models. . 51
5.14 Observed points on the Abaqus CAE model-undeformed shape. 53
5.15 Observed points on the ABAQUS CAE model — deformed shape. 53
5.16 Determination of Poisson's ratio for Point 1 and 2 54
5.17 Deformed shape for the numerical model. 55
5.18 Convergence study of the acceleration values. 56
5.19 Convergence study of the first ten eigenmodes. 57
5.20 Proposed set up for testing the dry foam. 58
5.21 Experimental vs. Abaqus FRF for the dry foam. 58
5.22 Experimental vs. Abaqus FRF for the dry foam with improved BC. 59
5.23 Influence of various values for Poisson's ratio on the FRFs. 61
5.24 Vibrator machine experiment proposed set up 62
5.25 Vibrator machine FEM model 63
5.26 FRF obtained using the vibrating machine 64
5.27 Modular setup with proposed mittigation solutions — experimental. 65

5.28 Modular setup with proposed mittigation solutions — numerical. 65
5.29 FRF for no mitigation. 66
5.30 FRF for active mitigation. 66

6.1 Tests configurations with single masses and double masses added on the ground surface. 71
6.2 The reference case with no added masses — single layer foam. 72
6.3 Results for single masses placed between source and receiver. 74
6.4 Results for double masses placed between source and receiver. 75
6.5 Results for multiple masses placed between source and receiver. 77
6.6 Detail with the parts used for the two layers test setup. 78
6.7 Tests configurations on the two-layers foam. 79
6.8 The reference state with no added masses — two layers foam. 80
6.9 Results for configuration S1 of the masses placed in the ground surface. . . 80
6.10 Results for configurations S2, S3, S4 of the masses placed in the ground surface. 81
6.11 Results for configurations D14 and Q of the masses placed in the ground surface. 82
6.12 Detail with the parts used for the two layers test setup. 84
6.13 The reference case with no masses. 84
6.14 Mitigation results provided by numerical analysis — two layers foam. 86
6.15 Active mitigation setup with a 15 cm screening barrier 88
6.16 Results for vibration screen influence-active tests. 89
6.17 Results for vibration screen influence-passive tests 90
6.18 Active mitigation with width variation 91
6.19 Passive mitigation with width variation 91

A.1 P-waves, S-waves particle motion(L.A-2006). 105

B.1 Force development over time. 107
B.2 Deflection of the beam for entire time interval 107
B.3 Force amplitude in Abaqus model. 108

C.1 Frequency response of the beam given by 2nd accelerometer — experimental analysis. 109
C.2 Frequency response of the beam given by 3rd accelerometer — experimental analysis. 110
C.3 Frequency response of the beam given by 4th accelerometer — experimental analysis. 110
C.4 Frequency response of the beam given by 5th accelerometer — experimental analysis. 111

C.5 Frequency response of the beam given by 2nd accelerometer — numerical analysis. 112
C.6 Frequency response of the beam given by 3rd accelerometer — numerical analysis. 112
C.7 Frequency response of the beam given by 4th accelerometer — numerical analysis. 113
C.8 Frequency response of the beam given by 5th accelerometer — numerical analysis. 113
C.9 FRFs from both experimental and numerical models — accelerometer 2. . . . 114
C.10 FRFs from both experimental and numerical models — accelerometer 3. . . . 114
C.11 FRFs from both experimental and numerical models — accelerometer 4. . . . 115
C.12 FRFs from both experimental and numerical models — accelerometer 5. . . . 115

List of Tables

2.1 Mittigation solution history. 16

3.1 Wave characteristics. 17
3.2 Mattress dimensions. 18

5.1 Plexiglas beam properties and dimensions. 41
5.2 Damping coefficients. 47
5.3 Force and displacement values for the two tests. 54
5.4 Plexiglas beam properties and dimensions. 55
5.5 Material properties for the soaked foam. 61

Part I

Appendix

Appendix A

Additional wave theory description

A.1 Derivation of the body wave velocities

The P-wave and S-wave are also called body or volume waves because they propagate through the entire volume of the soil. In the following, the velocities of these waves are expressed with the use of the Navier's equations.

A.1.1 Body waves

P-waves

In the absence of the body forces, Equation 2.2 becomes:

$$(\lambda + \mu)\frac{\partial^2 u_j}{\partial x_i \partial x_j} + \mu \frac{\partial^2 u_i}{\partial x_i \partial x_j} = \rho \frac{\partial^2 u_i}{\partial t^2}. \tag{A.1}$$

By taking the divergence of Equation A.1 yields

$$(\lambda + \mu)\frac{\partial^3 u_k}{\partial x_k \partial x_i \partial x_i} + \mu \frac{\partial^3 u_k}{\partial x_k \partial x_i \partial x_i} = \rho \frac{\partial^3 u_k}{\partial t^2 \partial x_k}. \tag{A.2}$$

If the particle motion of the wave is dilatational the Equation A.2 can be expressed as function of the dilation Δ

$$(\lambda + 2\mu)\frac{\partial^2 \Delta}{\partial x_i \partial x_i} = \rho \frac{\partial^2 \Delta}{\partial t^2}, \frac{\partial^2 \Delta}{\partial x_i \partial x_i} = \frac{1}{c_P^2}\frac{\partial^2 \Delta}{\partial t^2}. \tag{A.3}$$

Finally the wave velocity reads

$$c_P = \sqrt{\frac{\lambda + 2\mu}{\rho}}. \tag{A.4}$$

The above equations represent the wave equations in three dimensions. In this case c_P stands for the wave phase velocity associated with the P-wave.

S-waves

In contrast with the P-waves, S-waves are rotational. Extracting the rotation from Equation A.1 results the following three equations:

$$(\lambda + \mu)\varepsilon_{ijk}\frac{\partial^3 u_i}{\partial x_i \partial x_k \partial x_j} + \mu\varepsilon_{ijk}\frac{\partial^3 u_k}{\partial x_i \partial x_k \partial x_j} = \rho\varepsilon_{ijk}\frac{\partial^3 u_k}{\partial t^2 \partial x_j}. \tag{A.5}$$

Here ε_{ij} is the permutation symbol with 3 possible values 1, -1 or 0. The fraction of the first term is symmetric in the indices j and k while ε_{ij} is antisymmetric. Therefore the first term of the equation cancels out and the equation becomes

$$\frac{\partial^2 w_i}{\partial x_i \partial x_j} = \frac{1}{c_S^2}\frac{\partial^2 w_i}{\partial t^2}, \qquad c_S = \sqrt{\frac{\mu}{\rho}}. \tag{A.6}$$

The above equation is the three dimensional wave equation and the c_S represents the wave phase speed and $w_i = w_i(x,t)$ is the rotation of the displacement field which has the formulation

$$w_i = \frac{1}{2}\varepsilon_{ijk}\frac{\partial u_k}{\partial x_j} = \frac{1}{2}\varepsilon_{ijk}W_{kj}, \qquad W_{kj} = \frac{1}{2}\left(\frac{\partial u_i}{\partial x_j} - \frac{\partial u_j}{\partial x_i}\right). \tag{A.7}$$

Where $W_{ij} = W_{ij}(x,t)$ is the infinitesimal rotation tensor. Due to the fact that the infinitesimal strain is symmetric and the rotation tensor is anti-symmetric

$$\frac{\partial u_i}{\partial x_i} = \varepsilon_{ij} + W_{ij}. \tag{A.8}$$

Interpreting the above equation it is deduced that the total displacement is composed by a

dilatational part corresponding to the P-waves and a rotational part corresponding to the S-wave. The particle motions generated by these displacements can be seen in Figure A.1.

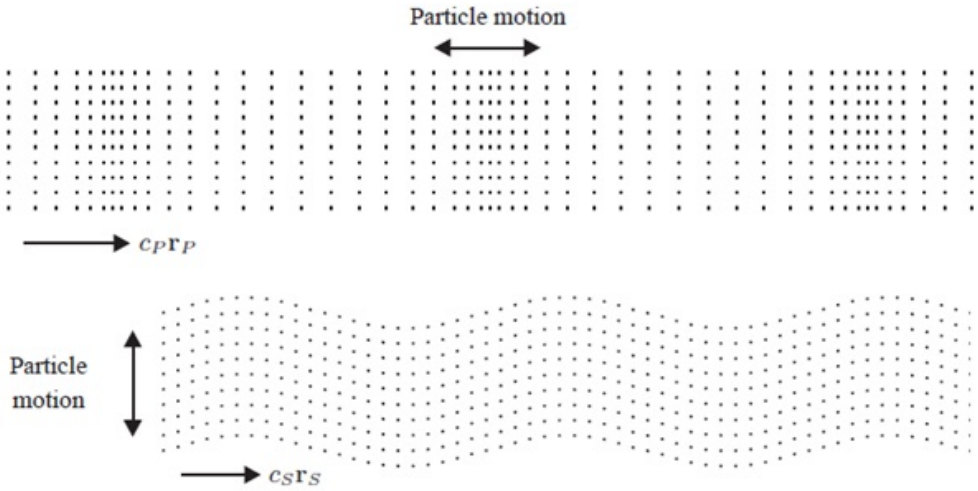

Figure A.1: P-waves, S-waves particle motion(L.A-2006).

Appendix B

Wave propagation-mathematical verification

B.1 Verification of Abaqus for wave propagation

In this section more details regarding the two models created both in MATLAB and Abaqus are presented. In Section 4.3 the results provided by the two models are presented and it was observed that the results match with small differences produced by the elements used in the analysis.

The force in the two models has to be harmonically applied in both models. In the MATLAB code the force it is applied in node 1 and its development over time can be seen in Figure B.1.

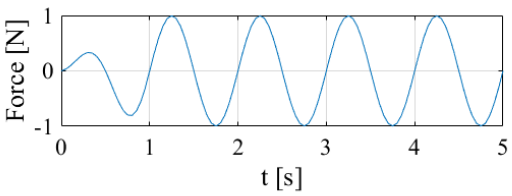

Figure B.1: Force development over time.

It is observed that the force has an amplitutde varying between $[-1,1]$ over the total time of 5 s. The beam's deflections can be observed in Figure B.2 over the whole time interval.

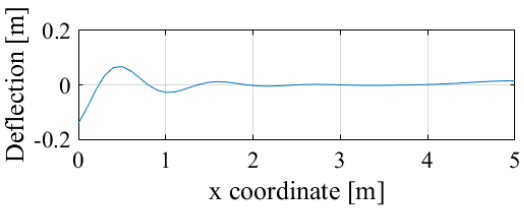

Figure B.2: Deflection of the beam for entire time interval

The beam dimensions in the Abaqus model are 5x0.1x0.1 m, being a 3D solid model regarded as a 1D wave propagation problem.

The force is applied at one end of the beam over the whole surface of $0.1\,\mathrm{m}^2$. A test has been made in order to check the differences between applying the force as a pressure or as a traction. The results confirmed that no influence of the results is made. For the model it has been used the pressure method of applying the force. It has been applied with a certain amplitude in order to simulate an harmonic excitation of the beam. The amplitude was created for a period of 1 sec following a sinusoidal behavior, see Figure B.3.

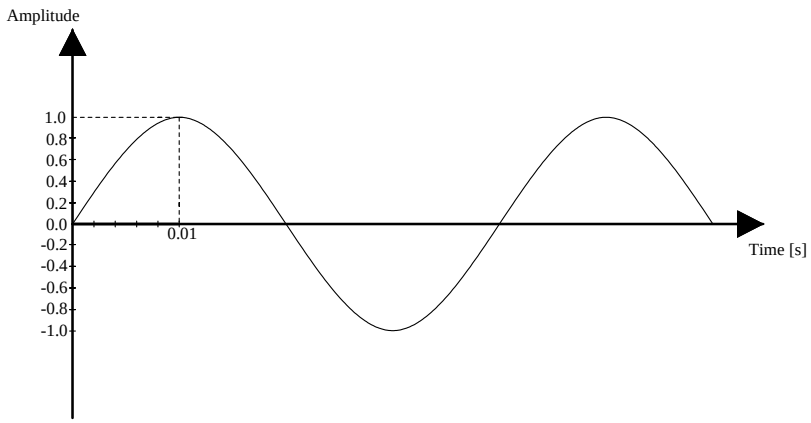

Figure B.3: Force amplitude in Abaqus model.

Beside the initial step in Abaqus, which is created automatically, a dynamic one - implicit step, has been created with a time period of 5 sec and maximum number of increments of 100. This process make the model more expensive regarding the time and the computational memory, but returns the desired accuracy.

Beside the Courant number when meshing, another criteria is the element type used for the mesh. For a linear element a minimum of 12 elements per wave length is required while for a quadratic element type 4 elements are enough. From Equation 4.4 the size of the element and time step is presented in Table B.1

Element	L_e	Δt
Quadratic	0.25	0.125
Linear	0.083	0.0415

For further calculation and for more accurate results the quadratic elements are preferred.

Appendix C

FRFs provided by analyzing the simple beam

C.1 Experimental results

The FRFs provided in the experimental analysis by the accelerometers 2, 3, 4 and 5 are presented in Figure C.1, C.2, C.3 and C.4.

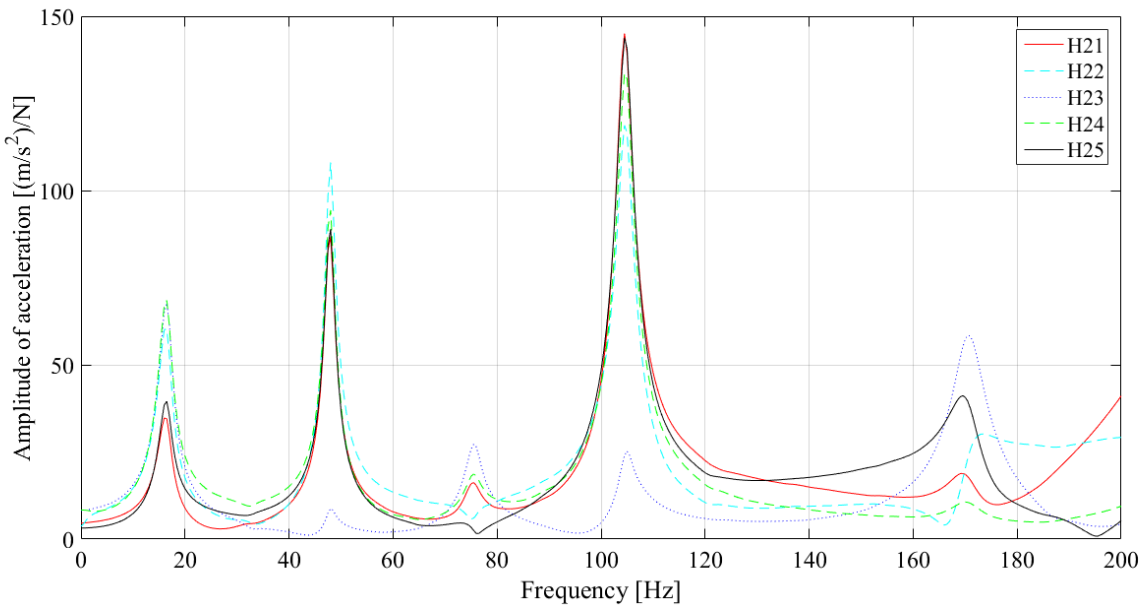

Figure C.1: Frequency response of the beam given by 2nd accelerometer — experimental analysis.

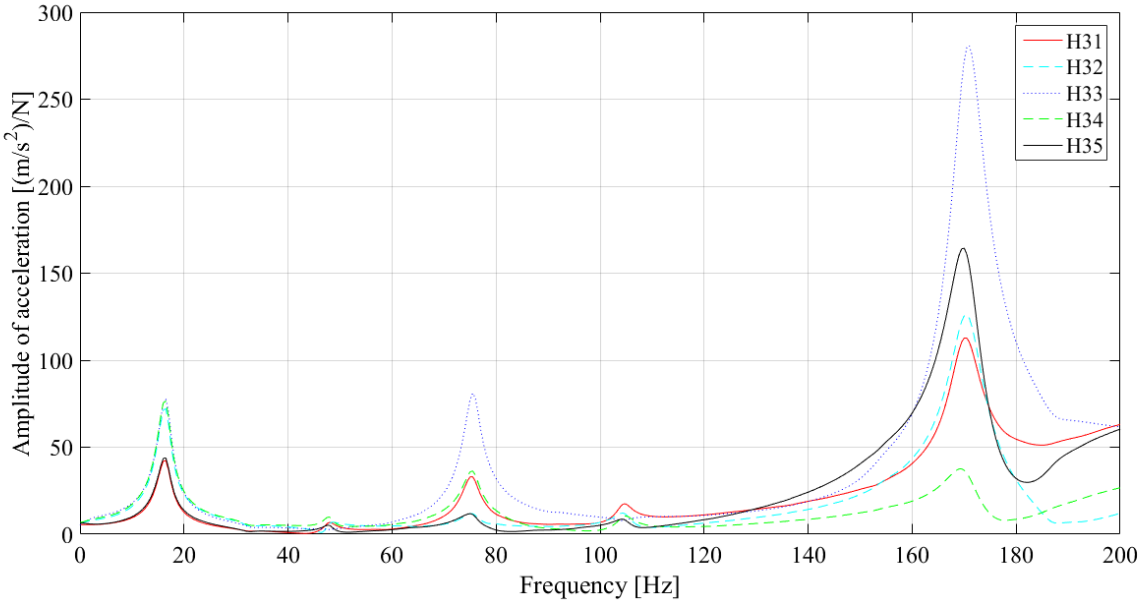

Figure C.2: Frequency response of the beam given by 3rd accelerometer — experimental analysis.

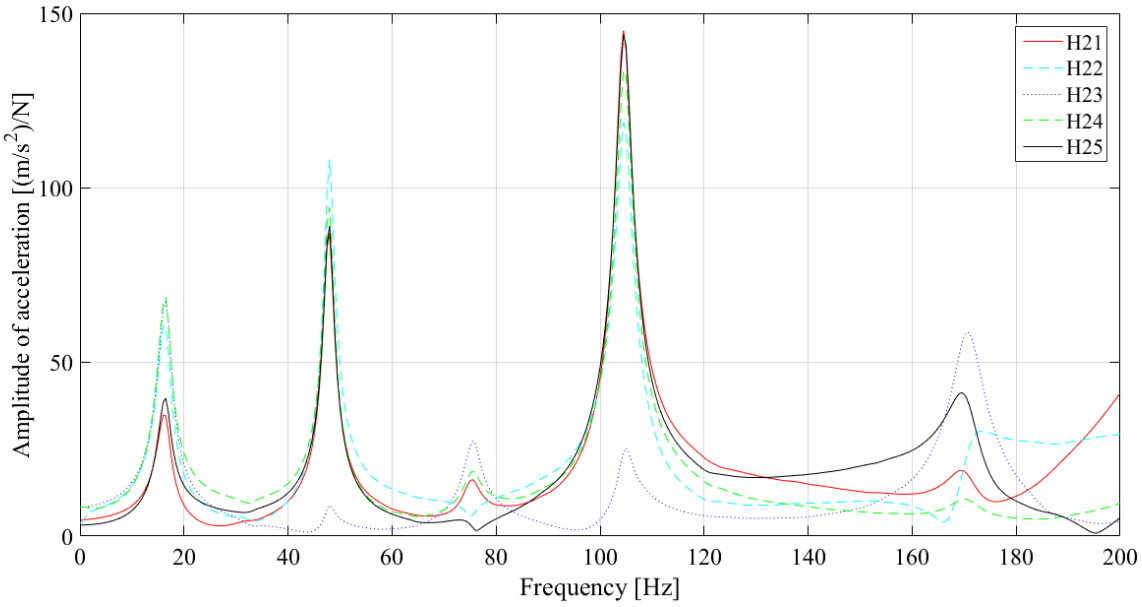

Figure C.3: Frequency response of the beam given by 4th accelerometer — experimental analysis.

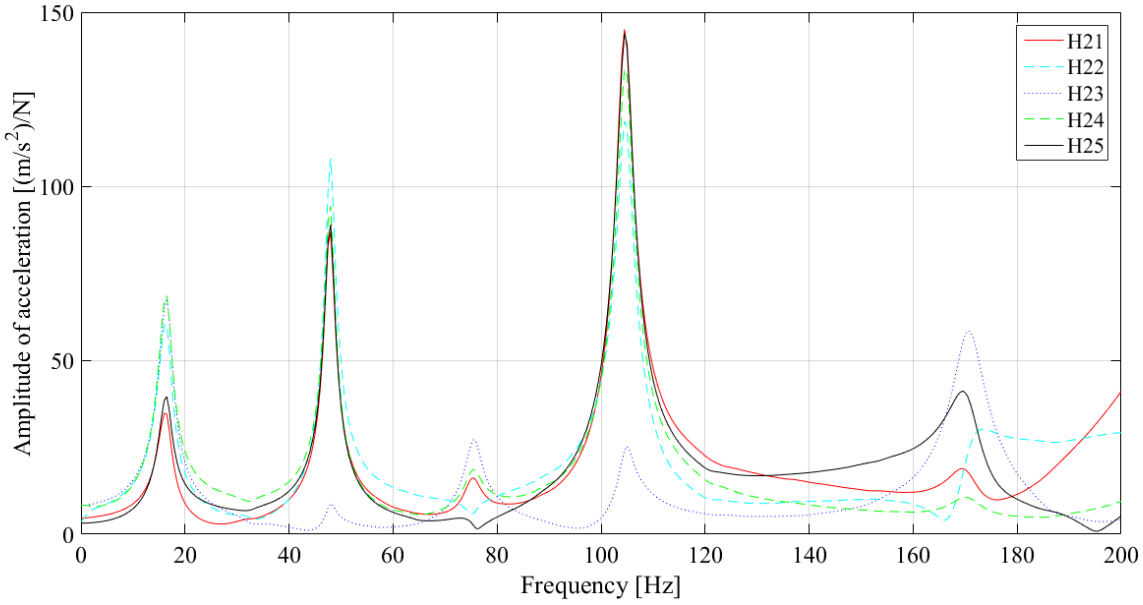

Figure C.4: Frequency response of the beam given by 5th accelerometer — experimental analysis.

C.2 Numerical results

The FRFs provided in the numerical analysis by the accelerometers 2, 3, 4 and 5 are presented in Figure C.5, C.6, C.7 and C.8.

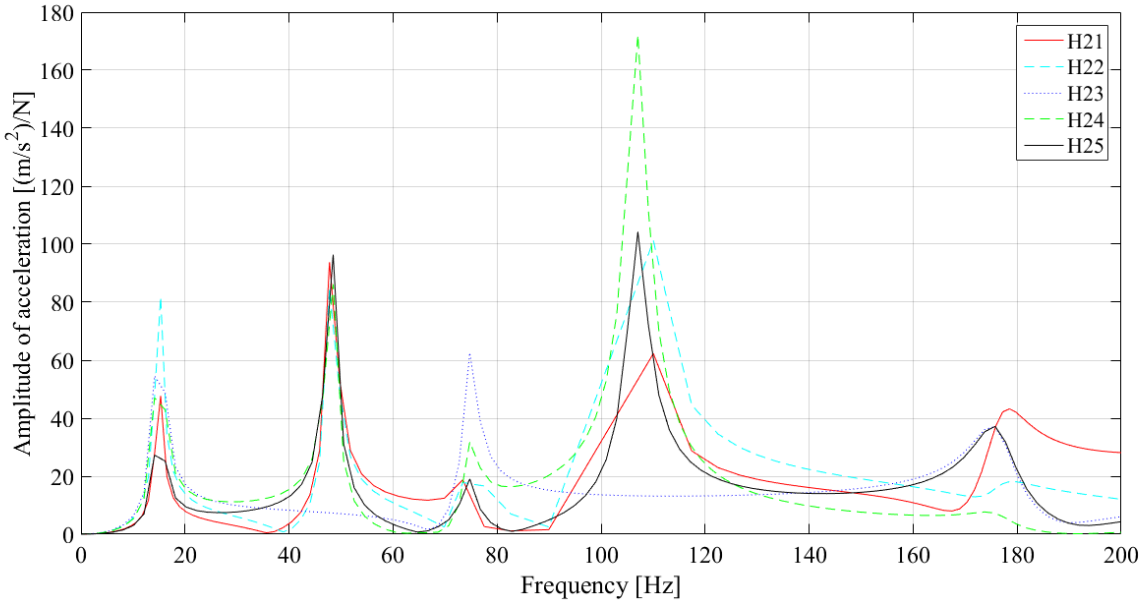

Figure C.5: Frequency response of the beam given by 2nd accelerometer — numerical analysis.

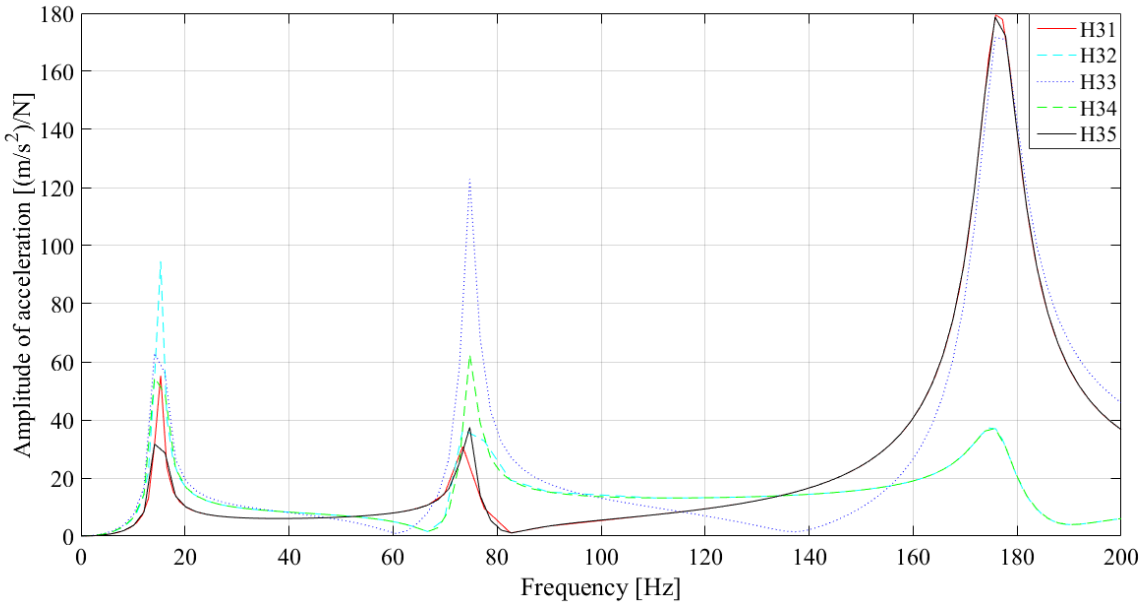

Figure C.6: Frequency response of the beam given by 3rd accelerometer — numerical analysis.

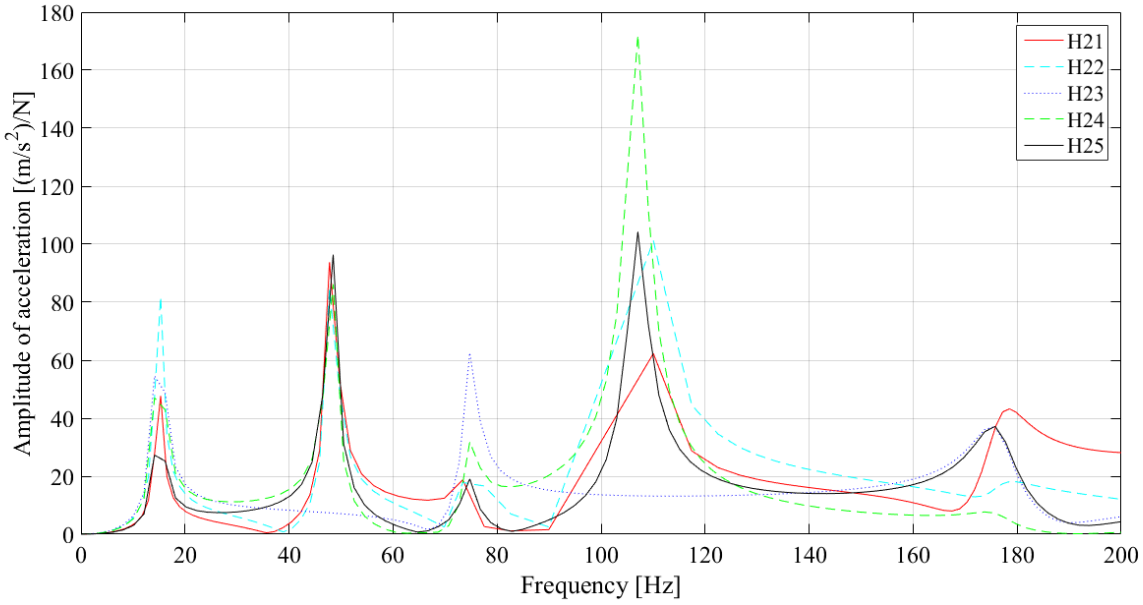

Figure C.7: Frequency response of the beam given by 4th accelerometer — numerical analysis.

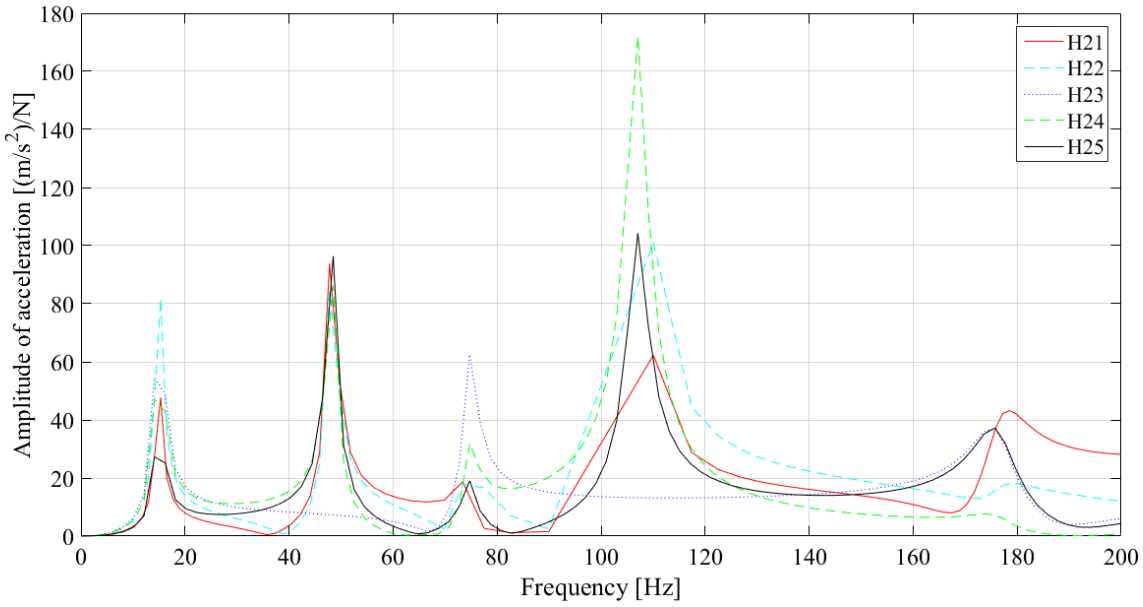

Figure C.8: Frequency response of the beam given by 5th accelerometer — numerical analysis.

C.3 Comparing the results

A comparison between the FRFs provided by the numerical and experimental results is presented Figure C.9, C.10, C.11 and C.12, for accelerometers 2, 3, 4 and 5.

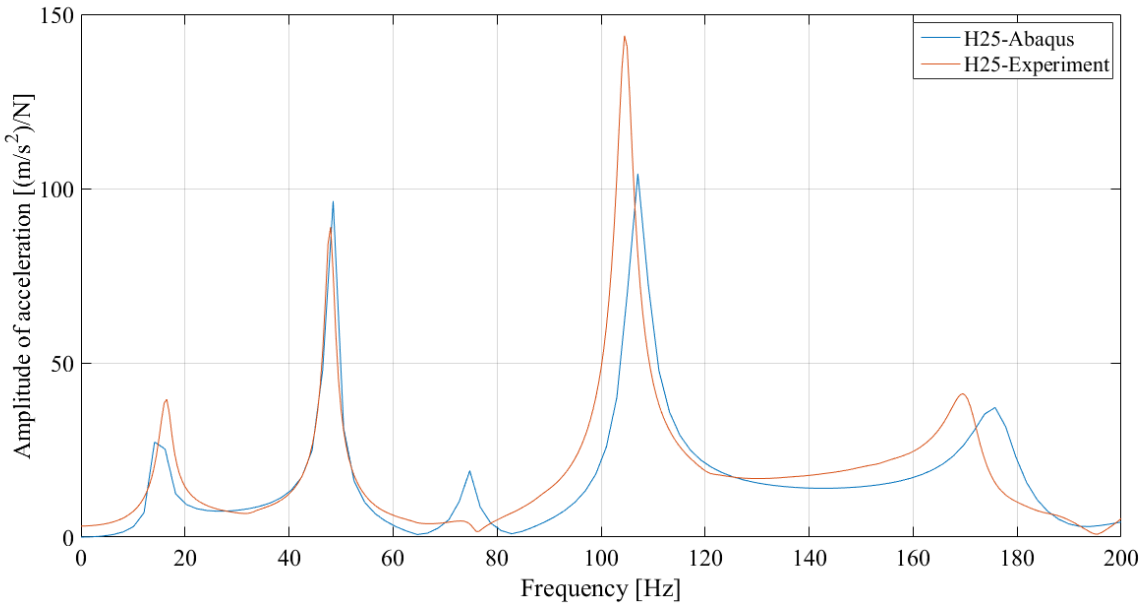

Figure C.9: FRFs from both experimental and numerical models — accelerometer 2.

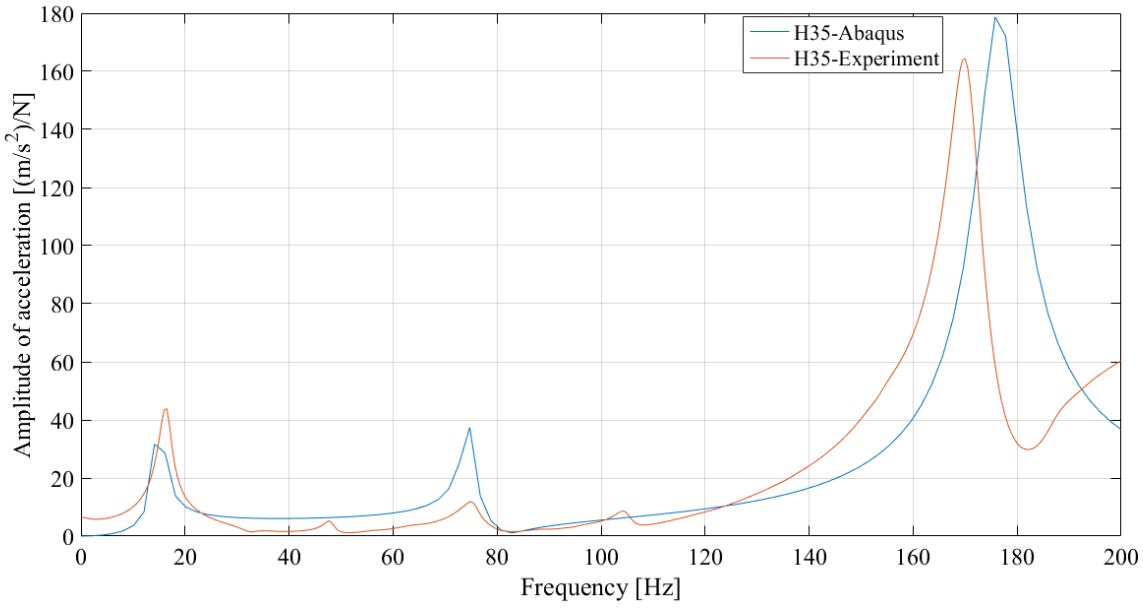

Figure C.10: FRFs from both experimental and numerical models — accelerometer 3.

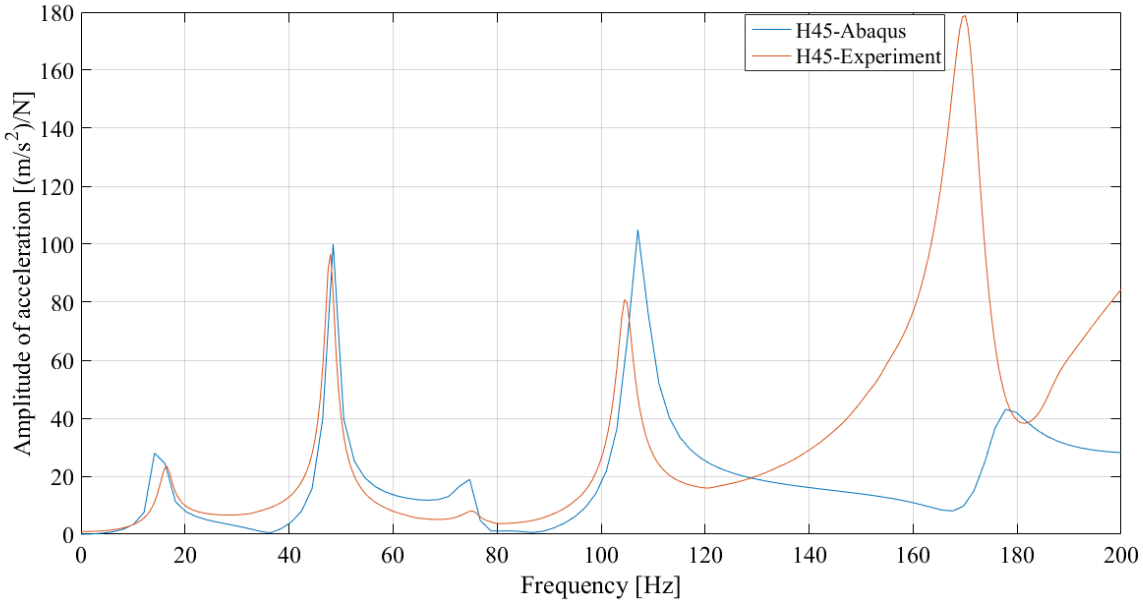

Figure C.11: FRFs from both experimental and numerical models — accelerometer 4.

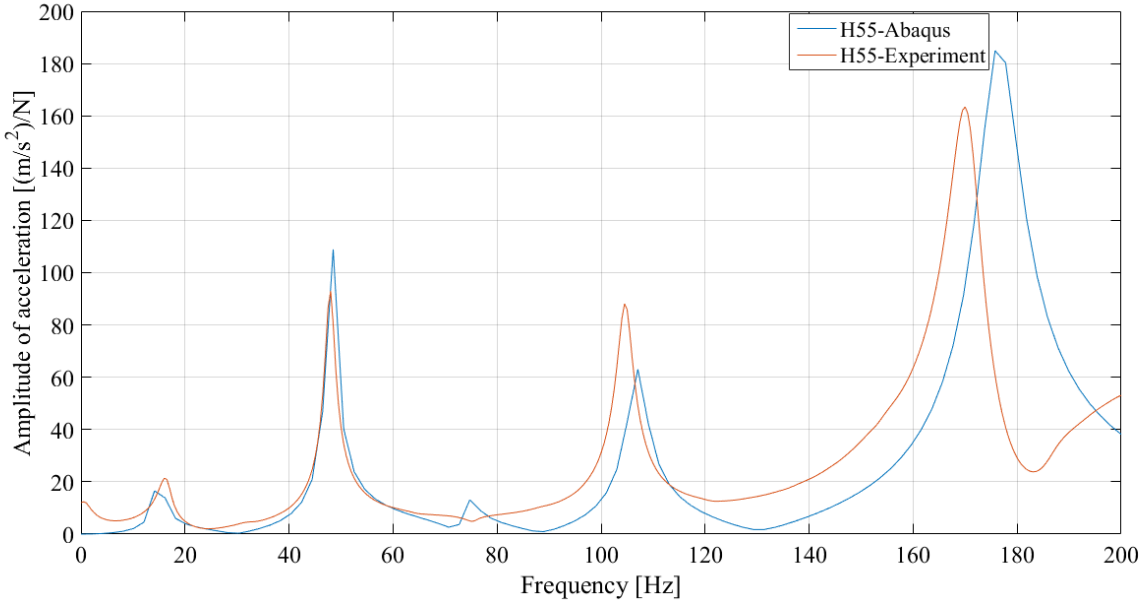

Figure C.12: FRFs from both experimental and numerical models — accelerometer 5.

Appendix D

Electronic appendix

The electronic appendix contains all the MATLAB and Abaqus models used in the project to analyse the experiment setups. The models are put on a data CD containing all the necessary files to run the Abaqus program. The CD contains folder for each part of the project.

Some MATLAB codes are based on Lars Andersen's provided coding for FEA of vibrations in infinite bar.

The data CD content:

- **Experimental data**
- **Numerical models**
- **Pictures from laboratory**
- **Report**